

**ADSORPTION OF REFORMER OFF-GAS ON NaX
ZEOLITE AND METAL ORGANIC FRAMEWORK
(MIL53(A1)): EQUILIBRIA AND KINETICS**

**A Thesis Submitted to
the Graduate School of Engineering and Sciences of
İzmir Institute of Technology
in Partial Fulfillment of the Requirements for the Degree of**

DOCTOR OF PHILOSOPHY

in Chemical Engineering

**by
Alev GÜNEŞ YERKESİKLİ**

**May 2013
İZMİR**

We approve the thesis of **Alev GÜNEŞ YERKESİKLİ**

Examining Committee Members:

Prof. Dr. S. Fehime ÇAKICIOĞLU ÖZKAN

Department of Chemical Engineering, Izmir Institute of Technology

Prof.Dr. Semra ÜLKÜ

Department of Chemical Engineering, Izmir Institute of Technology

Prof. Dr. Ş. Şeref HELVACI

Department of Chemical Engineering, Ege University

Assoc. Prof. Erol Şeker

Department of Chemical Engineering, Izmir Institute of Technology

Assoc. Prof. Yusuf SELAMET

Department of Physics, Izmir Institute of Technology

29 May 2013

Prof. Dr. S. Fehime ÇAKICIOĞLU ÖZKAN

Supervisor, Department of Chemical Engineering

Izmir Institute of Technology

Prof. Dr. S. Fehime ÇAKICIOĞLU ÖZKAN

Head of the Department of
Chemical Engineering

Prof. Dr. R. Tuğrul Şenger

Dean of the Graduate School of
Engineering and Sciences

ACKNOWLEDGEMENT

I would like to express my deepest gratitude to my advisor Prof. Dr. Seher F. ÇAKICIOĞLU ÖZKAN for her invaluable help, support and understanding during my thesis study. I am grateful for her patience, creative advice. I have learned too much from her and it has been a pleasure and great experience working under her supervision.

I wish to express my gratitude to my committee members, Assoc. Prof. Dr. Erol Şeker and Assoc. Prof. Dr. Yusuf SELAMET, Prof. Dr. Şeref Şerife HELVACI, Prof. Dr. Semra Ülkü for their insightful comments and constructive criticism, which helped to improve the overall quality of my thesis.

Special thanks to my friends; Özgün DELİİSMAİL, Ahmet Uğur ÇİÇEK, Yasemin ERTEN, Melda BÜYÜKÖZ for their friendship and interest.

I would like to express my heartfelt gratitude to my parents, Neşe and Mehmet Ali GÜNEŞ and brother, Batuhan GÜNEŞ for their continuous support and encouragement, which enabled me to overcome difficulties.

I wish to express my endless love to my dear husband and my life partner, Burç YERKESİKLİ who supported me, taught me and loved me. Finally, my warmest thanks belong to my dear daughter Ada YERKESİKLİ and my dear son Deniz YERKESİKLİ for their neverending love, and for being sunshines of my life. To them I dedicated this thesis...

ABSTRACT

ADSORPTION OF REFORMER OFF-GAS ON NaX ZEOLITE AND METAL ORGANIC FRAMEWORK (MIL53(Al)): EQUILIBRIA AND KINETICS

Synthetic gas produced from steam methane reforming (SMR off -gas) is a mixture of H₂, CO, CO₂, and CH₄ can be used in fuel cell after purification. In this study adsorption as a purification tool was used to obtain high H₂ content of gas mixture from SMR off gas. Zeolites and metal organic framework were used as an adsorbent. CO₂ equilibrium studies on K rich NaX zeolites, prepared with ultrasonic and traditional methods, and metal organic framework MIL53 (Al) shows high adsorption on zeolites than MIL53(Al) up to 1 atm. K rich zeolites give lower adsorption than NaX zeolite. Adsorption isotherms obtained for MIL53 (Al) is linear (favorable for zeolites). This makes MIL53(Al) is an promising adsorbent for high pressure application. Adsorption equilibrium at 5 atm shows that NaX zeolite is good adsorbent for the SMR off gas with the following orders: CO₂>CH₄>CO> H₂.

Kinetics of SMR off gas in MIL 53 (Al) were studied by using Zero Length Column (ZLC) method. The results show that the calculated diffusivities are strongly dependent on temperature but weakly dependent on purge flow rate. The study reveals that transport is controlled by intracrystalline diffusion. The activation energy on diffusion are nearly same (about 41 kJ/mol) and not change with respect to kinetic diameter of SMR off gases. Heat of SMR off gas adsorption on MIL53(Al) obtained from Henry's constant shows that adsorption is exothermic. The study shows that the ZLC method is an effective tool to investigate the diffusion kinetics of SMR off-gas gases in MIL53(Al).

ÖZET

REFORMER ÇIKIŞ GAZININ NaX ZEOLİTİ VE METAL ORGANİK AĞ YAPISI (MIL53(Al)) ÜZERİNDE ADSORPLANMASI: DENGE VE KİNETİK

Metanın buharla reformasyonundan üretilen sentetik gaz (SMR off-gas) H₂, CO, CO₂, ve CH₄ karışımdır, saflaştırmadan sonra yakıt hücresinde kullanılabilir. Bu çalışmada SMR çıkış gazı karışımından yüksek miktarda H₂ elde edebilmek için adsorpsiyon saflaştırma aracı olarak kullanılmıştır. Adsorbent olarak zeolitler ve metal organik ağ yapısı kullanılmıştır. Ultrasonik ve geleneksel metodla hazırlanmış K zengin zeolitler ve metal organik ağ yapısı MIL 53(Al) üzerindeki CO₂ denge çalışmaları 1 atm' e kadar zeolitlerde MIL53(Al) dan daha yüksek adsorplama göstermiştir. K zengin zeolitler NaX zeolitinden daha düşük adsorplama göstermiştir. MIL53 (Al) için elde edilen adsorpsiyon izotermi doğrusaldır. Bu MIL53 (Al) adsorbentini yüksek basınç uygulamaları için bir umut verici adsorbent yapar. 5 atm deki adsorpsiyon dengesi CO₂>CH₄>CO> H₂ sıralaması ile NaX zeolitinin SMR çıkış gazı için iyi bir adsorbent olduğunu göstermektedir.

SMR çıkış gazının MIL 53 (Al) üzerinde kinetiği zero length column (ZLC) yöntemi ile çalışılmıştır. Sonuçlar, hesaplanan difüzyon katsayılarının sıcaklığa güçlü şekilde bağlı ama akış hızına daha zayıf bağlı olduğunu göstermiştir. Çalışma, sistemin kristal içi difüzyon tarafından kontrol edildiğini ortaya koymaktadır. SMR çıkış gazlarının difüzyon üzerindeki aktivasyon enerjileri neredeyse aynıdır (yaklaşık 41 kJ/mol) ve SMR off gazlarının kinetik çapı ile değişmemektedir. MIL53(Al) üzerinde Henry sabitinden elde edilen SMR çıkış gazlarının adsorpsiyon ısıları adsorpsiyonun ekzotermik olduğunu göstermektedir. Çalışma ZLC yönteminin MIL 53 (Al) adsorbentinde reformer çıkış gazlarının difüzyon kinetiğini araştırmak için etkili bir araç olduğunu göstermektedir.

TABLE OF CONTENTS

LIST OF FIGURES	viii
LIST OF TABLES	x
CHAPTER 1. INTRODUCTION	1
CHAPTER 2. GAS ADSORPTION	4
2.1. Gas Adsorption Equilibrium.....	5
2.2. Gas Adsorption Kinetics.....	12
2.3. Zero Length Column (ZLC): Theory	16
2.4. Selectivity	20
CHAPTER 3. ADSORBENTS	23
3.1. Zeolites	23
3.2. Metal Organic Frameworks (MOFs)	27
3.2.1.Synthesis of MOFs.....	34
3.2.2.Application of MOFs	35
CHAPTER 4. GAS ADSORPTION PROPERTIES OF MOFs.....	38
CHAPTER 5. EXPERIMENTAL STUDIES	48
5.1.Materials	48
5.2.Preparation of the NaX and KNaX zeolite adsorbents	48
5.3. Characterization.....	48
5.4. Adsorption Equilibrium Studies	49
5.4.1. CO ₂ interaction with adsorbent surface	49
5.4.2. SMR Off-gas Adsorption	49
5.5. Adsorption Kinetic Studies: ZLC Adsorption System	51
5.6.Error Anlysis.....	53

CHAPTER 6.RESULTS AND DISCUSSIONS	55
6.1.Characterization of Adsorbents	55
6.1.1. Zeolite Adsorbents	55
6.1.2. MIL 53 (Al) Adsorbent.....	62
6.2. Adsorption Equilibrium Studes	64
6.2.1. CO ₂ interaction with Adsorbent Surface	65
6.2.2. SMR off-gas CO ₂ , CH ₄ , CO and H ₂ Adsorption	71
6.3. Adsorption Kinetic Studies: Zero Length Column (ZLC).....	78
CHAPTER 7. CONCLUSION	88
REFERENCES	90

LIST OF FIGURES

<u>Figure</u>	<u>Page</u>
Figure 2.1. Representative Zero Length Column	17
Figure 3.1. Faujasite structure showing cation sites (I, II, III) and locations of oxygen atoms	23
Figure 3.2. Metal components and ligands to create 1D, 2D or 3D MOF's (Schröder, 2010).....	27
Figure 3.3. View of MIL 53 structure with (SBUs, coordination bonds, linker)	29
Figure 3.4. Structural switching of the MIL 53 system on CO ₂ adsorption	30
Figure 3.5. Schematic representation of synthesis MOFs	34
Figure 5.1. Experimental apparatus	50
Figure 5.2. Zero Length Column configurations	52
Figure 6.1. SEM images of adsorbents: (a) NaX (b) S50 (76) (c) S70 (81) (d) U50 (79) (e) U70(83)	57
Figure 6.2. X-ray diffraction patterns of zeolite adsorbents.....	58
Figure 6.3. TG curves of zeolite adsorbents	59
Figure 6.4. DSC curves of zeolite adsorbents	59
Figure 6.5. FT-IR spectra of the zeolites between (a) 400-4000 and (b) 400-1600 cm- Wavelength	61
Figure 6.6. SEM images of MIL 53(Al).....	62
Figure 6.7. X-ray diffraction patterns of MIL53(Al)	62
Figure 6.8. TG curves of MIL 53 (Al).....	63
Figure 6.9. FT-IR spectra of MIL 53(Al)	64
Figure 6.10. CO ₂ adsorption isotherm of the zeolites and MOFs at 278K (a) and 298K (b)	66
Figure 6.11. CO ₂ adsorption isotherm of NaX zeolite at 298 K (error bar is obtained after two measurements)	67

Figure 6.12.	Adsorption isotherms of CO ₂ at 278 K of NaX zeolite (o: experimental, linecurve fittings Langmiur: — — — Freundlich:— — — Sips: — — — — Toth: —————model equations 68	68
Figure 6.13.	Change in heat of adsorption with loading 71	71
Figure 6.14.	CO ₂ , CH ₄ , CO, H ₂ adsorption equilibrium on zeolite NaX at 298 K (a), 313K(b)..... 72	72
Figure 6.15.	Change in amount adsorbed amount with charge pressure 73	73
Figure 6.16.	Adsorption isotherms of CO ₂ , CH ₄ , CO, H ₂ (●: experimental points at 298K and ○: experimental points at 313K, curve fitting lines Sips: — — — Langmiur— — — — Toth: —————model equations 75	75
Figure 6.17.	CO ₂ desorption curves at 100 °C for 3h, 6h, 20h regeneration periods (purge flow rate of 100 ml/min) 78	78
Figure 6.18.	Effect of purge helium flow rate on the desorption of CO ₂ , CH ₄ , H ₂ , CO 80	80
Figure 6.19.	Effect of temperature on the response curves of CO ₂ , CH ₄ , H ₂ , CO (Helium flow rate=100 ml/min)..... 83	83
Figure 6.20.	Variation of Henrys law constant and diffusivity and with temperature for adsorption of CO ₂ , CH ₄ , H ₂ , CO 85	85
Figure 6.21.	Figure 6.21. The kinetic selectivity, SA/B, for MIL 53(Al) 87	87

LIST OF TABLES

<u>Table</u>	<u>Page</u>
Table 2.1. The IUPAC classification for adsorption isotherms	6
Table 2.2. Studies with Zero Length Column (ZLC) technique in literature.....	15
Table 3.1. Zeolite: X	24
Table 3.2. Selected Studies for ion exchange in NaX zeolite	26
Table 3.3. Examples of MOFs structure (Adam et al. 2008)	28
Table 3.4: Some examples of rigid MOFs	31
Table 3.5. Some examples of flexible MOFs.....	33
Table 4.1. Properties of adsorbate gases used in this study	39
Table 4.2. Gas adsorption properties of some rigid MOFs	40
Table 4.3. Summary of gas adsorption in flexible MOFs	42
Table 4.4. CO ₂ adsorption properties of Zeolites and all-silica microporous solid, Aluminium phosphates, MOFs and amine modified mesoporous silica.	44
Table 6.1. Textural properties of adsorbents.....	56
Table 6.2. TG and DSC data of the zeolites	60
Table 6.3. Isotherm Model fitting for CO ₂ adsorption data	70
Table 6.4. Model Fitting and parameters of CO ₂ , CH ₄ , CO and H ₂ adsorption on NaX zeolite (± 95 % confidence interval)	76
Table 6.5. Variation of parameters with temperature and flow rate for CO ₂ , CH ₄ , H ₂ , CO on MIL 53 (Al)	82
Table 6.6. Sorbate properties and heat of adsorption, activation energy values	85

CHAPTER 1

INTRODUCTION

Hydrogen is an environmentally clean energy fuel. It produces from various resources. But in the world most of the hydrogen is produced by Steam Methane Reforming (SMR) processes because of its efficiency and lowest investment cost (Liu et al., 2005). Steam methane reformer off-gas (SMR-off gas) contains CO₂, (10-25%), CH₄ (1.3-8%), CO (0.25-10%) as impurities besides the hydrogen. Hydrogen can be used as an energy source into a fuel cell. However its application needs high purity hydrogen. For example PEM fuel cells hydrogen quality is given that at least %99.99. So these impurities must be removed. As a result of that, it is critical to remove impurities from the off-gas to separate and optimize the hydrogen production.

Gas separation techniques include cryogenic distillation, membrane-based, and adsorption-based technologies. Since the invention of synthetic-zeolites in the 1940s, with the emergence of various adsorbents and the development of adsorption-based separation processes, adsorption has become a key gas separation tool in industry (Yang, 2002). With the synthesis of more and more new sorbent materials with different porosity and surface properties for green separation procedures, adsorptive separation will become increasingly more important. Thus, adsorptive separation will likely play a key role in future energy and environmental technologies notable examples are H₂ and CH₄ purifications. Conceptually, adsorptive gas separation processes can be divided into two types: bulk separation and purification. The former involves adsorption of a significant fraction (10% or more by weight) from a gas stream, while the latter implies less than 10 wt% adsorption of a gas stream (usually less than 2 wt %).

A general process of adsorptive gas separation or purification includes passing a gas mixture through a column packed with adsorbents or fixed-bed adsorbents to yield a product enriched in the more weakly adsorbed component. This is then followed by desorption of the strongly adsorbed component so that adsorbent can be reused. The high separating power is the result of the continuous contact and equilibration between the gas and adsorbent.

In adsorptive separation processes, gas separation is achieved based on the differences of adsorption capability of different components in the adsorbent. The performance of any such process is directly determined by the characteristics of the adsorbent in both adsorption equilibrium and kinetics. The related basic principles of adsorption are described in detail in several monographs. In addition to acceptable textural properties, a promising adsorbent should possess not only good adsorption capacity and selectivity, but also favorable adsorption kinetics and regenerability. To satisfy these requirements, the adsorbent should first have a reasonably high surface area as well as relatively large pore sizes for porous materials to allow adsorbate molecules to approach the interior surface.

Adsorbent choosing is very important for the rational design of the off-gas adsorption process, where the adsorption equilibrium and diffusion coefficients in the crystals of adsorbents are also great importance. Commonly used materials for gas separation and purification in industry are mainly limited to four types: activated carbon, zeolites, silica gel, and activated alumina. In the last decade, MOFs as a new family of nanoporous materials (Yaghi et al., 1998) are assembled by directly bonding metal clusters with organic linkers, thus there is no need to use structure-directing agents as for zeolites. In contrast to the tetrahedral building blocks in zeolites, MOFs can be synthesized from a large selection of inorganic clusters (e.g. square-shaped, trigonal, tetrahedral and octahedral) and organic linkers (e.g. carboxylates, imidazolates and tetrazolates). Consequently, MOFs possess a wide range of surface areas and pore sizes, and have been considered versatile materials for adsorption (Luizei et al., 2004). MOFs have very high capacity at high pressures; however, at atmospheric pressures their capacity is lower as compared to other sorbents. Volumetric and manometric method most widely used for gas adsorption. However, they are time consuming methods. Zero length column (ZLC) method is relatively inexpensive method and can be used to measure the nature of the diffusion parameters, diffusion coefficient (D) and Henry constants (K) (Barcia et al., 2005).

The general objectives of this study are to provide fundamental adsorption data (equilibrium and kinetic) of SMR off-gases (CO_2 , H_2 , CH_4 , CO) on zeolite NaX and MOF adsorbents. The studies in this thesis have been discussed in 3 parts. In the first part, the development of the adsorbent for CO_2 , the highest impurity in the reformer off gas (10-25 %), is targeted. We studied CO_2 adsorption on two types of adsorbents: K rich NaX zeolites which were prepared with ultrasonic and traditional methods and

metal organic frameworks (MOFs): MIL 53. Even the adsorption of CO₂ in conventional ion-exchanged X zeolites has been studied previously (Walten et al., 2006). There has not been an investigation of ultrasound effect in the preparation of K exchanged NaX zeolite and its effect on CO₂ adsorption.

In the second part of this study, we have measured high-pressure adsorption equilibrium of SMR-off gases on zeolite NaX, MOF at 278, 298 K and pressures ranging (0 to 5) atm by constructed volumetric system in our laboratory. In the third part of this thesis, the diffusion of SMR-off gas in a MIL-53 adsorbent has been investigated by the ZLC method. In literature there are limited kinetic studies with ZLC technique. Also, there are no kinetic studies have been reported about MOFs with SMR-off-gas in literature with ZLC or without ZLC technique. The effect of purge flow rate and temperature on the diffusion character is investigated and the diffusion mechanism is also discussed. ZLC method validity was investigated and realistic diffusion coefficients in MIL-53 adsorbent were determined.

CHAPTER 2

GAS ADSORPTION

Adsorption is defined as the enrichment of one or more components in an interfacial layer between solid (adsorbent) and fluid (adsorptive). If one component of a mixture is adsorbed more strongly than the others, a surface phase rich in strongly adsorbed species (adsorbate) is created. This enrichment forms the basis of separation of mixtures by adsorption operations. There are a lot of applications of the adsorption technologies: separation of gases (air separation, air conditioning, air purification, sewage gas purification, flue-gas purification, hydrogen separation from primary gas mixture and etc.), pollution control, respiratory protection, biological application, heterogeneous reaction applications.

Key component of adsorption, adsorbents are classified according to the pores by The International Union of Pure and Applied Chemistry (IUPAC); microporous (diameter $< 20 \text{ \AA}$), mesoporous ($20 \text{ \AA} < \text{diameter} < 500 \text{ \AA}$), macroporous (diameter $> 500 \text{ \AA}$). This is the important criteria for choosing adsorbent in any adsorption-based technology.

Based on the nature of the bonding between the adsorbate molecule and the adsorbent surface, adsorption can be categorized as either physical adsorption, which doesn't involve chemical bonding or chemisorption which involves chemical bonding. Absorption should not be mixed up with adsorption. Adsorption occurs at any pressure and temperature and molecules of gases or liquids stick to the surface of a solid material. Absorption is bulk or volume phenomenon and pressure or temperature is not necessary for process (Keller and Staudt, 2005).

Besides to adsorption; cryogenic distillation, membrane processes, chemical absorption and physical absorption techniques can be also used to separate the mixtures. The unique advantage of adsorption over other separation methods is the higher selectivity that can be achieved by adsorbents. The effectiveness of separation is directly determined by the characteristics of the adsorbent in both adsorption equilibrium and kinetics.

2.1. Gas Adsorption Equilibrium

Adsorption equilibrium is established after considerable contact of the gas with the adsorbent surface. The relation between the amount adsorbed N , the equilibrium pressures P , and the adsorption temperature T can be represented in the general form:

$$f(N, P, T) = 0 \quad (2.1)$$

At the specific temperature T , Eq. 2.1 can be reduced by the adsorption isotherms as follows:

$$N = f(P)_T \quad (2.2)$$

And

$$P = f^{-1}(N)_T \quad (2.3)$$

The adsorption isotherms, Eq. 2.2, are most frequently used in studies of adsorption equilibrium and are represented by mathematical equations such as Langmuir, Freundlich, Sips, Toth model equations. Equation 2.1 also can be described by following form, and is called by the adsorption isoster:

$$P = f(T)_N \quad (2.3)$$




However, adsorption isoster can not be measured directly because it is impractical to hold N constant. Instead, the value of the adsorption isosteres can be interpolated from a group of the adsorption isotherms at various temperatures. Besides, the linearity of the isosteres has been employed as a useful criterion on the internal consistency of the experimental isotherms.

Adsorption isotherm gives information about the relationship between the gas amount adsorbed and pressure (or relative pressure) at constant temperature. The overall shape of an isotherm is governed by the nature of the gas-solid system, the pore structure of the adsorbent and the operational temperature. Adsorption isotherms are classified into microporous or mesoporous adsorbent and single or multilayer adsorption, according to IUPAC classifications (Table 2.1). IUPAC classifications are

used as general guidelines in studying the characteristics of gas adsorption on adsorbents.



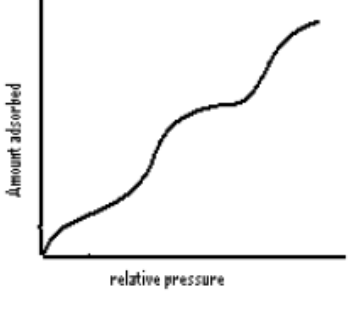
Table 2.1. The IUPAC classification for adsorption isotherms

(Source: Do, 1998).

<p>TYPE I</p> 	<p>Characteristics of microporous adsorbent having relatively small external surface area.</p> <p>The limiting uptake is governed by the accessible micropore volume rather than by internal surface area.</p>
<p>TYPE II</p> 	<p>Reversible non-porous or macroporous adsorbent.</p> <p>The linear section is often considered as a stage at which monolayer coverage is completed and multilayer adsorption increases progressively with increasing pressure.</p>
<p>TYPE III</p> 	<p>The isotherm indicates a weak adsorbate-adsorbent bonds but this type of isotherm is not common.</p>

(cont. on next page)

Table 2.1. (Cont.)

<p>TYPE IV</p> 	<p>A hysteresis loop which associated with capillary condensation that takes place in mesopores. The initial part of isotherm is attributed to monolayer-multilayer adsorption since it follows the same path as part of Type II isotherm.</p>
<p>TYPE III</p> 	<p>Type V isotherm is uncommon but also related to Type III where adsorbent-adsorbates interaction is weak.</p>
<p>TYPE IV</p> 	<p>The Type VI isotherm represents stepwise multilayer adsorption.</p>

An adsorption isotherm is a constant temperature equilibrium relationship between the quantity of adsorbate per unit of adsorbent and the equilibrium concentration of adsorbate. The adsorption models help to characterize the adsorbent for certain application. Adsorption equilibrium can be more described by adsorption isotherms. The parameters of these models indicate the extent of heterogeneity of the adsorbent being investigated. In this study, the interaction parameters of the zeolites and MOF adsorbents have been determined by using the models stated in this chapter.

Different model equations were applied to the adsorption data obtained from volumetric studies in order to get information regarding the heterogeneity of the adsorbent surfaces. The models applied to the data are Langmuir, Sips and Toth model equations. By making use of the data obtained from the heterogeneity parameters of the applied equations, interpretation of the results is made.

The simplest theoretical model for monolayer adsorption is due to the Langmuir model (Equation 2.4). The basic assumptions on which the model is based on are as follows;

The basic assumptions on which the model is based on are as follows;

- Molecules are adsorbed at a fixed number of well-defined localized sites.
- Each site can hold one adsorbate molecule.
- All sites are energetically equal.
- There is no interaction between molecules adsorbed on neighboring sites

$$q = \frac{q_m b P}{1 + b P} \quad (2.4)$$

Where q_m (mmol/g adsorbent) represents the monolayer adsorption capacity, P (kPa) is the gas pressure inside the pores in equilibrium with q_m and b (kPa⁻¹) is another adsorption equilibrium constant, related to the Henry constant by $K = b q_m$

Henry constant is in fact equilibrium constant and, shows the usual van Hoff temperature dependence. It measures the intrinsic affinity of the adsorbent for a specific adsorbate that can be used to provide quantitative comparisons of adsorption affinity. Parameter b , called as an affinity constant or Langmuir constant, is shows how strong an adsorbate molecule is attracted onto a surface. When the affinity constant b is large, the surface is covered more with adsorbate molecule as a result of the stronger affinity of adsorbate molecule towards the surface. Besides, increase in temperature decreases the amount physisorbed due to the greater energy acquired by the adsorbed molecule to desorp.

Tóth model is actually a modification of Langmuir model, which has the advantage of predicting the right adsorption limits when pressure approaches zero and infinite values, thus reducing deviation errors between experimental data and calculated values of adsorption equilibrium. This model is derived from the potential theory and assumes a quasi-gaussian energy distribution in which most of the adsorption sites have a smaller adsorption energy than the peak adsorption energy. Tóth equation has three adjustable parameters, and is a useful tool to describe adsorption equilibrium on heterogeneous systems and multilayer adsorption. 3-empirical extension of the Langmuir isotherm that leads to **Toth model equation**,

$$q = \frac{q_m b P}{(1 + (bP)^n)^{1/n}} \quad (2.5)$$

where n is Toth equation constant. Toth equation is reduced to the Langmuir equation for n= 1.

The Freundlich isotherm is first conceived as an empirical model, although it can be derived from the assumption that the surface is composed of “patches”, following an exponential decay energy distribution with a Langmuir-type isotherm behavior on each “patch”. However, the equation does not account for Henry’s law behavior at low surface coverage and for the saturation of the adsorbed phase. It is possible to interpret **Freundlich model equation** theoretically in terms of adsorption on an energetically heterogeneous surface.

$$q = kc^d \quad (2.6)$$

where k is a temperature-dependent constant, d is equation constant.

This equation often successfully correlates experimental data for low and intermediate values of amount adsorbed q as stated in literature (Do, 1998). However, this model gives no limit to adsorption capacity, making the amount adsorbed go to infinity when the concentration increases.

To overcome this limitation of Freundlich model, the **Sips model** isotherm which is a modified Freundlich equation that included the asymptotic saturation effect, can be used. Simply the Sips model in which describes the adsorption including

interactions between the adsorbate and adsorbent is generalization of both Langmuir and Freundlich models.

$$q = \frac{q_m b P^n}{1 + b P^n} \quad (2.7)$$

Sips and Freundlich equations are not obey Henry's law, not appropriate at low pressure. In general, the interpretation of experimental adsorption isotherms can be realized in terms of adsorption model equation. It is also important to note that a general theory of adsorption that includes all factors affecting a given process can lead to such a complicated model equation of isotherm. Therefore, the simplicity of a given theory can offer a great advantage in understanding adsorption phenomena of various adsorbate-adsorbent systems.

Physically, molecules prefer to adsorb onto sites of high energy and then as adsorption progresses molecules then adsorb onto sites of decreasing energy, resulting in a slower rise in the amount adsorbed versus pressure. The contribution of solid toward heterogeneity is the geometrical and energetical characteristics, such as the micropore size distribution and the functional group distribution (they both give rise to the overall energy distribution which characterizes the interaction between the solid and the adsorbate molecule). The contribution of the adsorbate molecule is its size, shape and conformation. All these factors will affect the system heterogeneity, which is macroscopically observed in the adsorption isotherm and dynamics. Therefore, by measuring adsorption equilibrium, isosteric heat, and dynamics, one could deduce some information about heterogeneity, which is usually characterized by a so called apparent energy distribution.

Heat of Adsorption

The heat evolved during adsorption, heat of adsorption can be determined by calculating the isosteric heats from adsorption isotherms, measured at two different temperatures. Heat of adsorption is related to the energy of bonds formed and thus represents a measure of the strength of the interaction (Yang, 1997).

It has been well known that the adsorption phenomena is accompanied by evolution of heat since adsorbate molecules are more stabilized on the adsorbent surface

than in the bulk phase. In addition, the amount of heat evolution by unit adsorption depends on the system adopted. Thus, information concerning the magnitude of the heat of adsorption and its variation with surface coverage can provide useful information concerning the nature of the surface and the adsorbed phase. The heat of adsorption at constant amount adsorbed N can be calculated from the slopes of the isosteres, using the Clausius-Clapeyron equation for adsorption:

$$\frac{q_{st}}{RT^2} = \left[\frac{\partial \ln P}{\partial T} \right]_N \quad (2.8)$$

The the isosteric heat of adsorption q_{st} is denoted as $-\Delta H$ at zero loading. If experimental isotherms are available at two different temperatures, the value of q_{st} is given by:

$$q_{st} = R \left[\frac{\ln P_1 - \ln P_2}{1/T_2 - 1/T_1} \right]_N \quad (2.9)$$

where P_1 and P_2 are the equilibrium pressures at temperatures T_1 and T_2 respectively, when the amount adsorbed N is constant. For useful description of adsorption equilibrium data at various temperatures, it is important to have the temperature dependence form of an isotherm equation. The temperature dependence of the Sips equation is given by equation 2.10.

$$q_{st} = Q - (\alpha RT_0)n^2 \ln\left(\frac{q_m}{q_m - q}\right) \quad (2.10)$$

The temperature dependence of the Toth equation is given by equation 2.11.

$$-\Delta H = Q - t(\alpha RT_0) \left[\ln\left(\frac{q}{q_m^t - q^n}\right)^{1/t} \right] - \frac{\ln(q_m)}{1 - (q/q_m)^t} \quad (2.11)$$

The parameters b and t are temperature dependent parameter of Toth model equation. Q (J/mol) and α values are calculated from equation 2.12 and 2.13,

respectively. Q (J/mol) value is a measure of the heat of adsorption and parameter α is calculated by using both model constants for different temperature values from equation 2.12 and 2.13. We have assumed that the temperature variation of q_m is negligible with this approach (Do, 1998).

$$b = b_0 \exp\left(\frac{Q}{R} \left(\frac{T_0}{T} - 1\right)\right) \quad (2.12)$$

$$\frac{1}{n} = \frac{1}{n_0} + \alpha \left(1 - \frac{T_0}{T}\right) \quad (2.13)$$

where b_0 , b and n , n_0 values are both model constants at different temperatures at T_0 and T respectively.

2.2. Gas Adsorption Kinetics

Pore diffusion has been widely studied in connection with its influence on the overall kinetics of gas adsorption. Four mechanisms of transport may be identified: molecular diffusion, Knudsen diffusion, transition diffusion and surface diffusion. The effective diffusivity is thus a complex quantity which often includes contributions from more than one mechanism. In the Knudsen diffusion regime, the molecules do not interact with one another, so that they move in straight lines between points on the pore channel surface. Molecular diffusion, often called simply diffusion, is the thermal motion of all gas particles at temperatures above absolute zero. The rate of this movement is a function of temperature, viscosity of the fluid and the size of the particles. In molecular diffusion the resistance to flow arises from collisions between diffusing molecules. Molecular diffusion will be the dominant transport mechanism when mean free path of the gas (average distance travelled between the molecular collisions) is small relative to the pore diameter. There must be a wide range of conditions under which both Knudsen and molecular diffusion are significant. In the transition regime both wall collisions and inter molecular collisions contribute to the resistance and effective diffusivity. There is in addition to possibility of direct

contributions to the flux from transport through the physically adsorbent layer on the surface of pore and this is referred to as surface diffusion.

A proper understanding of how a gas molecule adsorbs and diffuses in a porous adsorbent medium is crucial to the successful application of adsorption. However, the measurement of adsorption kinetics is also fundamental for modeling adsorption processes since the transport of mass into and out of the adsorbent can affect significantly the performance of industrial processes.

A variety of microscopic methods: pulsed field gradient Nuclear magnetic resonance (NMR), NMR relaxation, quasi elastic neutron scattering QENS and macroscopic methods: uptake rate measurement, frequency response, infrared spectroscopy and chromatographic methods, are used for the measurement of diffusivities in porous materials Bekkum et al., 2001; Karge and Weitkamp, 2008). NMR and QENS are the microscopic method and equilibrium measurements are made on a scale smaller than dimensions of an individual crystal by following the mean square displacement of the molecules in a known time interval. NMR technique is a non-invasive technique allows the observation of molecular transport in porous media without any disturbance of their intrinsic molecular dynamics. Pulsed-field gradient NMR (PFG NMR) is able to provide direct information about the rate of molecular migration in the intracrystalline space and follow molecular diffusion paths from 100 nm up to 100 μm (Rouquerol et al., 1999). Neutron spin-echo technique is also microscopic method and depends on measuring the rate of a catalytic reaction under diffusion-controlled conditions.

Single crystal membrane permeation, FTIR and the recently developed interference microscopy technique can be classified as mesoscopic methods and to be applied at the scale of the individual crystal.

Macroscopic methods measure the transport diffusion and depend on measuring the flux under a well defined gradient of concentration. If the small sample of adsorbent is subjected to change in ambient concentration (or partial pressure) of sorbate, it is the most obvious way to measure intracrystalline diffusion with direct measurement of the adsorption or desorption rate. If the diameter of the diffusing molecule is slightly smaller than the pore diameter, diffusion within an ideal micropore is fast and difficult to measure by macroscopic methods. Slow transport diffusion is easily measured macroscopically when the molecular diameter of the sorbate approaches the minimum diameter of the pore, the diffusional activation energy increases and the diffusivity

drops by orders of magnitude but it is inaccessible to microscopic techniques. Especially in batch measurements, transient uptake rate measurements are subject to intrusion of heat transfer limitations at low pressures.

Eic and Ruthven (Eic et al., 2002) developed a Zero Length Column (ZLC) chromatographical technique to overcome the effect of axial dispersion, the external mass transfer resistances and heat transfer on the diffusion, in the late 1980s. This technique directly measure transport diffusivities in porous adsorbent particles. Zero Length Column (ZLC) chromatographical technique involves a purge of a previously equilibrated sample to obtain a curve of fractional desorption versus time. The diffusion time constant can be obtained by matching the desorption dynamic curve to the theoretical solution of the diffusion equation. This method can eliminate the intrusion of axial dispersion, heat transfer and bed diffusion resistances by the use of large crystals, low adsorbate concentration and very small adsorbent sample amount as well as high carrier flow rate during desorption. It is a simple and inexpensive technique for obtaining the diffusion coefficient.

In this study, the diffusion of SMR-off gases in a MIL 53(Al) adsorbent has been investigated by the ZLC method. As you can see from Table 2.2. in literature there are limited kinetic study using ZLC method. Also, there are no kinetic studies have been reported about MOFs with SMR-off gases in literature. Krungleviciute et al.,(2008) have reported that in Cu-BTC the time to reach equilibrium was comparable for Ar and CF₄. They used these results to establish kinetic selectivity for the same two gases in another variety of MOF, RPM1-Co. Peralta et al., reported a kinetic studies for the separation of hydrocarbon in Cu-BTC (Peralta et al., 2009). Saha et al., studied metal-organic framework (MOF-177, MOF 5) for H₂ adsorption. The hydrogen adsorption equilibrium and kinetic data were measured (Saha et al., 2008).

Table 2.2. Studies with Zero Length Column (ZLC) technique in literature.

Studies	Adsorbent	Adsorbate	Gas analyzer	Reference
Sorption and Kinetics of CO ₂ and CH ₄ in binderless beads of 13X zeolite	13X zeolite	CO ₂	Mass spectrometer	Silva et al., 2001
Diffusion of linear paraffins in silicalite studied by the ZLC method in the presence of CO ₂	Silicalite	<i>n</i> -butane <i>n</i> -hexane <i>n</i> -octane <i>n</i> -decane and CO ₂	GC chromatograph	Guimarães et al., 2010
Evaluation of the main diffusion path in novel micro-mesoporous zeolitic materials with the zero length column method	UL-ZSM5 ZSM-5, ZSM-12 Al-Meso-100	<i>n</i> -heptane Toluene	GC chromatograph	Malekian et al., 2007
Diffusion of linear paraffins in NaCaA studied by the ZLC method	NaCaA	Linear Alkanes	GC chromatograph	Brandani and Gunadi, 2006
Measurement of adsorption equilibrium by the Zero Length Column (ZLC) Technique Part 1: Single Component system	CaA, NaLSX	CO ₂ , N ₂ CO, CH ₄ (pure / mixture)	Mass spectrometer	Brandani et al., 2003
Adsorption of propane and propylene onto carbon molecular sieve	Carbon molecular sieve CMS) 4A	Propane N35 propylene N24	GC chromatograph	Grande et al., 2003

(cont. on next page)

Table 2.2. (Cont.)

Improved estimation of zeolite diffusion coefficients from zero-length column experiments	Silicalite	Benzene Ethylbenzene	GC chromatograph	Loos et al., 2000
Analysis of ZLC desorption curves for liquid systems	NaX	Benzene Hexane	GC chromatograph	Ruthven and Brandani, 1995
Diffusion of light alkanes in silicalite studied by the zero length column method	Silicalite	n-butane Isobutane Propane	GC chromatograph	Huften and Ruthven, 1993

2.3. Zero Length Column (ZLC): Theory

In a zero length column, the assumptions used to obtain a mathematical expression for response curves are as follows:

- Adsorbents have spherical geometry.
- Gas behavior is ideal.
- The process is isothermal because of the small quantity of adsorbent.
- Perfect mixing throughout the ZLC cell, if the holdup in the fluid phase is neglected.
- Axial dispersion and mass transfer resistance can be neglected. Because instantaneous equilibration is assumed at the external surface of the adsorbent particles in the very small column (ZLC).
- The equilibrium relationship between adsorbed phase and fluid phase will be linear at sufficiently low concentrations. This linear relationship is commonly referred to as Henry's law (K).
- The self supported adsorbent has a porous structure containing micropores and the mass transfer control is limited by micropore diffusion, D_c , due to crystal structure.
- Micropore diffusion coefficient (or crystalline diffusivity), D_c , is constant and does not change with concentration.

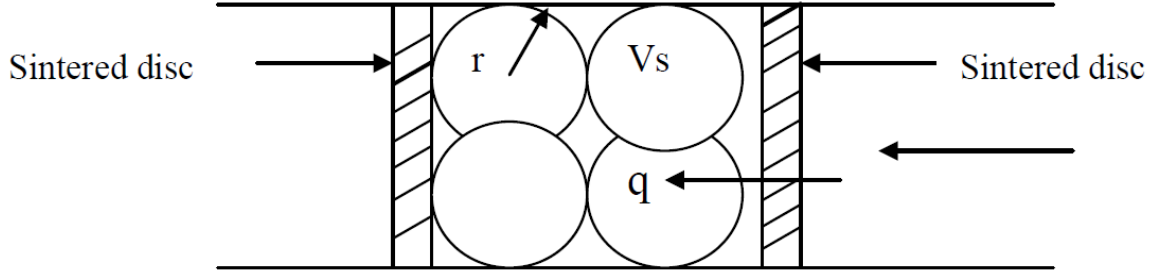


Figure 2.1. Representative Zero Length Column.

The mass balance around the adsorbent

$$\frac{\partial q}{\partial t} = D_c \left(\frac{\partial^2 q}{\partial r^2} + \frac{2}{r} \frac{\partial q}{\partial r} \right) \quad (2.14)$$

and into the fluid phase of the ZLC column

$$V_f \frac{dc}{dt} + V_s \frac{d\bar{q}}{dt} + F c = 0 \quad (2.15)$$

where \bar{q} is the overall amount adsorbed per unit particle volume, V_f (cm³) is the volume of fluid in column, V_s is the volume of solid phase, F is the purge volumetric flow rate, c is the gas-phase concentration of adsorbate, and t is time. Analytically solution of differential equations 2.14 and 2.15 with following the boundary and initial conditions

$$q(r, 0) = \bar{q}(0) = q_o = K C_o \quad C(0) = C_o \quad \left(\frac{\partial q}{\partial r} \right)_{r=0} = 0 \quad (2.16)$$

$$\bar{q}(t) = \frac{3}{r^3} \int_0^{r_c} q r^2 dr \quad (2.17)$$

Analytic solution equation for ZLC system (Crank 2003);

$$\frac{q_o - \bar{q}(t)}{q_o} = 1 - 6L^2 \sum_{n=1}^{\infty} \frac{\exp(-\beta_n^2 D_c t / r^2)}{\beta_n^2 [\beta_n^2 + L(L-1)]} \quad (2.18)$$

and

$$\beta_n \cot \beta_n + L - 1 = 0 \quad (2.19)$$

where L is the time constant ratio shows the relation between the flow rate and the controlling steps.

$$L = \frac{1 \text{ purge flow rate } r^2}{3 \text{ crystals volume } KD_c} = \frac{\left(\frac{r^2}{D_c}\right)}{\left(\frac{3KV_s}{F}\right)} \quad (2.20)$$

$$V_s = m_s / \rho_s = m_s / \rho(1 - \varepsilon_p) \quad (2.21)$$

where m_s is the sample mass, ρ is the pore wall density, ρ_s is the particle density, and ε_p is the particle porosity.

When the Equation 2.18 is differentiated and substituted into Equation 2.15 the gas phase concentration of adsorbate is expressed as;

$$\frac{C}{C_s} = 2L \sum_{n=1}^{\infty} \frac{\exp(-\beta_n^2 D_c t / r^2)}{\beta_n^2 + L(L-1)} \quad (2.22)$$

In ZLC technique, there are two alternatives for extracting the relevant parameters. One is the long-time (LT) asymptote of desorption curve (Eic et al., 2002) which is linear on a semilogarithmic plot. The other is the short time (ST) approximate method (Hufton et al., 1993) which fits the initial part of the response curve for obtaining the diffusion time constant. Both methods have their own disadvantage (Hufton et al., 1993) and may yield diffusivity values differing by as much as an order of magnitude. The reason is that both methods are simplified and have some deviations from experiment. Further, different time regions are chosen in fitting the desorption curve, and the nature of the errors is different in these regions. LT analysis uses only the data from the tail of desorption curve, which is the region of greatest experimental uncertainty. On the other hand, in ST analysis, the effect of any experimental error in initial time and dead-volume contribution is very significant. Moreover, when particle size is not uniform, larger deviation is caused if the same average diameter is used in the

two methods (Han et al., 1999). Some effort has been made to develop a full-time (FT) (Loos et al., 2000) method, in which diffusion parameters can be extracted by fitting the entire desorption curve, but they are not widely used because of their greater complexity.

For full time (FT) method, the experimental desorption curve was fitted to Eqs. (2.20-22) using a nonlinear least squares method to obtain the best fitting parameters D_c/R^2 and L . For the large values of t , only the first root of Equation 2.19 contributes to the summation part of the Equation 2.22, it reduces to;

$$\frac{C}{C_o} = \frac{2L}{\beta_1^2 + L(L-1)} \exp\left(-\frac{\beta_1^2 D_c t}{r^2}\right) \quad (2.23)$$

The micropore diffusion coefficient, D_c , and the dimensionless Henry constant, K , can be determined from the slope and intercept of a plot of $\ln(C/C_o)$ versus t . This procedure is referred to the LT method.

For small values of t , gas phase adsorbate concentration can be also expressed as in equation 2.24.

$$\frac{C}{C_o} = \left(\frac{r^2}{L^2 \pi D_c t}\right)^{1/2} - \frac{1}{L} \quad (2.24)$$

D and K are estimated from the slope and the intercept of a plot of C/C_o versus $t^{1/2}$ by the time analysis. This procedure is referred to as the ST method. Both LT, ST cases performed at high flow rates such that the effluent concentration is determined by the rate. This means that sorbate diffuses out of the adsorbent particles.

When the ZLC experiment is performed at a sufficiently low flow rate, then L is small and the desorption rate is controlled entirely by convection. In other words, the adsorbate phase is always in equilibrium with the gas phase as the following equation; (Brandani and Ruthven 2005).

$$\bar{q}(t) = KC(t) \quad (2.25)$$

When L is small, β is small and $\beta_n \cot \beta_n$ can be replaced by the first term of the Equation 2.25 and equal to approximately $L \approx \beta^2/3$. Then, the concentration response curve as the simple exponential form can be written as;

$$\frac{C}{C_0} = \exp\left(\frac{-Ft}{KV_s + V_f}\right) \quad (2.26)$$

The response curve is independent of the flow rate under equilibrium control. A plot of $\ln (c/c_0)$ vs. time should give a straight line through the origin with slope $-F/(KV_s + V_f)$. When K has a large value, KV_s value should be higher than V_f . The slope yields directly the value of the dimensionless Henry's Law constant (K).

The temperature dependence of the diffusivity is correlated by the Arrhenius form:

$$D = D_0 \exp(-E/RT) \quad (2.27)$$

E is the activation energy for surface diffusion can be obtained by

$$E = RgT^2\left(\frac{\partial \ln D}{\partial T}\right) \quad (2.28)$$

where D_0 ($m^2 s^{-1}$) is the pre-exponential factor of the diffusion process independent from the temperature, E_a ($J mol^{-1}$) is the activation energy for adsorbates in a given adsorbents, R ($J mol^{-1}K^{-1}$) is the gas constant, and T (K) is temperature. Further, the isosteric heat of adsorption at zero loading, q_{st} , is obtained from the Henrys law constant, K , following

$$q_{st} = R\left(\frac{\partial \ln K}{\partial (1/T)}\right) \quad (2.29)$$

2.4 Selectivity

Suitable adsorbent is the first step to provide efficiency of an adsorption separation process. Adsorbent with sufficiently high selectivity and capacity is required

for an economic separation process. The selectivity may depend on a difference either adsorption equilibrium or kinetics. However, most of the adsorption processes used depends on equilibrium selectivity. To consider the processes, separation factor can be defined as (Ruthven, 1984);

$$\alpha_{AB} = \frac{X_A / X_B}{Y_A / Y_B} \quad (2.30)$$

where X and Y are the mole fractions of component A or B in adsorbed and fluid phase at equilibrium, respectively.

Separation factor generally varies with temperature and composition. Therefore, suitable conditions must be selected to maximize the separation factor. However, separation factor is independent of composition and equal to the ratio of the Henry's law constants to relevant components for an ideal Langmuir system given in Equation 2.31. This approach works well for some systems such as CH₄-CO₂ in 5A and NaX zeolite and very quick and reliable method of estimating separation factors (Karge and Weitkamp, 2008; Ruthven, 1984).

$$\alpha_{AB} = \frac{q_A / p_A}{q_B / p_B} = \frac{K_A}{K_B} = \frac{(q_m b)_A}{(q_m b)_B} \quad (2.31)$$

where p_A and p_B are the sorbate pressure for A and B component, respectively. q_A and q_B are the adsorbed phase concentration for A and B component, respectively. The product (q_mb)_i corresponds to the initial slope of the isotherm, or Henry's constant (K), for component *i*. Hence, the adsorbent selectivity is equivalent to the ratio of the initial slopes of the isotherms of the two components, or K_A/K_B. It should be noted that the selectivity has resulted in a constant value simply because of the nature of the Langmuir isotherm.

The chromatographic methods have also the advantage to provide information on the adsorption kinetics. Kinetic separations are used especially with molecular sieve adsorbents. The kinetic selectivity is determined by the ratio of intracrystalline diffusivities for the components (Ruthven, 2011; Ruthven and Reyes, 2007) given in Equation 2.32.

$$S_{AB} = \frac{K_A}{K_B} \sqrt{\frac{D_A}{D_B}} \quad (2.32)$$

CHAPTER 3

ADSORBENTS

Aluminosilicate zeolites, activated carbon, activated clays are used generally for the separation of gas and vapor mixtures.

3.1. Zeolites

Zeolites comprise a three-dimensional crystal network of Si and Al atoms, which are present in the form of SiO_4 and $(\text{AlO}_4)^-$ tetrahedral. Tetrahedrons join together in shared oxygen atoms with various regular arrangements, to form hundreds of different three-dimensional crystal frameworks (Kaduk et al., 1995).

The three dimensional zeolite channels have 12 ring windows. The crystal structure of a zeolite consists of cages and supercages. The molecules to be adsorbed reach the cages and supercages by the windows. The cages are the smaller cells than the supercages which may even contain cages as seen in Figure 3.1 (Savitz et al., 1999).

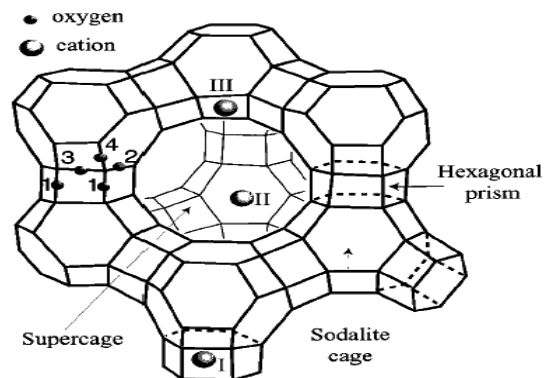


Figure 3.1. Faujasite structure showing cation sites (I, II, III) and locations of oxygen atoms

Zeolite has negative charges compensated by Na^+ ions. The pore size openings which can be tuned by exchange of the sodium ions against other mono-, di-, or trivalent cations allow the separation of gas mixtures for example; SMR off-gas separation, CO_2 capture from flue gas by a molecular sieve effect consisting in the

sorption uptake of smaller molecules and hindering of adsorption of larger molecules relate to the critical diameter of the pore opening (Buhl et al., 2004).

Aluminosilicate zeolites have pores of uniform size contrary to the other adsorbents. The NaX is a synthetic aluminosilicate zeolites composed of Si, Al, Na, and O atoms. Its chemical formula is $\text{Na}_{86}[(\text{AlO}_2)_{86}(\text{SiO}_2)_{106}].264\text{H}_2\text{O}$. Data related to structures of X zeolites are summarized in Table 3.1.

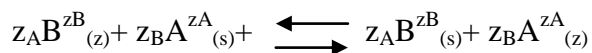
Table 3.1. Zeolite: X
(Source: Breck, 1974)

Chemical Composition	
Typical oxide formula	: $\text{Na}_2\text{O}.\text{Al}_2\text{O}_3.2.5\text{SiO}_2.6\text{H}_2\text{O}$
Typical unit cell contents	: $\text{Na}_{86}[(\text{AlO}_2)_{86}(\text{SiO}_2)_{106}].264\text{H}_2\text{O}$
Variations	: Si/Al=1 to 1.5 and Na/Al=0.7 to 1.1
Crystallographic Data	
Symmetry	: Cubic
Density	: 1.93g/cc
Unit cell volume	: 15,362-15,670 Å ³
Structural Properties	
Framework	: Truncated octahedra, β cages, linked tetrahedrally through D6R2s in arrangement.
Contains	eight cavities, ~13 Å in diameter in each cell
Void Volume	: 0.50 cc/cc
Framework density	: 1.31 g/cc
Channel system	: Three-dimensional
Hydrated free apertures	: 12-ring, 7.4 Å, and 6-ring, 2.2 Å
Dehydrated free apertures	: 7.4 Å
Largest molecule adsorbed	: $(\text{C}_4\text{H}_9)_3\text{N}$
Kinetic diameter	: 8.1Å

Adsorption properties of zeolite can be changed with modification such as cation exchange, impregnation. These techniques are used to introduce metal into zeolites. Impregnation in which pores are filled with a solution of metal salt of sufficient concentration to give correct loading is the simplest and most direct method. Ion

exchange is the reversible interchange of ions between a solid and a liquid. There is no permanent change in the structure of the solid, which is the ion exchange material. Usually, contacting a zeolite with a salt solution of different cation performs ion exchange; one type of cation is replaced with other.

The ion exchange process:



Where z_A and z_B are the charges of the exchange cation A and B and the subscript z and s refer to the zeolite and solution, respectively.

A widely recognized modification of adsorbent is to replace the Na^+ ions with other metal ions (e.g., Li^+ , K^+ , Mg^{2+} , Ca^{2+} , Ce^{3+}) and then reduce them in situ so that the metal atoms are deposited within the framework. The resultant material displays the properties associated with a supported metal catalyst. Ion exchanged cation can induce new catalytic features in many reactions especially in liquid phase reactions, by their different size and chemical structure (Sheldon et al., 1998).

The ultrasound increases Li^+ , Ca^{2+} and Ce^{3+} ion exchange rate in comparison with the undisturbed (Kaya et al., 2012) changes the size distribution and character of crystal (Nishida 2004). In literature, ultrasonic method as compared to the traditional exchange method was found to be very effective on the exchange amount at equilibrium (Kaya et al., 2012). Ultrasound acted like a co-driven force of concentration of counter ions in solution due to cavitation effect of ultrasound field and increased the equilibrated values in ion exchange process.

Literature review for ion exchange performed generally with traditional method was given in Table 3.2. Even the adsorption of CO_2 in conventional ion-exchanged X zeolites has been studied previously (Walten et al., 1998). There has not been an investigation of ultrasound effect in the preparation of K exchanged NaX zeolite and its effect on CO_2 adsorption. Among the adsorbents zeolites are most commonly used adsorbents for CO_2 adsorption at 1 atm. Acidic CO_2 molecule can adsorb on the basic surfaces. Barthomeuf suggested that the base strength of zeolites increased along with an increase of the aluminum content because of the lower electronegativity of aluminum compared to that of silicon. (Barthomeuf, 2003). The presence of aluminum atoms in zeolites introduces negative framework charges that are compensated with exchangeable cations such (extraframeworkcations).The modification of zeolites via the

introduction of large and electropositive, polyvalent cations enhance the adsorption of acidic CO₂. Walten et al showed that the CO₂ adsorption of the X zeolites increased as the cation ionic radii decreased: in the order Cs⁺ < Rb⁺ < K⁺ < Na⁺ < Li⁺ (Walton et al., 2006).

Table 3.2. Selected Studies for ion exchange in NaX zeolite

Studies	Counter ions (the amount exchanged %)	Ion exchanger/ Adsorbent	Reference
Water softening by combination of ultrasound and ion exchange	Ca ²⁺ , Mg ²⁺	Co-polymer of styrene and divinylbenzene	Entezari and Tahmasbi, 2009
Kinetics of alkylation of phenol with methanol over Ce-exchanged NaX zeolite	Ce ³⁺ (1.74-10.43)	NaX	Barman et al., 2006
CO ₂ adsorption in Y and X zeolites modified by alkali metal cation exchange	Li ⁺ (76), K ⁺ (88.7) Rb ⁺ (75.4) Cs ⁺ (55)	NaY, NaX	Walton et al., 2006
Cerium uptake by zeolite A synthesized from natural clinoptilolite tuffs	Ce ³⁺	Zeolite A	Faghihian et al., 2005
Li-X type zeolite mediated Michael addition of thiols to cyclic enones and its application in the synthesis of 13-thiaprostaglandins	Cs ⁺ (52) K ⁺ (88) Li ⁺ (75)	NaX	Shinde et al., 2004
Hydrothermal stability of the novel zeolite type LSX in comparison to the traditional 13X modification	Li ⁺ (74) Na ⁺ (100) K ⁺ (85) Ca ²⁺ (98) Ba ²⁺ (93)	LSX, 13X	Buhl et al., 2003
Li ⁺ - and H ⁺ - exchanged low silica X zeolite as selective nitrogen adsorbent for air separation	Li ⁺ , H ⁺	LSX	Kim, 2003
Thermodynamics of nitrogen and oxygen sorption on zeolites LiLSX and CaA	Li ⁺ , Ca ²⁺	NaLSX, A zeolite	Shen et al., 2001

3.2. Metal Organic Frameworks (MOFs)

Metal organic frameworks, MOFs known as coordination polymers (Uemura, et al., 2006, Kitagawa et al., 2006), hybrid organic-inorganic materials (Forster et al., 2002) and organic zeolites (2) are composed of metals (as nodes) and ligands (as linkers) which form extended networks via coordinated bonds (Figure 3.2). Each has its own focusing point. The use of “coordination polymer” emphasizes the nature of bonding. On the other hand, “metal organic framework” emphasizes the composition.

The one-dimensional (1D), two-dimensional (2D) or three-dimensional (3D) metal organic framework structures built by linking linear or nonlinear organic linkers and metal clusters often lead to open voids that can hold molecules so called “guest molecules” (Figure 3.2).

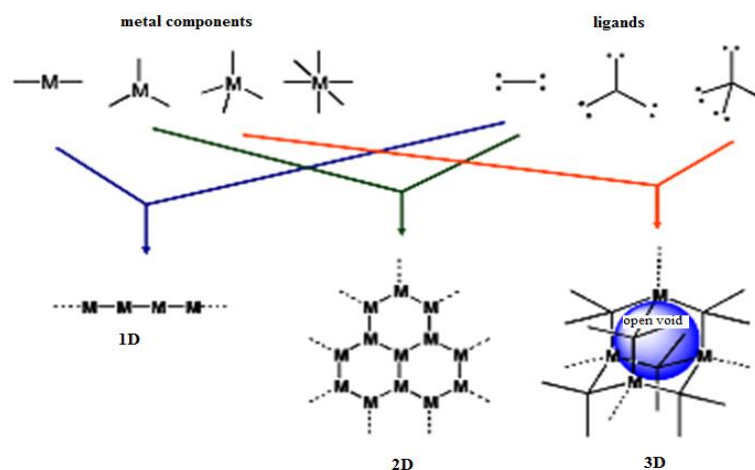


Figure 3.2. Metal components and ligands to create 1D, 2D or 3D MOF's

(Source: Schröder, 2010)

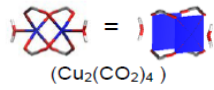
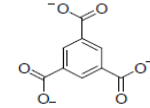
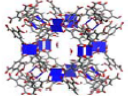
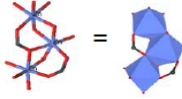
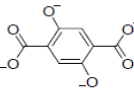
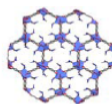
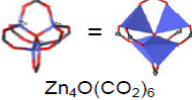
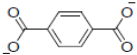
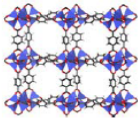
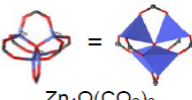
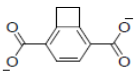
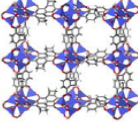
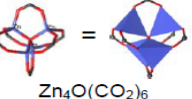
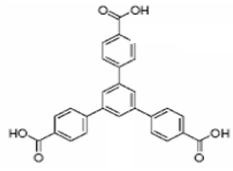
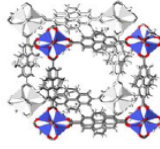
Choice of metal components and bridging ligands, specific framework topologies are very important, while functionalisation and modification of the ligand and metal centers can fine-tune the electronic and chemical nature of the resultant framework surface. By appropriate design of metal nodes, ligand bridges, solvent, synthetic conditions and templates, MOF materials showing porosity and open structures can be prepared. In literature the ultimate goal is to gain full control and understanding over the framework structure and synthesis at a predictive level. Such design and control remains difficult to achieve in practice (Yaghi et al., 1998) but series of analogous materials have been successfully synthesized to afford systematic

variations of pore size, shape and functional groups at the pore surface as you can see in below Table 3.4 and Table 3.5.

The most important characteristics for nodes and linkers are their connection numbers and their overall geometries. Figure 3.2 illustrates some of the basic motifs generated by combinations of different metal nodes and organic linkers. For example, Cu (I) ions are known to connect in a tetrahedral stereochemistry to four 4, 4'-bipyridyl ligands, and the resulting cationic frameworks $\{[\text{Cu} (4, 4'\text{-bipyridyl})_2]^+\}$ have an overall polymeric diamonded structure. By manipulation of metal stereochemistry and the angular nature of the ligand linkers, highly complex topologies can be generated.

Most of the porous MOFs are built upon metal clusters, so called secondary building units (SBUs). The SBUs serve as “nodes” and coordinate to organic linkers to form frameworks. Some examples MOF structure with their inorganic SBUs and organic linkers drawn in Table 3.3. It is a metal cluster connected by organic linkers. Because of the large size of SBUs, the resultant structures of MOFs are usually porous and could have relatively large pores (Chui et al., 1999, Yang et al., 2002). Pore size can also be modified by introducing different length organic linkers.

Table 3.3. Examples of MOFs structure
(Source: Adam et al., 2008)

Inorganic SBU	Organic Linker	MOF structure ^a
 (Cu ₂ (CO ₂) ₄)		 HKUST-1 CuBTC
 Zn ₃ [(O) ₃ (CO ₂) ₃]		 MOF-74
 Zn ₄ O(CO ₂) ₆		 IRMOF-1 MOF 5
 Zn ₄ O(CO ₂) ₆		 IRMOF-6
 Zn ₄ O(CO ₂) ₆		 IRMOF-10 MOF 177

Most porous MOFs are microporous and their pore diameters less than 2 nm. The most advantageous features of these materials are: well-characterized pores, small pore diameter, high micropore volume, and high surface area. Their pore structure can often be modified not only to adjust pore size and/or shape but also to enhance sorbate-sorbent interactions (Fletcher et al., 2005). These microporous MOFs show low thermal stabilities (decomposition occurs at $T > 300^{\circ}\text{C}$). Longer and linear ligands give rise to frameworks with less stability (Müller et al., 2006). They have also low hydrolytic stability. Decomposition of the framework occurs rapidly if the gas or liquid phase contains a few percents of H_2O which imposes severe limitations on their usage in catalytic oxygenation reactions, where water constitutes a major reaction product (Suh et al., 2008).

MOFs can be categorized into rigid and flexible/dynamic classes. Some examples rigid and flexible MOFs with their inorganic and organic units are given in Table 3.3 respectively. Rigid MOFs have comparatively stable and robust porous frameworks with permanent porosity, similar to zeolites and other inorganic porous materials, whereas flexible MOFs possess dynamic, “soft” frameworks that respond to external stimuli, such as pressure, temperature, and guest molecules (Suh et al., 2008).

For MOFs, the entire framework is supported by coordination bonds and/or other weak cooperative interactions such as H-bonding, $\pi-\pi$ stacking, and van der Waals interaction (Figure 3.3). The flexibility is thus expected even under mild conditions (Suh et al., 2008).

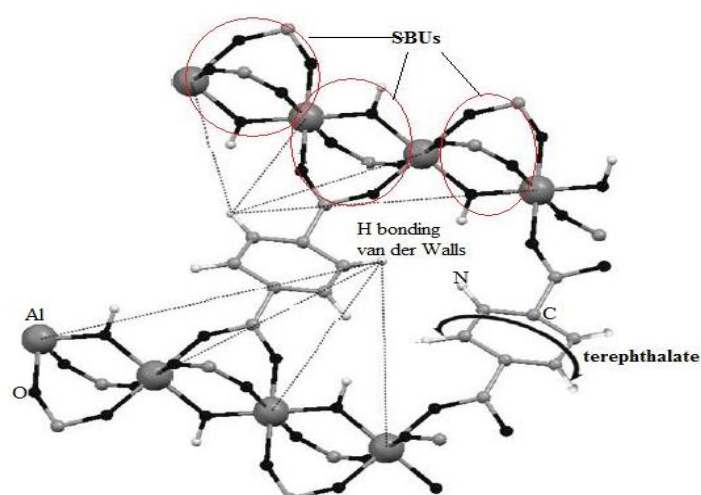


Figure 3.3. View of MIL 53 structure with (SBU's, coordination bonds, linker)

The most common flexible MOF, MIL (Material Institute Lavoisier)-53 (Al) (Table 3.4) built up from chains of octahedra sharing-OH vertices linked by terephthalate moieties is superior adsorbent for CO₂ adsorption as shown in Figure 3.4. This behavior corresponds to two consecutive reversible structural transitions from a large-pore (LP) to a narrow-pore (NP) form at very low CO₂ loading, and from the NP to the LP form at higher CO₂ concentration. This structural switching (Figure 3.4) implies a 38% change in unit-cell volume, from 1072 Å³ (NP) to 1486 Å³ (LP). Furthermore, both of these transitions are accompanied by a mixed-phase (NP/LP) domain whose composition varies with CO₂ pressure to give the pure NP or LP form (Sales et al., 2009). The MIL-53 framework is made of parallel one-dimensional M(OH) chains (M = Al, Cr), linked together by 1,4- benzene dicarboxylate (BDC) ligands to form linear diamond shaped channels that are wide enough to accommodate small guest molecules.

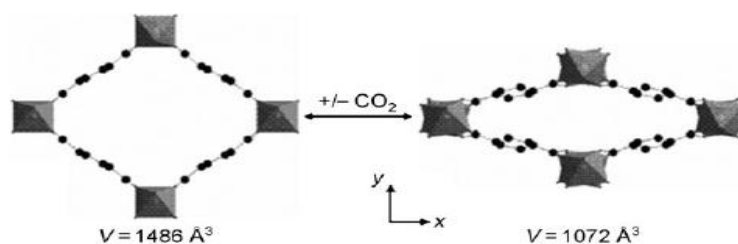
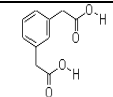
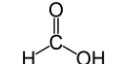
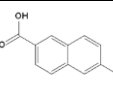
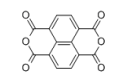
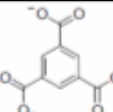
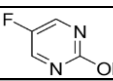
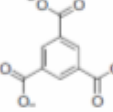
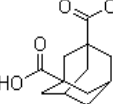


Figure 3.4. Structural switching of the MIL 53 system on CO₂ adsorption (Source: Sales et al., 2009).

Table 3.4: Some examples of rigid MOFs

Rigid MOF's ^(a)	pore size (Å)	pore volume (cm ³ /g)	Inorganic part	Organic part		References
				name	structure	
<i>Er</i> ₂ (<i>pda</i>) ₃	3,4	0,005	Er(NO ₃) ₃	1,4-phenylendiactic acid		Pan et al., 2003
<i>Mn</i> (<i>HCOO</i>) ₂	4,5	0,19-0,22	MnCl ₂	Formic acid		Dybtsev et al., 2004
<i>Mn</i> (<i>ndc</i>)	4	0,4	Mn(NO ₃) ₂ ·H ₂ O	2,6-naphthalene dicarboxylic acid		Moon et al., 2006
<i>Cr</i> ₃ O(<i>H</i> ₂ O) ₂ <i>F</i> (<i>ntc</i>) _{1,5} (<i>MIL-100</i>)	4,4	0,2	Cr(NO ₃) ₃ ·9H ₂ O	naphthalene-1,4,5,8-tetracarboxylic acid		Surble et al., 2006
<i>Al</i> ₂ O(<i>OH</i>) ₁₈ (<i>H</i> ₂ O) ₃ (<i>Al</i> ₂ (<i>OH</i>) ₄₉ (<i>btc</i>) ₆) (<i>MIL-96</i>)	2,5-3,5	0,32	Al(NO ₃) ₃ ·9H ₂ O:	1,3,5-benzenetricarboxylic acid		Loiseau et al., 2006
<i>Cu</i> (<i>F-pymo</i>) ₂	2,9	0,06	Cu(NO ₃) ₂ ·3H ₂ O	5-fluoro-2 hydroxypyrimidine		Navarro et al., 2008
<i>CuBTC</i>	10.8-11.8	1.96	CuNO ₃ ·2.5H ₂ O	Trimesic acid		Yazaydin et al., 2009
<i>Zn</i> ₄ (<i>OH</i> ₂ O) ₃ (<i>adc</i>) ₃ -(<i>PCN-13</i>)	3,5	0,3	Zn(NO ₃) ₂ ·6H ₂ O	1,3-adamantanedicarboxylic acid		Ma et al., 2007

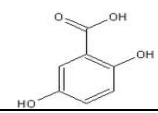
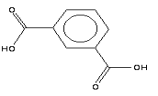
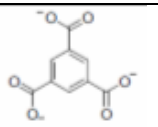
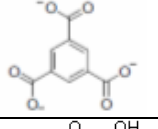
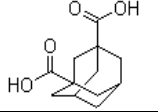
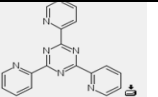
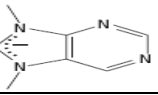

(cont. on next page)

Table 3.4. (Cont.)

$Zn(cbIM)_2(\mathbf{ZIF-95})$	3,65	0,59	$Zn(NO_3)_2 \cdot 4H_2O$	$(C_7H_5N_2Cl)$ 5-chlorobenzimidazole	cbim	Wang et al., 2008
$Zn_2(cnc)_2(dpt)$	3,7	0,27	$Zn(NO_3)_2 \cdot 4H_2O$	4-Carboxycinnamic acid		Xue et al., 2008
$Zn_3(OH)(p-cdc)_{2,5}$	3	0,6	$Zn(NO_3)_2 \cdot 4H_2O$	1,12-dihydroxy-dicarbonyl- 1,12-dicarba-closododecaborane		Bae et al., 2008
$Zn_4O(bt b)_2(\mathbf{MOF 177})$	7.1-7.6	1,31	$Zn(NO_3)_2 \cdot 4H_2O$	1,3,5-Tris(4- carboxyphenyl)benzene		Li et al., 2007
$Zn(ndc)_2(dpni)$	4-5	-	$Zn(NO_3)_2 \cdot 4H_2O$	2,6-naphthalenedicarboxylate		Bae et al., 2008
$Sm_4CO_3(pyta)_6(H_2O)$	3,5	0,08	$Co(NO_3)_2 \cdot 6H_2O$	2,4,6-pyridinetricarboxylic acid		Li et al., 2008
$Mg_3(ndc)_3$	3,46-3,64	0,62	$Mg(NO_3)_2 \cdot 6H_2O$	2,6-naphthalenedicarboxylic acid		Dinca et al., 2005
$Cd_3(OH)_2(L)_4(H_2O)_2$	5,4	0,12	$Cd(NO_3)_2 \cdot 4H_2O$	4-aminophenyl-1H-tetrazole		Zou et al., 2007
$Yb_4(m_4-H_2O)(tatb)_{(8/3)}(SO_4)_2$ (PCN-17)	3,5	0,37	Yb(NO₃)₃	4,4',4''-s-triazine-2,4,6- trilytribenzoate		Ma et al., 2008

^(a) Abbreviations: **pda** = 1,4-phenylendiacetate, **ndc** = 2,6-naphthalenedicarboxylate, **ntc** = naphthalene-1,4,5,8-tetracarboxylate, **btc** = 1,3,5-benzenetricarboxylate, **adc** = 9,10-anthracenedicarboxylate, **apt** = 4-aminophenyltetrazolate, **pyta** = 2,4,6-pyridinetricarboxylate, **btb** = 1,3,5-benzenetribenzoate, **F-pymo** = 5-fluoropyrimidin-2-olate, **nim** = 2-nitroimidazole, **cbim** = 5-chlorobenzimidazole, **cnc** = 4-carboxycinnamic, **dpt** = 3,6-di-4-pyridyl-1,2,4,5-tetrazine, **tatb** = 4,4'-S-triazine-2,4,6-trilytribenzoate; **p-cdc** = 1,12-dicarba-closo-dodecaborane-1,12-dicarboxylate, **DMF** = dimethylformamide, **dpni** = N,N'-di-(4-pyridyl)-1,4,5,8-naphthalene tetracarboxydiimide

Table 3.5. Some examples of flexible MOFs

Flexible MOF's ^(a)	pore size (Å)	Inorganic part	Organic part		References
			name	structure	
$Cu(dhbc)_2(4,4'-bipy)$	3.3	$Cu(NO_3)_2 \cdot 3H_2O$	2,5-dihydroxybenzoic acid		Kiteura et al., 2003
$Cu(bdc)_2(4,4'-bipy)_{0.5}$	4.2	$Cu(NO_3)_2 \cdot 3H_2O$	1,3-benzenedicarboxylic acid		Kiteura et al., 2003
$Al(OH)(bdc)$ (MIL-53)	8.5	$Al(NO_3)_3 \cdot 9H_2O$	1,3,5-benzenetricarboxylic acid		Bourrelly et al., 2005
$Cr(OH)(bdc) \cdot H_2O$ (MIL-53)	8.5	$Cr(NO_3)_3 \cdot 9H_2O$	1,3,5-benzenetricarboxylic acid		Llewellyn et al., 2006
$Zn(adc)(4,4'-bpe)_{0.5}$	3.4	$Zn(NO_3)_2 \cdot 4H_2O$	9,10-Anthracenedicarboxylic acid		Chen et al., 2007
$H_2Ni_3O(H_2O)_3(tatb)_2H_2O$ -(PCN-5)	5.7	$Ni(NO_3)_2 \cdot 6H_2O$	4,4',4''-s-triazine-2,4,6-triyl-tribenzoic acid		Ma et al., 2007
$Zn(Pur)_2$ (ZIF-20)	2.8	$Zn(NO_3)_2 \cdot 4H_2O$	Purinate		Hayashi et al., 2007
$Cu(fma)(4,4'-bpe)_{0.5}$	3.6	$Cu(NO_3)_2 \cdot 3H_2O$	fumaric acid		Chen et al., 2007

^(a) Abbreviations: **dhbc** = 2,5-dihydroxybenzoate, **bpee** = 4,4'-(E)-ethene-1,2-diyl-dipyridine, **Pur** = purinate, **bdc** = 1,4-benzenedicarboxylate, **tatb** = 4,4',4''-S-triazine-2,4,6-triyltribenzoate **bipy**= bipyridine, **fma**=fumarate

3.2.1. Synthesis of MOFs

Synthesis procedure of MOF (Figure 3.5) involves four main steps: crystallization, purification, activation and post synthesis treatments (Meek et al., 2010). The synthesis is very sensitive to the conditions such as starting metallic salt, solvents and especially the temperature has a high impact and can lead to different structures (Farha et al., 2010). MOF crystals are produced almost exclusively by hydrothermal/solvothermal, vapor diffusion, microwave and sol gel techniques (Meek et al., 2010). Microwave synthesis can reduce the crystallization time considerably (Kuppler et al., 2009). The crystals are slowly grown from a hot solution of metal precursor and bridging ligands. At low temperatures, the crystal growth can be controlled by vapor diffusion. For synthesis at temperatures above 100 °C, solvothermal synthesis is used. Solvothermal synthesis involves the use of a solvent (organic or inorganic) at elevated temperatures and pressures in a closed system, often in the vicinity of its critical point (Sheldrick et al., 1997, Rabenau et al., 1985). The most commonly used solvent is water but other solvents such as alcohol, dialkyl formamides and pyridine are also used. When water is used as a solvent, the reactions are referred as hydrothermal.

Selection of the solvent is very important, because some metal sources and organic linkers have very low solubility or are even insoluble. In order to increase the solubility, two or three solvents can be mixed or another solvent may be added to increase solubility.

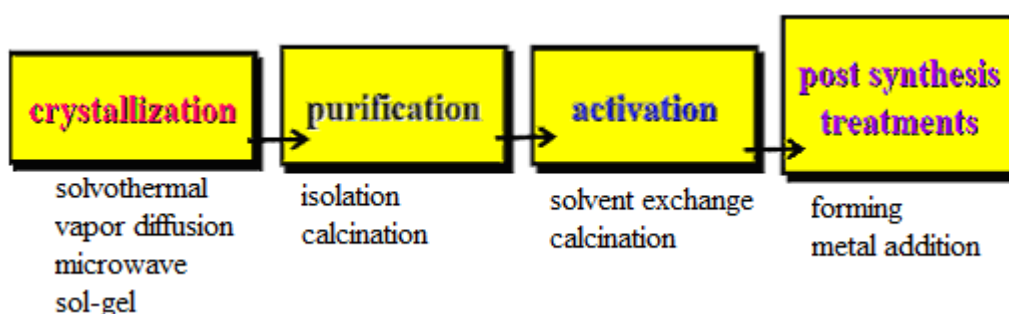


Figure 3.5. Schematic representation of synthesis MOFs

Metal–organic framework materials (MOFs) are inherently insoluble. This renders impossible the **purification** of MOFs via the conventional methods such as distillation, recrystallization, chromatography, sublimation, etc. Purification consists of isolation or calcinations to remove starting materials. Purification of MOF materials relies upon differences in density between desired and undesired products, filtration and calcinations. In a solvent with appropriate density, one phase of the MOF product mixture floats while the others sink. This method is both straight forward and broadly applicable (Meek et al., 2010).

For most applications, it is necessary to remove guest solvent molecules from the pores of the MOF without the loss of porosity, a process termed “**activation**”. The removal of the guest molecules (solvent or water from synthesis) without damaging the structural integrity of the material is often an additional challenge in activation. Traditional activation entails methods for heating the MOF material under vacuum. Unfortunately, in many instances this leads to partial or even full loss of porosity. Eddaoudi and co-workers were the first to address this problem (Eddaoudi et al., 2002). They showed that by exchanging the MOF-incorporated solvent remaining from synthesis for a lower boiling point solvent and then removing the solvent under relatively mild conditions, MOF porosity could often be retained.

Post-synthetic treatments of MOFs open up another dimension of structural possibilities that might not be achieved by conventional synthesis. A great deal of recent work explores covalent modification of the bridging ligands by forming graphite and polymer and metal addition.

3.2.2 Application of MOFs

MOFs possess a wide array of potential applications (Kitagawa et al., 2004). They are summarized as follows:

- Adsorption
- Catalysis, Luminescence
- Drug Delivery
- Optic
- Magnetic
- Catalysis

- Ion Exchange
- Sensing
- Polymerization

The use of MOFs as solid catalysts is particularly interesting because the pore size and functionality of the framework can be adjusted over a wide range for a variety of catalytic reactions. It is still an enormous challenge to find out whether the metal centers, the ligands or functionalized ligands, or even metal–ligand interactions or differences in particle size, can cause unusual catalytic properties. Advantages of MOFs as catalyst are seen in the easy separation of a heterogeneous catalyst, the tailoring of the pore size to yield selectivity, and/or shape and size selectivity by creating an appropriate environment around the catalytic center in the restricted space available (Kupler et.al., 2009).

MOFs can work as catalysts through;

- (i) coordinatively unsaturated nodes (metal centers),
- (ii) ligands functionalized with organic groups (organocatalysis),
- (iii) metal-complexes (as in homogeneous catalysis) which are incorporated into the linking ligand (e.g. as metalloligands) or the pores.

MOFs that have magnetic or luminescence properties together with size- or shape-selective sorption can be potentially applied in sensor devices. For the sensing properties of MOFs a direct contact with an electrically conducting material would be desirable. Luminescent networks can be prepared by utilizing luminescent organic building blocks and/or luminescent metal building blocks, or by utilizing the ligand-to-metal charge transfer (Zacher et al., 2008).

MOFs present as optimal drug-delivery materials due to the adjustability of the framework's functional groups and the tunable pore size. With MOFs, the benefits of using organic materials (biocompatibility and the ability to uptake large amounts of drugs) and inorganic materials (controlled release) may both be utilized (Horcajada et.al.2006).

Gas separation by adsorption is the most domain application for porous MOFs. Compared to zeolites and activated carbon materials, porous MOFs exhibit exceptionally high surface areas and large pore volumes so they are become a new adsorbent for gas separation applications. The development of a new adsorbent in industry for gas separation by adsorption normally goes through multiple steps. These

steps are materials design and preparation, selective gas adsorption studies, materials evaluation, adsorbents preparation scale-up, and separation process design and optimization. Currently, the investigation of MOFs as adsorbents in gas separation is in its early stage. Most of the research is focused on selective gas adsorption studies based on adsorption/desorption isotherm measurements of single gas components, which provide the predominant information for adsorbent screening. Nanospaces of MOFs are ideal to adsorb various strategic gases like H₂ (Müller et al., 2006), CH₄ (Düren et al., 2007), CO₂ (Babarao et al., 2008). The adsorption performance of MOFs depends on the crystallization and activation steps in synthesis (Chowdhury et al., 2009).

In this thesis we used MOF (MIL 53(Al)) for the separation of hydrogen from steam methane reformer off gas.

CHAPTER 4

GAS ADSORPTION PROPERTIES OF MOFs

Adsorptive separation process needed porous solid materials. Zeolites, activated carbons, and silica gels are traditional adsorbents. With an increasing need for a more efficient, energy-saving procedure for gas separation and environmentally benign adsorbents with tailored structures and tunable surface properties must be found. Metal–organic frameworks (MOFs) are promising candidates as adsorbents for gas separations due to their large surface areas, adjustable pore sizes and controllable properties, as well as acceptable thermal stability. A survey of selective gas adsorption in rigid, flexible MOFs has been given in Table 4.2 and 4.3 respectively.

The selective adsorption of H₂ but not N₂ due to size exclusion was also observed in Mg₃(ndc)₃ (Dinca et al., 2005), Cu(F-pymo)₂ (Navarro et al., 2008) at 77 K as shown in Table 4.1. PCN-17 (Ma et al., 2008) led to selective adsorption of H₂ over N₂ and CO. This material may thus have applications for the separation of N₂ and the separation of H₂ from CO in fuel-cell applications, as well as the H₂ enrichment of the N₂/H₂ exhaust.

MIL-96 (Loiseau et al., 2006) and Zn₂(cnc)₂(dpt) (Xue et al., 2008) were also found to selectively adsorb CO₂ over CH₄ based on size/shape exclusion. These materials may be useful in the separation of CO₂ and CH₄, which is an essential industrial process for natural-gas purification and landfill-gas separation. Adsorbates used in this study are CO, CO₂, CH₄ and H₂ and their properties are given in Table 4.1. Gas kinetic diameters obtained from the mean free path are given below.

Table 4.1: Properties of adsorptive used in this study

Properties	Adsorptives			
	CO ₂	CO	CH ₄	H ₂
Normal B.P(K)	216.55	81.66	11.66	20.27
Tc(K)	304.12	132.85	190.56	32.98
Vc(cm ³ mol ⁻¹)	94.07	93.10	98.6	64.20
Pc(bar)	73.74	34.94	45.99	12.93
kinetic diameter (Å)	3.3	3.690	3.758	2.89
Polarizabilityx10 ²⁵ /cm ³	29.11	19.5	25.93	8.042
Dipole momentx10 ¹⁸ /esu.cm	0	0.10	0	0
Quadruple momentx10 ²⁶ /esu.cm ²	4.3	2.5	0	0.662

Several MOFs (Mn(HCOO)₂, MIL-100, MIL-96, ZIF-95, Zn₂(cnc)₂(dpt), Mn(ndc)) can selectively adsorb CO₂ over CH₄ because CO₂ has a large quadrupole moment whereas CH₄ has none (a seen in Table 4.3). The adsorption isotherms of this MOF indicated that CO₂ was more preferentially adsorbed than CH₄.

Table 4.2. Gas adsorption properties of some rigid MOFs

Rigid MOF's ^(a)	Uptake(mmol/g), (T(K), P(atm))					References
	CO ₂	CH ₄	CO	H ₂	N ₂	
<i>Er</i> ₂ (<i>pda</i>) ₃	0.5(273,1)				None(273,1)	Pan et al., (2003)
<i>Mn</i> (<i>HCOO</i>) ₂	4.65(195,1)	None(195,1)		4.5(78,1)	None(78,1)	Dybtsev et al., (2004)
3(<i>ndc</i>) ₃				2.3(77,1)	None(77,1)	<i>Dinca et al., (2005)</i>
<i>MIL-100</i>	3.4(304, 30)	1,4 (304, 30)			1 (304, 30)	Surble et al., (2006)
<i>MIL-96</i>	3.7(303, 3.5)	0.8 (303, 3.5)				Loiseau et al., (2006)
<i>PCN-13</i>			5.1(77, 1)	2.07(77, 1)	3.2(77, 1)	Ma et al., (2007)
<i>Cd</i> ₃ (<i>OH</i>) ₂ (<i>apt</i>) ₄ (<i>H</i> ₂ <i>O</i>) ₂	3.1(195, 1)			3(195, 1)	None(77,1)	Zou et al., (2007)
<i>Sm</i> ₄ <i>CO</i> ₃ (<i>pyta</i>) ₆ (<i>H</i> ₂ <i>O</i>)	0.9(77, 1), 2(195, 1)					Li et al., (2008)
<i>Cu</i> (<i>F-pymo</i>) ₂				3.5(77,1)	None(77,1)	Navarro et al., (2008)
<i>ZIF-68</i>	1.48(273,1)		0.14(273, 1)			Banerjee et al., (2008)
<i>ZIF-95</i>	0.87 (298,1.2)	0,27(298, 1,2)	0,2(298, 1,2)		0,08 (298, 1)	Wang et al., (2008)
<i>Zn</i> ₂ (<i>cnc</i>) ₂ (<i>dpt</i>)	6.65(195, 1)	3.25(195, 1)				Xue et al., (2008)
<i>Mn</i> (<i>ndc</i>)	1,5 (273, 1), 3 (195, 1)	0,8 (273,1), 1,7(195, 1)				Moon et al., (2006)
<i>PCN-17</i>			0.88(77, 1)	4.5(77, 1)	0.89(77, 1)	Ma et al., (2008)
<i>Zn</i> ₃ (<i>OH</i>)(<i>p-cdc</i>) _{2,5}	0,58 (298,0,5)	0,07 (298, 0,5)				Bae et al., (2008)
<i>Zn</i> ₃ (<i>OH</i>)(<i>p-cdc</i>) _{2,5} <i>DMC</i>	0,27(298, 0,5)	0,068(298, 0,5)				Bae et al., (2008)
<i>MOF 177</i>				0.1(298,1)		Li et al., (2007)
<i>CuBTC</i>	6-10(298,5)			None(298,5)		Yazaydin et al.,(2009)
<i>Zn</i> (<i>ndc</i>) ₂ (<i>dpni</i>)	4.3(296, 17.5)	2.5(296,17.5)				Bae et al., (2008)

^(a)Abbreviations: **pda** = 1,4-phenylendiacetate, **ndc** = 2,6-naphthalenedicarboxylate, **ntc** =naphthalene-1,4,5,8-tetracarboxylate, **btc** =1,3,5-benzenetricarboxylate, **adc** = 9,10-anthracenedicarboxylate, **apt**=4-aminophenyltetrazolate, **pyta** = 2,4,6-pyridinetricarboxylate, **btb**=1,3,5-benzenetribenzoate, **F-pymo** = 5-fluoropyrimidin-2-olate, **cbim** = 5-chlorobenzimidazolate, **cnc** =4-carboxycinnamic, **dpt** = 3,6-di-4-pyridyl-1,2,4,5-tetrazine, **dpni** = N,N₀-di-(4-pyridyl)-1,4,5,8-naphthalene tetracarboxydiimide

Mn(ndc) is a 3D microporous MOF with 1D channels in which there exist coordinatively unsaturated Mn^{II} sites (Moon et al., 2006). The adsorption measurements showed that this MOF has much higher adsorption capabilities for CO_2 than for CH_4 at ambient temperatures. These results have shown that open metal sites in a MOF can aid in the separation of (quadru) polar/ non-polar gas pairs such as CO_2/CH_4 . Thus, this MOF-based material may have a potential application in PSA units for CO_2/CH_4 separation

It is also of interest that recently developed zeolitic imidizolate frameworks (ZIFs) have shown high CO_2 storage ability and can capture CO_2 from CO_2/CO mixtures (Banerjee et al., 2008). These frameworks contain large cages interconnected by small apertures. For example, in ZIF-68, the large cages have diameters of 7.2 Å which is connected by apertures of sizes 4.4Å. At 273 K, the CO_2 and CO adsorption isotherms showed that all of these ZIFs have a high affinity and capacity for CO_2 . The selective adsorption was further confirmed by breakthrough experiments, which showed complete retention of CO_2 and passage of CO when they were exposed to a stream containing a 50:50 v/v binary mixture of CO_2 and CO at room temperature. This selectivity can be attributed to the equilibrium effect based on different quadruple moments of CO_2 and CO, but not the molecular sieve effect because the pores in these ZIFs are large enough to allow both gas molecules to enter.

$\text{Er}_2(\text{pda})_3$ (Pan et al., 2003) which has a 3D framework structure with 1D circular channels and coordinatively unsaturated ErIII sites. The effective dimension of the channels is approximately 3.4Å in diameter. Adsorption measurements showed selective adsorption of CO_2 over Ar and N_2 , which was attributed to the combined effects of size and of host–guest interactions by the authors.

At room temperature, ZIF95 showed a high affinity and storage capacity for CO_2 over CH_4 , CO, and N_2 . The high selectivity for CO_2 was ascribed to the combined effects of the size of the pore apertures being similar to CO_2 and the strong quadrupolar interactions of CO_2 with N atoms present on the pore surface, whereas it is also relevant to the higher critical point of CO_2 than those of other gases. In addition, it should also be noted that for the same MOF, the adsorption properties may be distinct at different temperatures. One such example is $\text{Mn}(\text{HCOO})_2$ (Samsenenko et al., 2007).

As demonstrated above, rigid MOFs have great application potential in CH_4 , CO_2 , CO, H_2 , N_2 separations because both their pore size and shape and their surface

properties can be easily tuned by the selection of metal or metal clusters, ligand design and functionalization, as well as by post-synthetic modification.

Many flexible MOFs have been synthesized but only a few were used for gas adsorption (Table 4.3). Comparatively, the gas adsorption in flexible MOFs is more complicated than that in rigid MOFs. In most cases, the adsorption isotherms show hysteretic behaviors due to framework rearrangements during adsorption-desorption processes. Besides size/shape exclusion and adsorbate-surface interaction, structural rearrangement must also be taken into account.

Table 4.3. Summary of gas adsorption in flexible MOFs

<u>Flexible MOF's</u> ^(a)	<u>T</u> <u>(K)</u>	<u>P</u> <u>(atm)</u>	<u>Uptake (mmol/g)</u>					<u>References</u>
			CO ₂	CH ₄	CO	H ₂	N ₂	
<i>Cu(dhbc)₂(4,4'-bipy)</i>	298	100	3.69	2.9			2	Kiteura et al., 2003
<i>Cu(bdc)₂(4,4'-bipy)_{0.5}</i>	298	10	3.15					Kiteura et al., 2003
<i>Al(OH)(bdc) (MIL-53)</i>	304	30	10	6		no		Bourrelly et al., 2005
<i>Cr(OH)(bdc)-H₂O (MIL-53)</i>	304	20	7,5	none				Llewellyn et al., 2006
<i>Zn(adc)(4,4'-bpe)_{0.5}</i>	77	1			none	3.12	none	Chen et al., 2007
<i>H₂Ni₃O(H₂O)₃(tatb)₂(H₂O)- (PCN-5)</i>	195	1	4.6	1.88				Ma et al., 2007
<i>Zn(Pur)₂(ZIF-20)</i>	273	1	3.15	0.61				Hayashi et al., 2007
<i>Cu(fma)(4,4'-bpe)_{0.5}</i>	77	1			none	4		Chen et al., 2007
	195	1	4.5	1.42				

^(a) Abbreviations: **dhbc** = 2,5-dihydroxybenzoate, **bpee** = 4,4'-(E)-ethene-1,2- diyl dipyridine, **Pur** = purinate, **bdc** = 1,4- benzenedicarboxylate, **tatb** = 4,4',4''-S-triazine-2,4,6-triyltribenzoate **bipy**= bipyridine

When adsorbates enter the pores, frameworks can alter their pore sizes through the adjustment of inter-framework distances. Systematic tuning of the dicarboxylate and bi-pyridine type ligands has led to a series of this type of MOF, indicating that the “rational design” approach is useful in tuning the micropores of such MOFs for their separation of CO₂, CO, CH₄ molecules (Chen et al., 2007).

The structure of the MIL-53 is built up from infinite chains of corner-sharing MO₄(OH)₂ (M = Al³⁺, Cr³⁺). This results in a 3D metal organic framework containing 1D diamond shaped channels with pores of free diameter close to 0.85 nm. The chemical formula of the metal benzenedicarboxylate MIL-53 is M(OH)(O₂C-C₆H₄-CO₂) where M denotes the trivalent chromium or aluminum. MIL-53 a flexible MOF, showed different adsorption behaviors for CH₄ and CO₂ (Bourrelly et al., 2005). The adsorption isotherm of CH₄ was typical for a microporous material, whereas the CO₂ isotherm exhibited two steps; above the first step at low pressure the CO₂ adsorption capacity greatly exceeded that of CH₄. The difference between the CH₄ and CO₂ isotherms was attributed to the quadrupole moment of the CO₂ molecules. For MIL-53, (Liywellyn et al., 2006) the adsorption isotherm of CO₂ showed very little uptake at pressures up to 10 bar, while a distinct high uptake occurred in the 12-18 bar pressure range. However, the adsorption isotherm of CH₄ showed almost no uptake below 20 bar. This was attributed to the repulsive effect of the water molecules in the host framework and the nonpolar CH₄ molecules.

The selective adsorption of CO₂ over CH₄ was observed in ZIF-20, (Hayashi et al., 2007) which has a 3D porous structure with large cages connected by small windows. At 273 K, the CO₂ uptake at 760 torr is five times higher than that of CH₄ suggesting a stronger interaction between the pore surface and the CO₂ molecules. It is interesting to note that the maximum pore aperture (2.8 Å as measured from the crystal structure) of ZIF-20 is smaller than the kinetic diameter of CO₂ and CH₄. Therefore, it was believed that the large cage space in the structure becomes accessible through a dynamic window-widening process wherein the ligands swing to allow gas molecules to pass. This result demonstrated that molecules with dipole and quadrupole moments seem to have a distinct effect on the framework flexibility of some MOFs.

Cu(dhbc)₂(4,4'-bpy), (Kiteure et al., 2003) which in its hydrated form has a 2D sheet motif (Kiteure et al., 2003). The sheets have interlocking ridges and hollows furnished by the dhbc benzene planes in an upright fashion and are mutually interdigitated to create 1D channels with a cross section of 3.6 x 4.2 Å. N₂, O₂, CO₂, and

CH₄ adsorption isotherms showed initially a flat curve indicative of zero adsorption in the low pressure region, followed by an abrupt increase at a specific gate opening pressure in each case. For each gas, the adsorption isotherm showed an abrupt decrease at another pressure, the gate-closing pressure, leading to a hysteresis loop of sorption.

CO₂ adsorption is a key step in separation of H₂ from SMR-off gas mixture because of its highest percentage (10-25%) in the mixture. Adsorption separation by a porous material is one of promising methods considered for separation of CO₂ from flue gas. Table 4.3 lists the novel adsorbents and conditions used for CO₂ adsorption. As you can see from table, MOFs showed higher CO₂ adsorption capacities than other adsorbents at high pressure range. MOFs have large surface areas, adjustable pore sizes and controllable properties, as well as acceptable thermal stabilities. These unique structure properties of MOFs, make them attractive as adsorbents for CO₂ separation with properties better than other porous materials, such as silicates, carbons, and zeolites.

Table 4.4. CO₂ adsorption properties of Zeolites and all-silica microporous solid, Aluminium phosphates, MOFs and amine modified mesoporous silica.

<u>Adsorbents</u>	<i>T(K)</i>	<i>P(kPa)</i>	<i>n(mmol/g)</i>	<i>Reference</i>
<i>Zeolites and all-silica microporous solid</i>				
<i>NaX</i>	306,295	0.67, 1	5.4, 4.5	Dume et al., 1996 Harlich et al., 2004
<i>NaY</i>	295,295	1,1	4.1, 1	Harlich et al., 2004
<i>Na-ZSM-5, H-ZSM-5</i>	297,295	0,67, 1	1.8, 1.9	Dume et al., 1996 Harlich et al., 2004
<i>Silicalite</i>	295	1	1.4	Dume et al., 1996 Harlich et al., 2004
<i>NaA</i>	298	0.93	4.1	Breck 1956
<i>Beta-zeolite</i>	303	1	1.8	Xhe et al., 2009
<i>Na-mordendite</i>	308	10	2.8	Delgado et al., 2006
<i>Herschelite</i>	298	0.69	2	Fisher et al., 2003

(cont. on next page)

Table 4.4. (Cont.)

<i>Aluminium phosphates</i>				
<i>ALPO4-5</i>	165	1	3.3	Martin et al., 1998
<i>ALPO4-14</i>	290	1	2.2	Zhoe et al., 2009
<i>SAPO4-34</i>	298	1	3.4	Ramos et al., 2008
<i>MOFs</i>				
<i>MOF-177</i>	298	30	32	Millward et al., 2005
<i>IRMOF-1/MOF-5</i>	298	30	21	Millward et al., 2005
<i>IRMOF-6</i>	298	30	18	Millward et al., 2005
<i>IRMOF-3</i>	298	30	18	Millward et al., 2005
<i>ZIF-69</i>	273	1	3.1	Hayashi et al., 2007
<i>ZIF-20</i>	273	1	3.1	Wang et al., 2008
<i>ZIF-100</i>	298	1.1	0.95	Baurelly et al., 2005
<i>MIL 53(Al)</i>	304	16	9	Llewelyn et al., 2008
<i>MIL-100</i>	303	60	18	Llewelyn et al., 2008
<i>MIL-101(Cr)</i>	298	50	40	Llewelyn et al., 2008
<i>Cu(BTC)</i>	298	30	11	Millward et al., 2005
<i>Activated carbon</i>	303	40	11.7	Drage et al., 2009
<i>Amine modified mesoporous silica</i>				
<i>MCM-41</i>	298	1	2.2	Hvang et al., 2003
<i>Xerogel</i>	298	1	1.2	Hvang et al., 2003

Millward and coworkers synthesized and studied the sorption properties of CO₂ and N₂ (among other gases) in a range of MOFs (Table 4.4). MOF-177 showed a very high capacity for adsorbing CO₂ at partial pressures above 15 bar, however, the capacity was low at small CO₂ pressures (Millward et al., 2005). The coordinating metal ion was Zn²⁺, and the organic linker was the benzene 1, 3, 5-tribenzoate group. The observed sigmoidal shape of the adsorption isotherm, for MOF-177 and similar MOFs, is still under scientific discussion. Walton et al., (2008) demonstrated that the shapes of the adsorption isotherms of CO₂ in MOF 177. They claimed that the sorbate–sorbate electrostatic interactions were essential for predicting the inflections and steps of the adsorption isotherms.

The adsorption equilibrium and diffusion of CO₂ on microporous metal–organic framework crystals (MOF-5, or IRMOF-1) were studied by Zhao et al., (2009). The

Freundlich adsorption isotherm equation can fit well the CO₂ adsorption and MOF-5 as found to be an attractive adsorbent for separation of CO₂ from flue gas.

Bastin et. al (2008) examined a microporous MOF Zn(bdc)(4,4'-bipy)_{0.5} (MOF-508b,) for the adsorption of CO₂. Barcia et al., (2008) studied the adsorption of CO₂, N₂, and CH₄ on crystals of MOF-508b, at temperatures in the range 303–343 K and at partial pressures up to 450 kPa. MOF-508b was found to be very selective for CO₂, and the loadings of CH₄ and N₂ were practically temperature independent. The Langmuir isotherm model provided a good representation of the equilibrium data.

Zeolitic imidazole frameworks (ZIFs) have structures formed by heterocyclic and nitrogen-containing linkers with topologies very similar to those of zeolites. Metals play a similar role on ZIFs to that of Si and Al atoms on zeolites, by mainly contributing with electrostatic interactions, the vdW contributions can be ignored. This fact makes ZIFs substantially different from other MOFs. Using high-throughput experimental techniques, Yaghi and coworkers identified a range of candidate materials with a high capacity for CO₂ adsorption (Hayashi et al., 2007, Wang et al., 2008).

Cr³⁺ and Al³⁺ ions can be used as the coordinating metals in MOFs. Llewellyn and coworkers studied the uptake of CO₂ in a series of MOFs, in which Cr³⁺ and Al³⁺ had been substituted at the coordinating cation positions (Baurelly et al., 2005). The Materials Institute of Lavoisier (MIL) solids have been shown to yield large CO₂ uptakes. In particular, MIL-100 and MIL-101 showed very high capacities for CO₂ adsorption at high pressures (Llewellyn et al., 2008). In particular as mentioned earlier, MIL-53 shows “breathing” phenomenon upon or host–guest interactions. Such flexible and dynamic frameworks are interesting as they open potential applications for high-performance molecular recognition and high selectivity for guest inclusion and release.

Hammon et al., studied binary adsorption of CO₂ and CH₄ in MIL-53(Cr), and discussed the possibility of using these MOFs for the PSA applications for CH₄ and CO₂ adsorption (Hamon et al., 2009).

CuBTC was first reported by Chui et al., (1999) as HKUST-1. CuBTC has symmetry and pores of 1.02 nm and 1.2 nm and octahedral side pockets of 0.48 nm which are connected to the larger pores by windows of 0.35 nm (Gelb and Gubbins 1999). The accessible porosity is about 0.34 cm³/g (Chui et al., 1999).

Wang et al., (2002) measured the isotherms of N₂, CO₂, CO, CH₄, O₂, N₂O, C₂H₄, C₂H₆, n- C₁₂H₂₆ and H₂O up to 1 bar at 295 K on the CuBTC. Senkovska and Kaskel (2008) measured methane adsorption up to 200 bar at 303 K. Wang et al., (2002)

measured CO₂ up to 20 bar at 298 K in addition to the low pressure data results. Millward and Yaghi (2005) also measured carbon dioxide at 298 K up to 42.5 bar, exceeding the amount adsorbed by Wang et al., (2002). Different syntheses and activation procedures were followed leading to the discrepancies. Recently, Chowdhury et al., (2009) investigated the influence of different synthesis methods on the adsorption performance of CuBTC. Two CuBTC samples were synthesized, one based on the procedure described by Wang et al., (2002) giving a BET surface area of 857 m²/g, and the other one using the synthesis method given by Liu et al., (2007a) resulting in a BET surface area of 1482 m²/g. Measuring the adsorption of N₂, O₂, Ar, CO₂, C₃H₈ at 295.25 K and 318.15 K, a strong influence of the synthesis on the adsorption performance was found.

Yazaydin et al., (2009) used molecular simulation techniques to predict that CO₂ uptake and selectivity with respect to N₂ and CH₄ in the Cu-BTC MOF were significantly increased by the presence of water molecules coordinated to open metal sites in the framework. Yang et al., performed a GCMC simulation of the adsorption and separation of CO₂ from flue gases (mixtures of CO₂/N₂/O₂) in Cu-BTC MOF, and found this a promising material for separating CO₂ from flue gases. Keskin et al (2009) studied gas adsorption and diffusion in Cu- BTC on the atomic level to predict the performance of Cu-BTC membranes for the separation of H₂/CH₄, CO₂/CH₄, and CO₂/H₂ mixtures. They found this membrane to have higher selectivities for all three mixtures than did MOF-5 membranes. Liang et al., (2009) experimentally studied Cu-BTC for its potential for CO₂ adsorption, and determined the isotherms for CO₂, CH₄, and N₂ at various pressures and temperatures. The authors observed a quadrupled capacity for CO₂ adsorption compared with NaX. Cu-BTC was shown to be unstable at moderate temperatures and humid conditions.

Krungleviciute et al., (2008) have reported that in Cu-BTC the time to reach equilibrium was comparable for Ar and CF₄. They used these results to establish kinetic selectivity for the same two gases in another variety of MOF, RPM1-Co. Peralta et al., reported a kinetic studies for the separation of hydrocarbon in Cu-BTC (Peralta et al., 2009). Saha et al., studied metal-organic framework (MOF-177, MOF 5) for H₂ adsorption. The hydrogen adsorption equilibrium and kinetic data were measured (Saha et al., 2011, 2012).

CHAPTER 5

EXPERIMENTAL STUDIES

5.1. Materials

Binderless NaX zeolite (CAS: 63231-69-6) (Aldrich) and metal organic framework (MIL53(Al)) (Basolite A100) (Sigma Aldrich) were used as adsorbents. KCl.9H₂O (Merck) was used to prepare salt solution in ion exchange experiment. High purity of H₂ (> 99.999 %), CH₄ (> 99.95 %) and CO₂ (> 99.995 %), CO (> 99.995 %), were used as adsorbates.

5.2. Preparation of the NaX and KNaX zeolite adsorbents

Binderless NaX zeolite with unit cell formula of Na₈₆(Al₈₆Si₁₀₆O₃₈₄) 264H₂O, and Si/Al:1.23 was used in preparation of KNaX zeolites. The ultrasound enhanced introduction of K⁺ cations into NaX frameworks was performed and compared with traditional one. 2 g of zeolite were mixed with 20 mL of 1 M KCl solution for 2h at 50 or 70 °C with water bath shaker (GFL 1092) at 130 rpm or ultrasonic processor (Sonics-Vibracell-VC 505, frequency; 16 kHz). After ion exchange, the mixtures were centrifuged and then zeolite phases were washed with water until Cl⁻ free solution was obtained. In adsorbent codes, U and S are expressed as ion exchange method ultrasound and shaker respectively. 50, 70 are expressed as synthesis temperature (°C) and Na exchange amount (%) are given in parenthesis.

5.3. Characterization

Thermal properties of the adsorbents were analyzed by thermo balance (Shimadzu TGA-51/51H) with scanning up to 1000 °C at heating rate of 10 °C/min. Nitrogen atmosphere (40 ml/min) were used for all analyses. Mineralogy and crystallinity of the adsorbents were determined by X-ray diffraction (Philips X-Pert Pro Diffractometer) using CuK α radiation at 45 kV and 40 mA in the 2 θ range of 50-70°

with 0.2° step size. The micrographs of the adsorbents were taken by using scanning electron microscopy (SEM, Philips XL 30S) with LFD and ETD detector at 5.00 and 3.00 kV under vacuum conditions.

Fourier Transform Infrared Spectroscopy (FTIR) analysis was carried out in the spectral region of 400-4000 cm^{-1} using an FTIR spectrophotometer (Shimadzu FT-IR 8201). 3 mg of a powder form of adsorbents were taken and completed to 150 mg with KBr to remove scattering effects. This powder mixture is then pressed into a pellet with a thickness of about 1mm to form homogenous and transparent in appearance. Chemical composition of the adsorbents was determined by Inductively Coupled Plasma Atomic Emission Spectroscopy (ICP-AES, 96, Varian). Textural properties of adsorbents were determined by using a volumetric N_2 adsorption instrument (Micromeritics, ASAP 2010M) at 77K. Prior to adsorption, the samples were degassed for 24 h under vacuum better than 10^{-5} mbar at 350 °C.

5.4. Adsorption Equilibrium Studies

Adsorption equilibrium studies were divided into two parts. The first part included the CO_2 adsorption up to 1 atm. Second part explained the SMR Off-gas Adsorption up to 5 bars.

5.4.1. CO_2 interaction with adsorbent surface

Adsorption equilibrium of CO_2 , on the adsorbents was measured by using volumetric adsorption apparatus (Micromeritics ASAP 2010 M) at 278 and 298 K. The isotherm data fitted to the Toth and Sips models equations by using Sigma Plot 6.01 statistical software program.

5.4.2. SMR Off-gas Adsorption

SMR off-gas (CO , CO_2 , CH_4 and H_2) adsorption was carried out in the home-made volumetric adsorption system (Figure 5.1). System mainly consist of adsorption cell (sample chamber(Parr/USA-4563).) , charge vessel, vacuum section. The sample

chamber volumes were nominally 600ml. To evaluate the amount of adsorbed gas, which is necessary for measuring equilibrium isotherms, a charge vessel were used. The vacuum section of the volumetric adsorption system was used to regenerate the adsorbent. A vacuum pump (1400N50 Welch Chemstar) with active pirani gauge (KJL 6006, Kurt J. Lesker) was used in this system. All connections in the apparatus were made with 1/4 in. (6.35 mm) stainless-steel tubing and proper swagelok fittings. System pressure measurements were accomplished through the use of pressure transducer (Cole Parmer, model C 206) operating in the range of 0 to 500 kPa with accuracy \pm 0.1 kPa. The determination of the true dead volume of the sample chamber and their associated piping was accomplished by a Helium expansion method. To evaluate the amount of adsorbed gas, which is necessary for measuring equilibrium isotherms, a charge chamber with a total volume of 1000 cm³ was used.



Figure 5.1. Experimental apparatus

The experimental procedure for measuring pure gas adsorption isotherms at 5 atm is as follows. A known mass of adsorbent (10 g in these experiments) was charged into the adsorption cell and was regenerated prior to each isotherm measurement at 573 K under vacuum (10 mbar) for 4h. Gas was introduced into the charge chamber and its pressure and temperature were measured. These measurements provided the initial number of moles of the gas, n_1 , by using the virial equations as the equation of state.

The gas was then allowed to contact the adsorbent by opening the valve of adsorption column. The pressure and temperature were measured after equilibrium has been achieved and the number of moles gas remaining in the system, n_2 , was calculated at the new condition. The number of moles introduced to sample chamber was then obtained by difference (i.e. $n_1 - n_2$). A part of this number of moles was adsorbed by adsorbent and the other was in the gas phase. In order to know the amount of adsorbed gas by adsorbent, thus, one may measure the number of moles in gas phase. Before starting adsorption experiments, the dead space V_d is determined with helium gas at ambient temperature and low pressure. All calculations were done by using Matcad 14 software program. The expected uncertainties in the amounts adsorbed were estimated using error propagation in all the measured variables and were confirmed by replicate runs.

5.5. Adsorption Kinetic Studies: ZLC Adsorption System

CO, CO₂, CH₄ and H₂ adsorption on the MIL53 (Al) was studied to determine diffusion coefficient by using the home-made ZLC system (Figure 5.2) as given detail in previous study (Erten Kaya, 2012). The system includes adsorbent zero length column, oven (Binder ED 53), gas flow controllers (Aalborg, DFC 26)) and mass spectrometer (Hiden HPR 20). Water vapour trap (Agilent) was placed before the mass flow controllers to reduce deteriorate effect of water vapor on gas adsorption. Simplified zero length column configurations were seen in Figure 5.2.

The ZLC cell consists of a small amount of adsorbent (≈ 2 mg) in powder form sandwiched between two sintered discs (35 μ m) (Alltech) in a 1/8-in. Swagelok fitting. Quartz wool was used to close remaining space of ZLC cell and prevent zeolite crystals to escape the mass spectrometer (MS). All the connections in the system were periodically inspected for leakage with a solution of water and soap.

The ZLC is located into an oven to regenerate and perform the adsorption experiments at desired temperature. Regeneration at 200 °C (1 Kmin⁻¹ heating ramp) removes water vapor and some impurities by using a flow of helium at 10ml/min for 3 or 14 h. The adsorbent into ZLC was exposed to a diluted stream of an adsorptive in an inert (helium) gas. Therefore, 3 % volume of adsorptive as the initial concentration was applied in order to describe the equilibrium by Henry's law. Adsorption measurements were carried out at 303, 343 and 373 K. Finally, purging with He gas was carried out at

30, 50, 70, 100 ml/min to obtain desorption (response) curves. The flow rates of both the adsorptive and purge streams were controlled by mass flow controllers. The effluent concentration of the desorption /response curves was recorded in digital form for data processing.

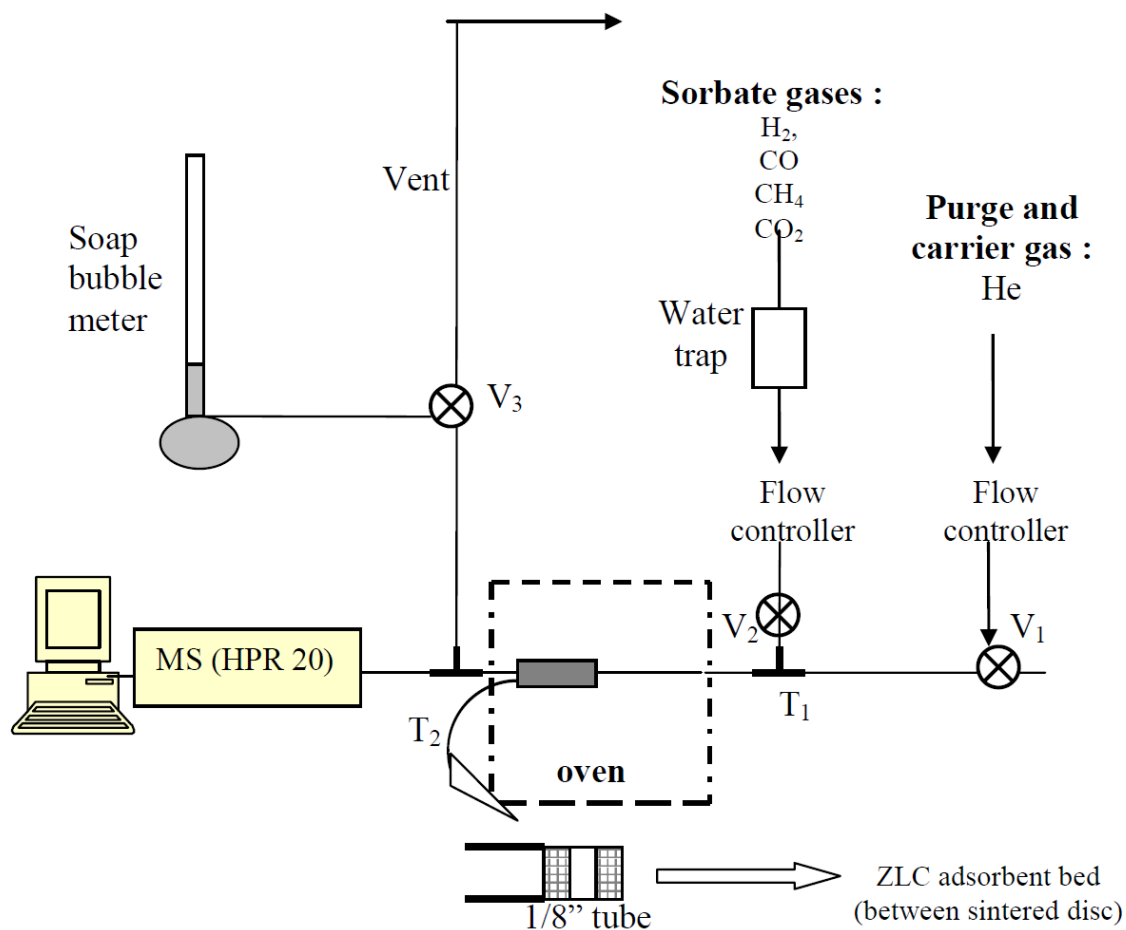


Figure 5.2. Zero Length Column configurations

5.6. Error Analysis

Adsorption equilibrium of CO₂, CH₄, CO, H₂ were evaluated and compared with isotherm models. All the model parameters were evaluated by nonlinear regression using the data fit software (Sigma Plot). The optimization procedure required an error function to be defined in order to be able to evaluate the fit of the equation to the experimental data. Apart from the regression coefficient (R²), the residual or sum of square error (SSE) and the standard error (SE) of the estimate were also used to gauge the goodness-of-fit:

$$SSE = \sum_{i=1}^m (Q_i - q_i)^2 \quad (5.1)$$

And

$$SE = \left[\frac{1}{m - p} \sum_{i=1}^m (Q_i - q_i)^2 \right]^{0.5} \quad (5.2)$$

where q_i is the observation from the batch experiment i , Q_i is the estimate from the isotherm for corresponding q_i , m is the number of observations in the experimental isotherm, and p is number of parameters in the regression model. The smaller SE and SSE values indicate the better curve fitting. F-ratio is the ratio of the mean square of the predicted model to the mean square of the true error (residual). The F-ratio is a test statistic for multiple independent variables. It is calculated as

$$F \text{ ratio} = MS_M / MS_R$$

where

$$MS = SSE / \text{doff} = \text{degrees of freedom}$$

Subscripted M means 'Model' and indicates the expected systematic variance. This is often measured as between measures variation; Subscripted R means 'Residual' and indicates the random, unsystematic variance. A good model will have a high mean

square for the model; therefore, the larger this ratio, the better the model “fits” the experimental data.

The average uncertainties for measurements were obtained by

$$\text{Average uncertainty:} = \left[\frac{ts}{\sqrt{n}} \right] \quad (5.3)$$

where t is the student t factor, s is the standart error, n is the number of measurements

The correlation coefficient, R^2 , SE, SSE, F-ratio, and predicted q_m (wherever applicable) values were used to determine the best fit adsorption isotherm model. So as to evaluate the goodness obtained fits, the sum of squares due to the errors (SSE), R^2 , the residual degrees of freedom and standard error of estimate associated with the output model results were calculated with the help of Sigma Plot software program.

In the kinetic study, desorption curves for CO_2 , CH_4 , CO , H_2 and MIL 53 were obtained. Good agreement is observed between experiment and theoretical model that described in above ZLC theory section. The Sum of square error for the determination of model constants was defined as

$$SSE = \left(\sum_{i=1} \frac{C(t_i)}{C_0} - F(t_i) \right)^2 < 10^{-7} \quad (5.4)$$

where $F(t_i)$ is the observation $\frac{C(t_i)}{C_0}$ from the batch experiment i, $\frac{C(t_i)}{C_0}$ is the estimate

from the theoretical ZLC model for corresponding $\frac{C(t_i)}{C_0}$.

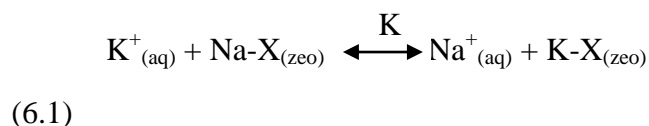
CHAPTER 6

RESULTS AND DISCUSSION

6.1. Characterization of Adsorbents

6.1.1. Zeolite Adsorbents

K^+ rich NaX zeolite (KNaX) was prepared with the exchange reaction between the counter ions, K^+ , and NaX zeolite;



Where K is the rate constant of the exchange reaction. Exchange percentage amount of Na^+ ion (η_{Na}) was calculated;

$$\eta_{Na} = \left(\frac{q_o - q_{Na}}{q_o} \right) \times 100 \quad (6.2)$$

where q_o and q_{Na} ($mg\ g^{-1}$) are the amount of Na^+ ions into zeolites initially and at any time t , respectively. The maximum Na exchange amount was obtained as 83% and 81% at 70 °C by using ultrasonic processor and shaker, respectively. Although no significant effect of the methods on exchange percent was noted. It was observed that temperature were more effective on the exchange of K in NaX zeolite when ultrasound processor is used. Textural properties of the adsorbents are given in Table 6.1. In adsorbent codes, U and S indicate respectively exchange methods: ultrasound and shaker; 50 and 70 numbers display exchange temperature (°C) respectively; the numbers in parenthesis are exchange percent of Na.

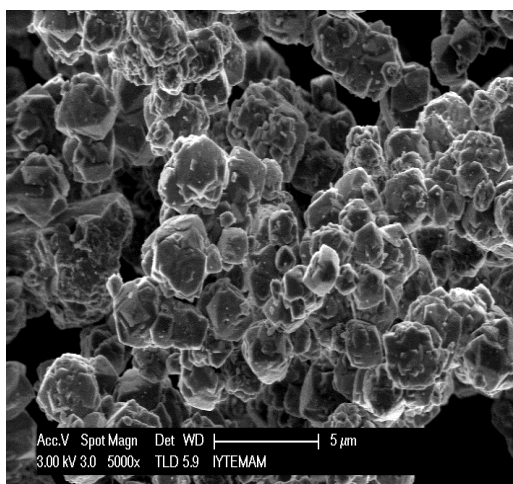
Table 6.1. Textural properties of zeolite adsorbents

Adsorbent codes	$A_L/m^2 g^{-1}$	$V_{mic}/cm^3 g^{-1}$	$d_m/\text{Å}$
NaX	1058	0.37	7,47
S50 (76)	1036	0.34	7,15
U50 (79)	902	0.33	6,55
S70 (81)	899	0.31	6,48
U70 (83)	857	0.31	5,67

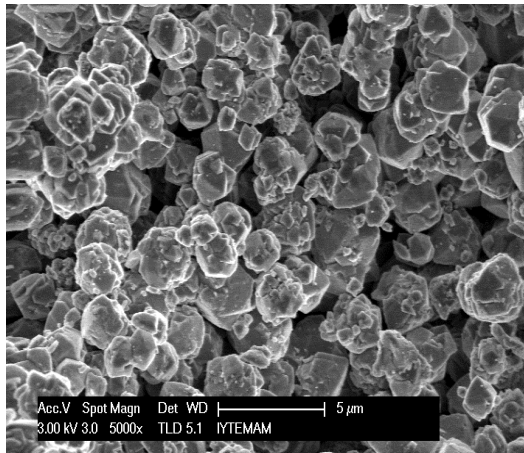
A_L : Surface area from Langmuir method; V_{mic} and d_m : micropore volume and median pore diameter from Howard–Kawazoe Method

As seen from Table K rich NaX zeolites have lower langmuir surface area and micropore volume than NaX zeolite. This can be explained with the restriction of K^+ ions, bigger ions than Na^+ ($R_{K^+} > R_{Na^+}$).

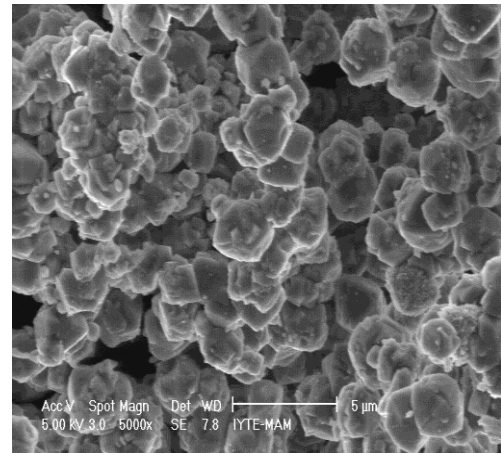
The micrographs of the surface obtained from scanning electron microscope show that the crystal size (2 μm) of NaX zeolite did not change with ultrasonic source or the methods used in K^+ ion exchange.



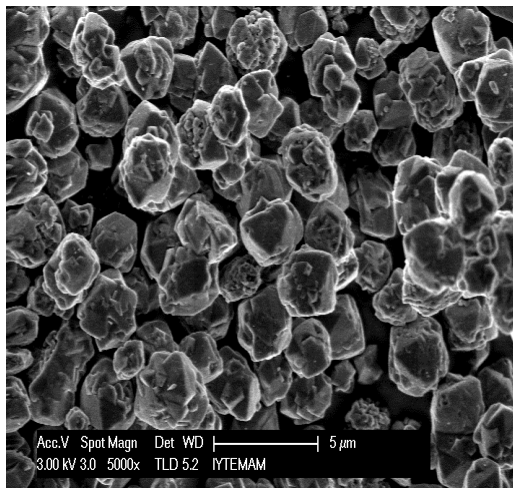
(a)



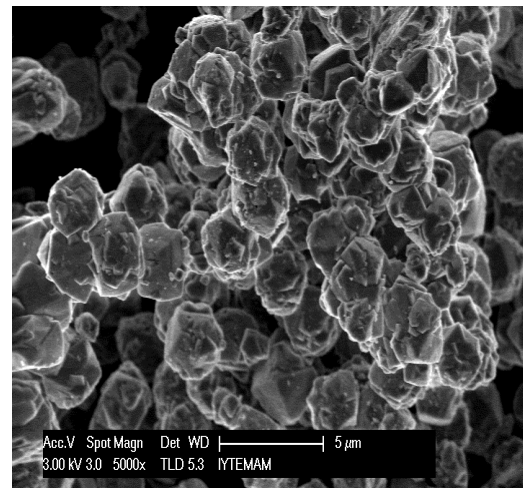
(b)



(c)



(d)



(e)

Figure 6.1. SEM images of adsorbents: (a) NaX (b) S50 (76) (c) S70 (81) (d) U50 (79) (e) U70(83)

Figure 6.2 shows the X-ray diffractogram of the zeolite adsorbents. From the XRD spectra of zeolite adsorbents K^+ ion exchange does not affect the skeleton, just changes the local pore in zeolites. The cation exchange resulted in decrease in the peak intensity as mentioned in the literature (Jasra et al., 2003; Buhl et al., 2003). As seen from the Figure 6.2, the NaX zeolite has the highest peak intensities and highly crystalline material but it is reduced with potassium exchange process. This means that X-ray diffraction studies of zeolites in powders confirm migration of cations to zeolite extraframework sites.

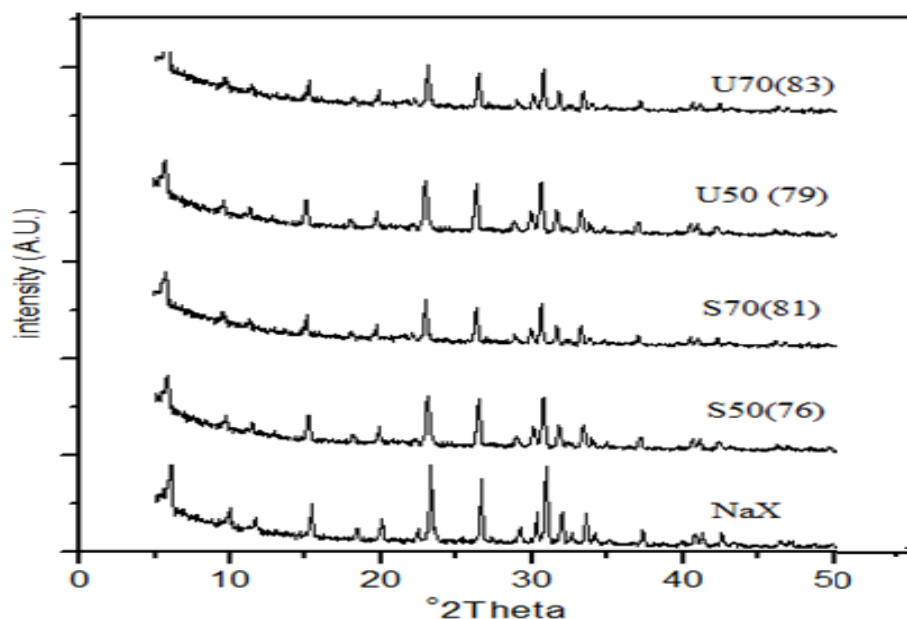


Figure 6.2. X-ray diffraction patterns of zeolite adsorbents

Thermal analyses including TG/DSC were used to investigate the change in thermal properties of the zeolites such as dehydration behavior. Zeolites were heated under N_2 flow to high temperatures to complete dehydration. Figure 6.3 shows the smooth mass loss of the zeolites from TG curves. As seen from the TG data tabulated S50(76) showed the highest dehydration and (the order is: S50(76)>NaX>U70(83)>S70(81)>U50(79) (Table 6.1). As seen from the thermal gravimetric analyze (TGA) curve (Figure 6.3), the weight loss was occurred up to 200 °C due to desorbing free mobile water in the supercages. Between 200-350 °C the water is desorbed from the hydrated cation complexes in which water is bounded to framework oxygens in the small pores of the zeolites as stated by Akbar et al., (2007).

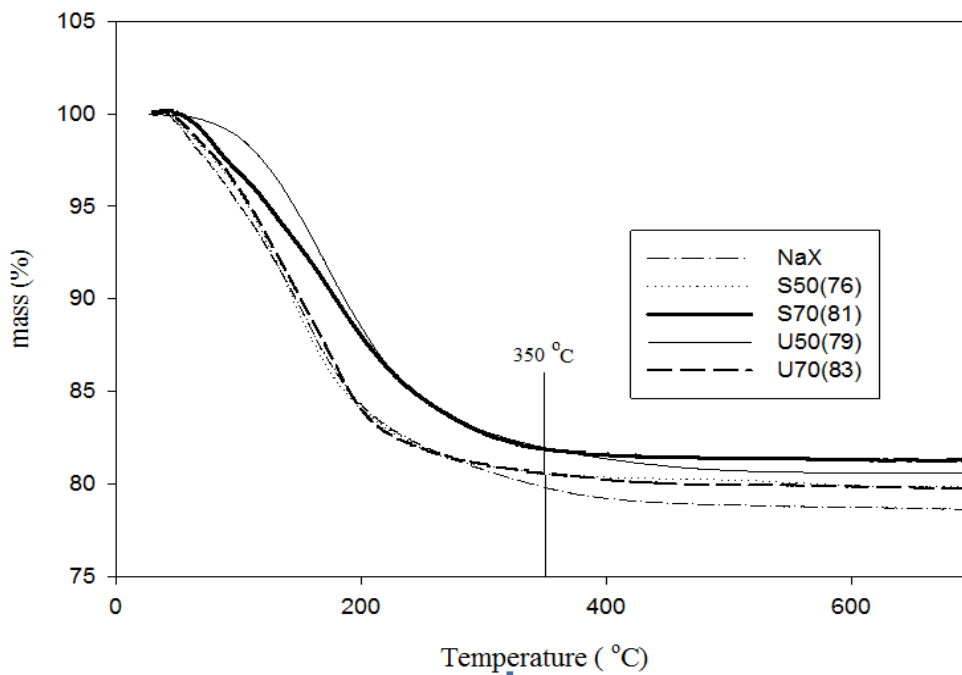


Figure 6.3. TG curves of zeolite adsorbents

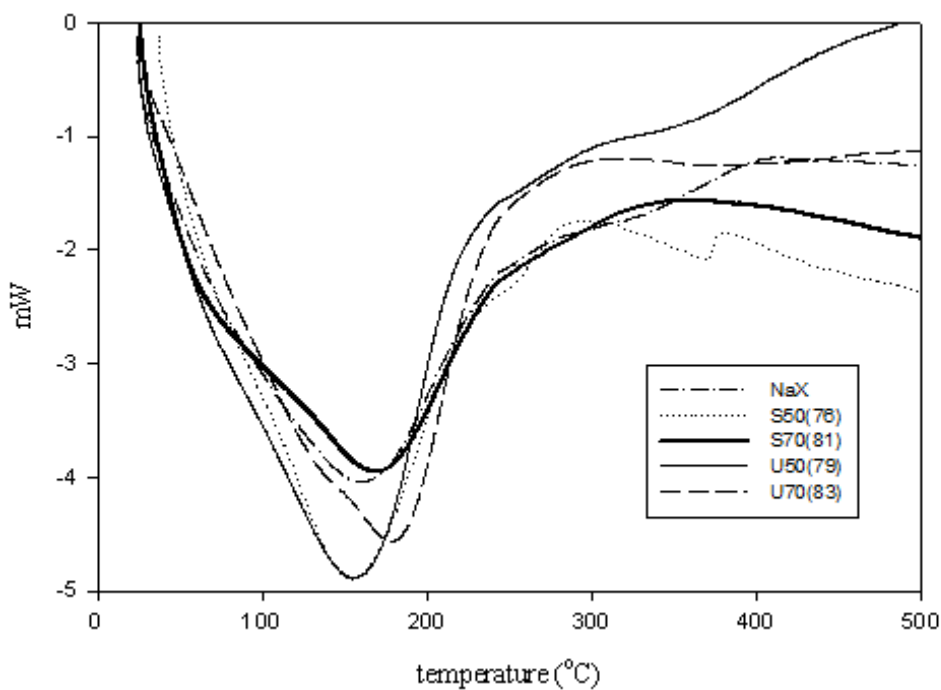


Figure 6.4. DSC curves of zeolite adsorbents

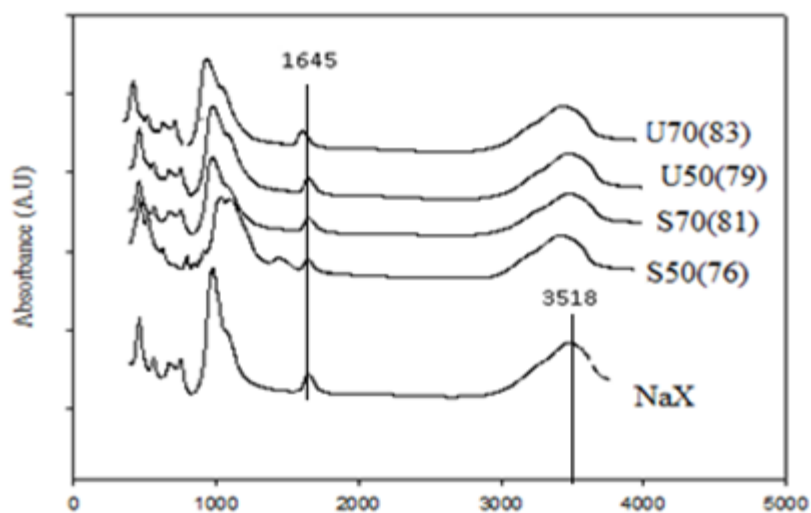
According to DSC curve free and bounded water, were removed with heating up to dehydration temperature (Table 6.2). The DSC curve gives an endothermic peak due to desorption of water for zeolites below 200°C as shown in Figure 6.4. This water is related to physically adsorbed water by means of cation. The enthalpy change (ΔH)

value is obtained from peak area above DSC curves and tabulated. Enthalpy change values of water in zeolites were found higher than vaporization enthalpy of pure water (≈ 2230 J/g at 100 °C) which shows how small pores was obtained for K rich adsorbents.

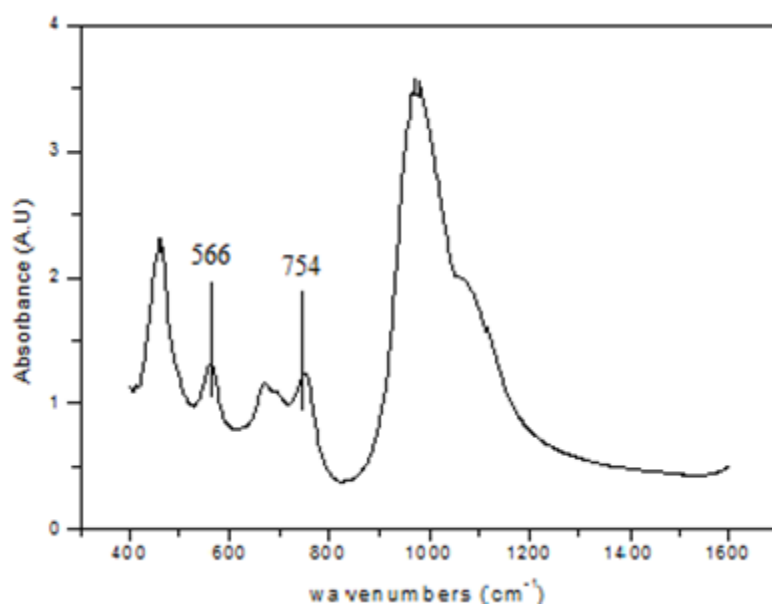
Table 6.2.TG and DSC data of the zeolites

Zeolites	Mass loss (%)	Number of water molecules desorbed per unit cell	Dehydration temperature (°C)	ΔH (J/g zeolite)	Moisture content (g water/100 g zeolite)	ΔH (J/g water)
NaX	22.5	133	431	1100	21.4	5140
S50(76)	19.9	126	407	791	18.7	4207
S70(81)	21.6	156	412	847	20	4131
U50(79)	21.4	131	422	883	20.2	4350
U70(83)	20.5	112	503	1130	19.3	5824

FT-IR spectroscopy was used to measure changes in the character of a particular symmetric stretching band at 754 cm^{-1} and the double-ring vibration band at 566 cm^{-1} , characteristic of faujasite zeolites as stated by Zhan et al., (2002).



(a)



(b)

Figure 6.5. FT-IR spectra of the zeolites between (a) 400-4000 and (b) 400-1600 cm^{-1} wavelength

The band at 1645 cm^{-1} is the characteristic of the bending mode in the water molecule. Fourier transform infrared spectroscopy showed a decrease in acidity upon ion exchange of zeolite as observed from the reduction in the intensity of the peaks corresponding to acidic hydroxyl groups (3518 cm^{-1}) on the surface of the sodalite cages (Jasra et al., 2003).

6.1.2. MIL 53 (Al) Adsorbent

Metal organic framework MIL 53 (Al) with demonstrate higher surface area (1278 m²/g) and micropore volume (0.4 cm³/g) than zeolites has small cubic particles shape (Figure 6.6).

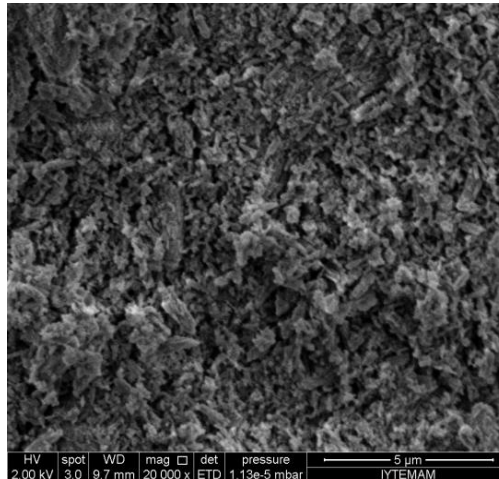


Figure 6.6. SEM images of MIL 53(Al)

MIL 53(Al) is crystalline material (Figure 6.7) the main peaks are located at between 10 and 20 2Theta values which is compitable with literature (Loiseau et al., 2006).

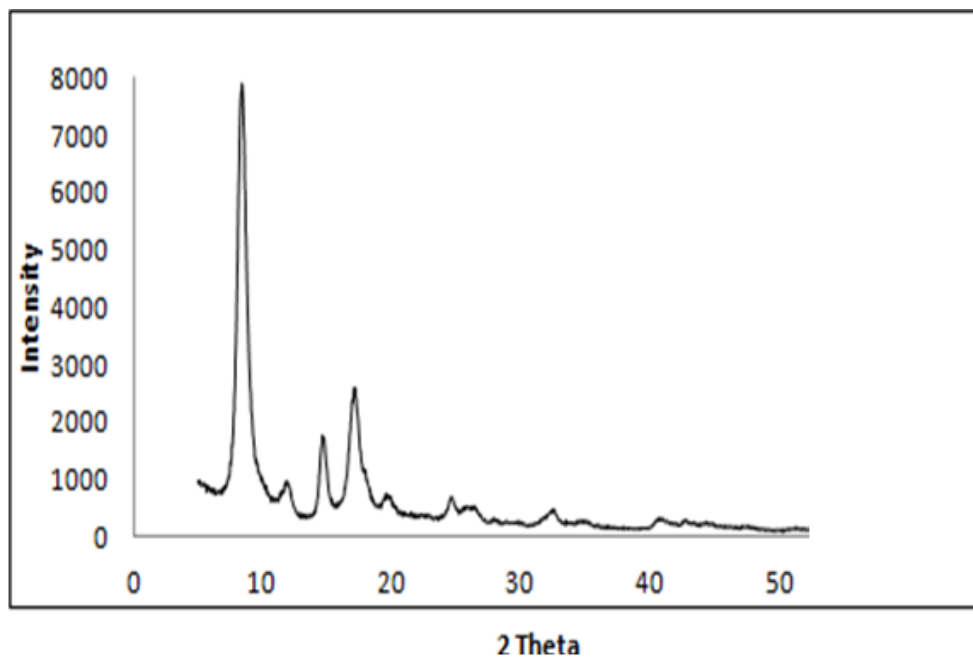


Figure 6.7. X-ray diffraction patterns of MIL53(Al)

TG curve of MIL 53 (Al) given (Figure 6.8) exhibited two-stage weight loss. The first weight loss occurred below 120 °C, indicating the removal of the occluded water from the structure. In the first weight loss below 120°C, samples show a negligible weight loss (about 5 wt %). The dehydrated structure, which is stable up to 560 °C, eventually collapses with the departure of the bound Benzene dicarboxylic acid (BDC) acid. At 640 °C, the final residue is an amorphous form of Al₂O₃

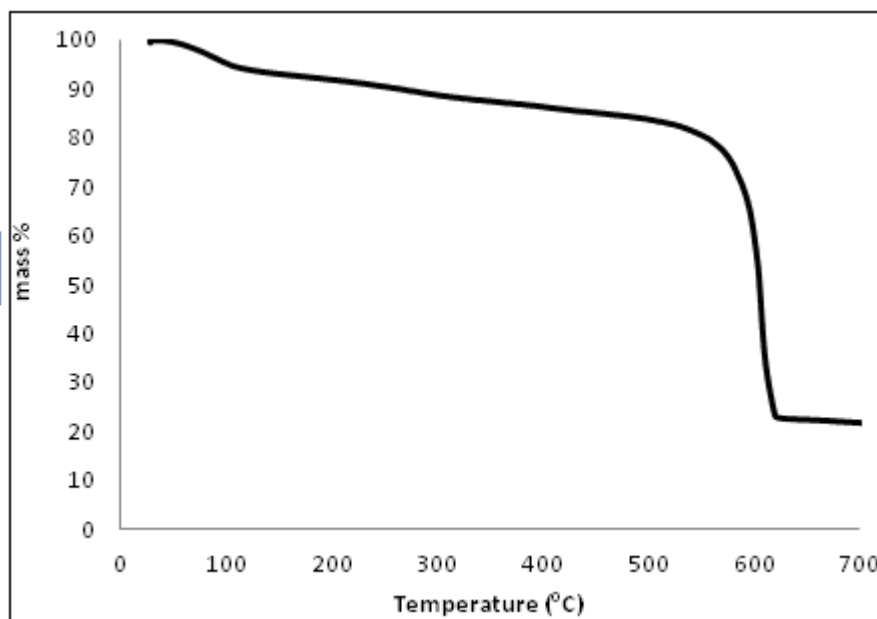
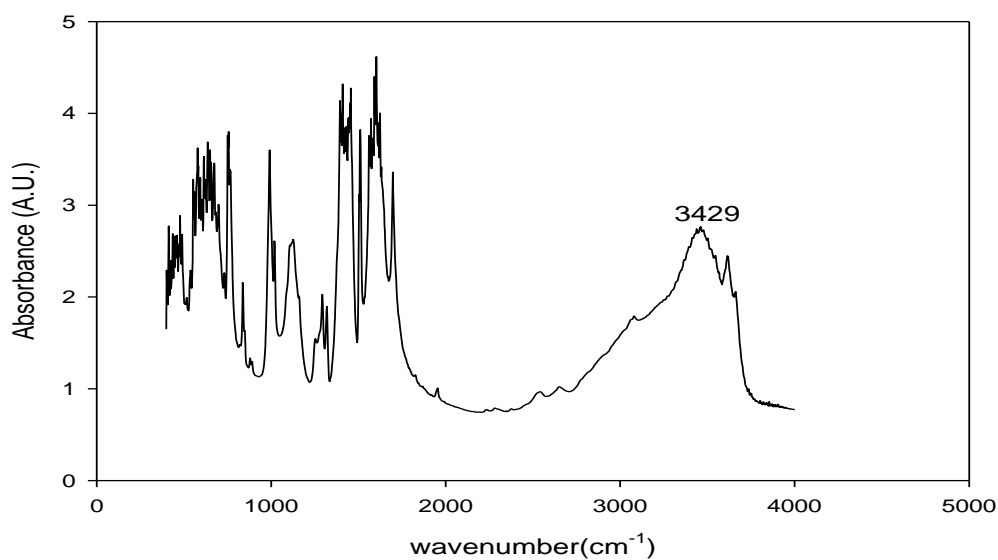
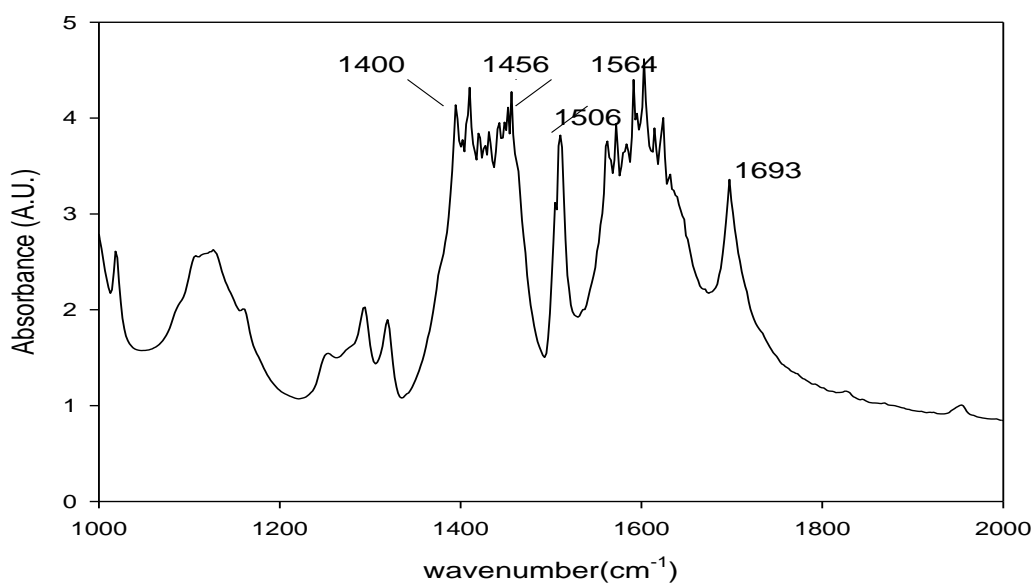


Figure 6.8. TG curves of MIL 53 (Al)

Figure 6.9 (a,b) shows the IR spectrum of the MIL 53 (Al). The observation of the two strong vibrational bands located at 1400 and 1456 cm⁻¹ assigned to -CO₂ symmetric stretchings whereas bands at 1506 and 1564 cm⁻¹ assigned to -CO₂ asymmetric stretchings of which are coordinated to aluminum. The presence of the bands characteristic of the framework -COO⁻ groups indicated the presence of the dicarboxylate within MIL 53(Al) sample. The peak at 3429 cm⁻¹ attributed to OH stretching. The peak at 1693 cm⁻¹ for the final sample is the characteristic peak for water.



(a)



(b)

Figure 6.9. FT-IR spectra of MIL 53(Al)

6.2. Adsorption Equilibrium Studies

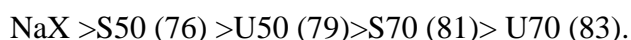
Equilibrium studies can be classified as CO₂ interaction and gas adsorption studies. In the former one the aim is to understand the interaction (energy distribution, heterogeneity etc.) of CO₂ with the adsorbent surface in the volumetric adsorption

system (ASAP 2010) at 1 atm. CO₂, CH₄, CO and H₂ adsorption were also studied in home-made volumetric system operating at pressure up to 4 bar.

6.2.1. CO₂ interaction with Adsorbent surface

Equilibrium isotherm data of CO₂ on the zeolite and MIL 53 (Al) adsorbents were obtained at 278K and 298K. Langmuir, Freundlich, Sips and Toth model equations were applied to the data. CO₂ isotherms of the adsorbents at 278 and 298K are given in Figs. 6.10. a and b respectively. As shown in Figures similar and highly favorable adsorption isotherms which are of type 1 according to IUPAC classification was observed for zeolite adsorbents. CO₂ adsorption show linear isotherm for MIL53(Al) adsorbent.

As the temperature increased the adsorbed amount decreased since adsorption is an exothermic process. With the introduction of K ions the effect of temperature on adsorption for zeolite adsorbents considerable and the orders as follows;



Similar order showing that NaX zeolite has the highest adsorption capacity and among the modified zeolites can be concluded. Acidic CO₂ molecule can adsorb on the basic surfaces. The basicity increases by increasing electropositivity of counter balance cation. K⁺ ion has lower electropositivity and ionic radius than those of Na⁺ ion. As it is expected, as ion exchange percentage increases from 76 to 83, the CO₂ amount adsorbed decreases. Barthomeuf suggested that the base strength of zeolites increased along with an increase of the aluminum content because of the lower electronegativity (higher electropositivity) of aluminum compared to that of silicon. (Barthomeuf, 2003). The presence of aluminum atoms in zeolites introduces negative framework charges that are compensated with exchangeable cations, namely, counter-balance cations or extra-framework cations. The modification of zeolites via the introduction of larger and more electropositive polyvalent cation enhance the adsorption of acidic CO₂. Walten et al., showed that the CO₂ adsorption of the X zeolites having monovalent counter ions increased as the cation ionic radii decreased: in the order Cs⁺ < Rb⁺ < K⁺ < Na⁺ < Li⁺ (Walton et al., 2006).

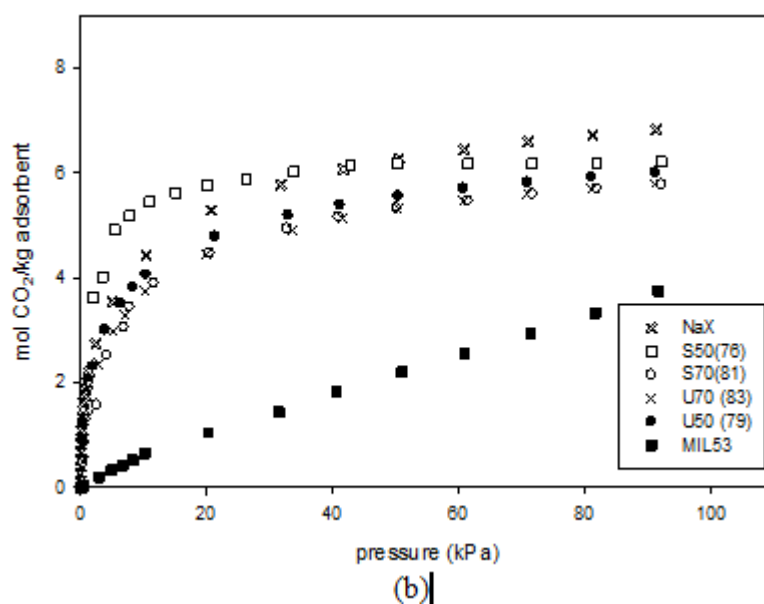
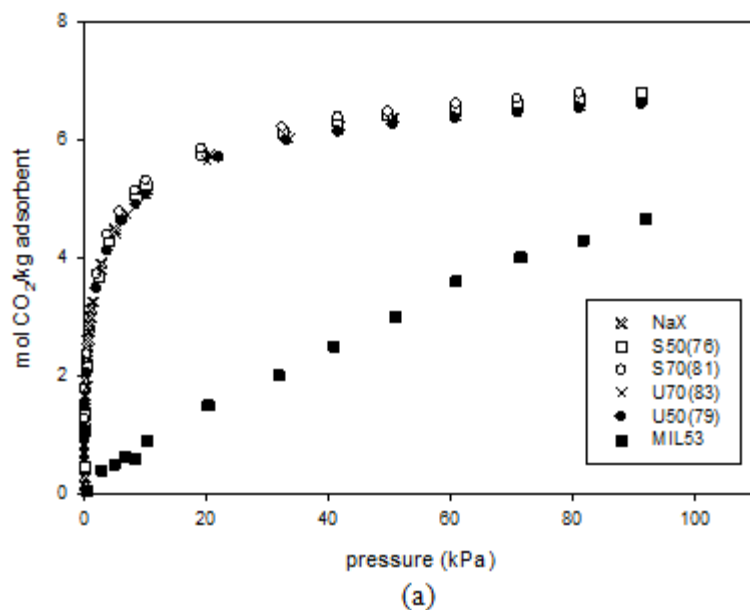


Figure 6.10. CO₂ adsorption isotherm of the zeolites and MOFs at 278K (a) and 298K (b)

Error analysis was applied to the isotherm data. The average uncertainties for CO₂ adsorption on NaX zeolite at 298K was approximately 0.9% (0.001 mmol/g) as depicted by the error bars in Figure 6.11. Good agreement between the replicate runs was obtained. This yield an expected uncertainty of about 0.9% Again, we have been concluded that, the repeated isotherms confirmed the estimated precision of the measurements.

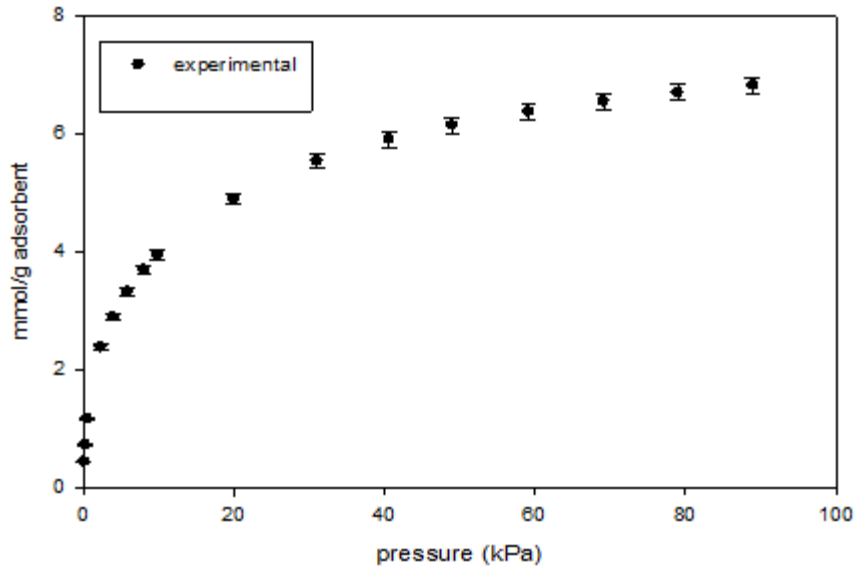


Figure 6.11. CO₂ adsorption isotherm of NaX zeolite at 298 K (error bar is obtained after two measurements)

Langmuir, Freundlich, Toth and Sips model equations were applied to the adsorption data obtained in order to get information regarding the heterogeneity of the adsorbent surfaces. Although the adsorption data were fitted to Langmuir, Freundlich, Toth and Sips models, (as shown in Figure 6.12 representatively), the data did not fitted well with Langmuir and Freundlich model. Toth and Sips isotherm models well described the experimental data obtained in this work with high regression coefficient ($R^2 > 0,98$), F ratio values and smaller standart error values.

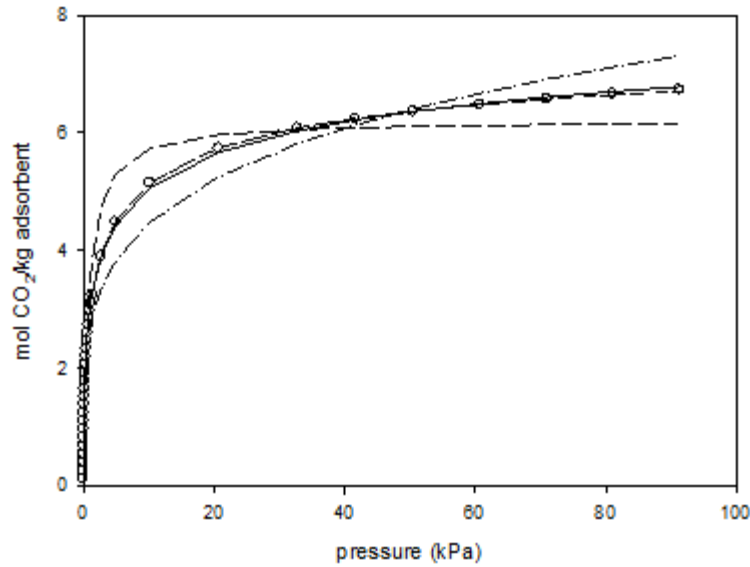


Figure 6.12. Adsorption isotherms of CO₂ at 278 K of NaX zeolite (o: experimental, linecurve fittings Langmiur: - - - Freundlich:— · — Sips: — — — Toth: ————model equations

For Sips and Toth model equations, usually larger of n value than 1 and lower t value than 1, respectively, is the characteristic of the heterogeneous system. System heterogeneity has been confirmed the ability of adsorbate of preferentially adsorption sites (Cavanati et al., 2004). As we have seen in Table 6.3, the Toth model was found to give the best fit for the adsorption data. All t values were found to be smaller than unity. It is confirming the sysyem heterogeneity of the adsorbent. It can be emphasized that surface heterogeneity favors the adsorption of CO₂, since MIL 53 (Al) that show the lowest adsorption capacity at two different temperatures, have also the lowest n (highest t) values for each temperatures, and therefore the lowest surface heterogeneity. However, this information does not point to what is the source of the heterogeneity, whether it is the solid structural property, the solid energetical property or the sorbate property. In other words, heterogeneity is not a solid characteristic alone but rather it is a characteristics of the specific solid and adsorbate pair (Do 1998, Yang 1997). We have noted from the table that the parameter t increased with temperature, suggesting that the system was "apparently" less heterogeneous as temperature increased (Do 1990). When the t values are compared at both temperatures, it can be determined that at 278K, adsorbate-adsorbent system is more heterogeneous since the t values are generally greater at 298K.

According to Table 6.3, NaX has the lowest t value (0.24 and 0.29 respectively) for 278K and 298K indicating that CO_2 -NaX pair is the most heterogeneous system. As it is expected t value increases; the heterogeneity of the system decreases with increasing ion exchange percentage from 76 to 83. The surface heterogeneity favors the adsorption of CO_2 , since U70 (86) which show the lowest adsorption capacity at two different temperatures, it has also the lowest n (highest t) values for each temperature, and therefore the lowest surface heterogeneity between the zeolite adsorbents. Our results are agreed with the results obtained in the literature (Walton et al., 2006). The KNaX of their study was exchanged 76%, while we achieved 86%.

Parameter b for Sips and Toth models, called as affinity constant also shows how strong an adsorbate molecule is attracted onto a surface. When the affinity constant b is large, the surface covered with adsorbate molecule as a result of the strong affinity of adsorbate molecule towards the surface. Besides, as temperature increases, the b values decreases. Among the adsorbents highest b value was obtained for MIL 53(Al) adsorbent. This is expected because of the linear isotherm shape of the MIL 53 (Al) adsorbent isotherms. For zeolite adsorbents highest b value was obtained as 0.34 for NaX zeolite adsorbent at 298K.

Table 6.3. Isotherm Model fitting for CO₂ adsorption data

		Adsorbents											
		NaX		MIL 53 (Al)		S50(76)		U50(79)		S70(81)		U70(86)	
Isotherm model	Parameters	278K	298K	278K	298K	278K	298K	278K	298K	278K	298K	278K	298K
Sips $q = \frac{q_m (bP)^{1/n}}{1 + (bP)^{1/n}}$	$q_m(SE)$	7.98(0.24)	7.65(0.08)	2.32(0.8)	1.51(0.2)	7.3(0.1)	7.6(0.2)	7.32(0.1)	6.51(0.3)	7.4(0.09)	6.47(0.1)	7.7(0.06)	6.5(0.2)
	$b(SE)$	0.34(0.04)	0.31(0.004)	7.7(0.003)	7.6(0.001)	0.31(0.02)	0.23(0.0007)	0.22(0.04)	0.2(0.01)	0.19(0.002)	0.17(0.009)	0.15(0.006)	0.14(0.005)
	$n(SE)$	2.1(0.1)	2(0.02)	1.3(0.01)	1.2(0.03)	1.85(0.03)	1.79(0.03)	1.73(0.08)	1.6(0.16)	1.53(0.04)	1.48(0.06)	1.34(0.02)	1.19(0.08)
	R^2	0.9968	0.9998	0.9999	0.9989	0.999	0.9995	0.9956	0.9954	0.9991	0.9978	0.9997	0.9951
	SE	0.01	0.02	0.03	0.031	0.06	0.05	0.15	0.05	0.05	0.09	0.3	0.12
	SSE	0.16	0.008	0.0008	0.009	0.14	0.05	0.32	0.02	0.03	0.1	0.018	0.19
	$F\text{-ratio}$	2196	34051	113630	4533	17756	23790	1583	6173	6353	2784	22422	1436
Toth $q = \frac{q_m bP}{(1 + (bP)^t)^{(1/t)}}$	$q_m(SE)$	7.1(0.4)	6.89(0.4)	1.7(0.9)	1.4(0.1)	7.3(0.23)	7.1(1)	7.1(0.24)	6.5(0.47)	6.9(0.12)	6.69(0.21)	7.7(0.07)	6.54(0.34)
	$b(SE)$	0.28(0.04)	0.24(0.04)	18(0.3)	14(0.01)	0.22(0.01)	0.21(0.03)	0.19(0.02)	0.171(0.02)	0.17(0.01)	0.166(0.01)	0.15(0.009)	0.139(0.008)
	t	0.24(0.02)	0.29(0.01)	0.71(0.07)	0.82(0.07)	0.35(0.008)	0.4(0.01)	0.43(0.03)	0.5(0.07)	0.54(0.01)	0.61(0.03)	0.67(0.005)	0.69(0.09)
	R^2	0.9973	0.9994	0.99999	0.98	0.9993	0.9990	0.9964	0.9994	0.9994	0.9986	0.9999	0.995
	SE	0.09	0.04	0.0036	0.11	0.05	0.07	0.13	0.04	0.04	0.07	0.02	0.13
	SSE	0.13	0.02	0.001	0.001	0.1	0.14	0.026	0.01	0.02	0.06	0.007	0.21
	$F\text{-ratio}$	2596	12334	672295	15310	243357	13049	1950	6590	9433	4351	55712	1301

P: pressure (kPa), q, q_m are the amount adsorbed (mmole CO₂/ g zeolite) at any pressure and monolayer coverage respectively

Isosteric heat of CO₂ adsorption

The isosteric heat of adsorption is an important parameter to evaluate the adsorption performance of adsorbents. It was calculated by using the Toth equation which gives the best result in fitting of experimental data.

Figure 6.13 shows the variation of the isosteric heat of adsorption for adsorbents with loading. The decrease of the isosteric heat with loading physically means that CO₂ molecules prefer to adsorb onto the sites of high energy. As you can see in Figure 6.13, there is a decreasing trend in isosteric heats as adsorbate loading increases, which shows that all adsorbent samples are strongly heterogeneous and this was also supported by the heterogeneity parameters of the Sips and Toth Models (n and t respectively). This high Q_{st} is attributed to the strong interaction between the quadrupole moments of CO₂ with cations.

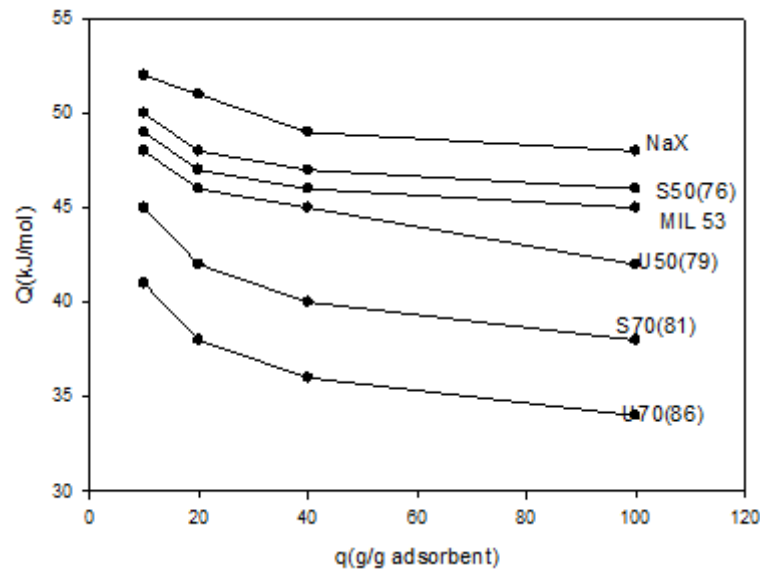


Figure 6.13. Change in heat of adsorption with loading

6.2.2. SMR off-gas CO₂, CH₄, CO and H₂ Adsorption

CO₂, CH₄, CO and H₂ adsorption isotherms on NaX zeolite measured at 298K and 313K in our home made volumetric system are shown in Figure 6.14(a,b) respectively.

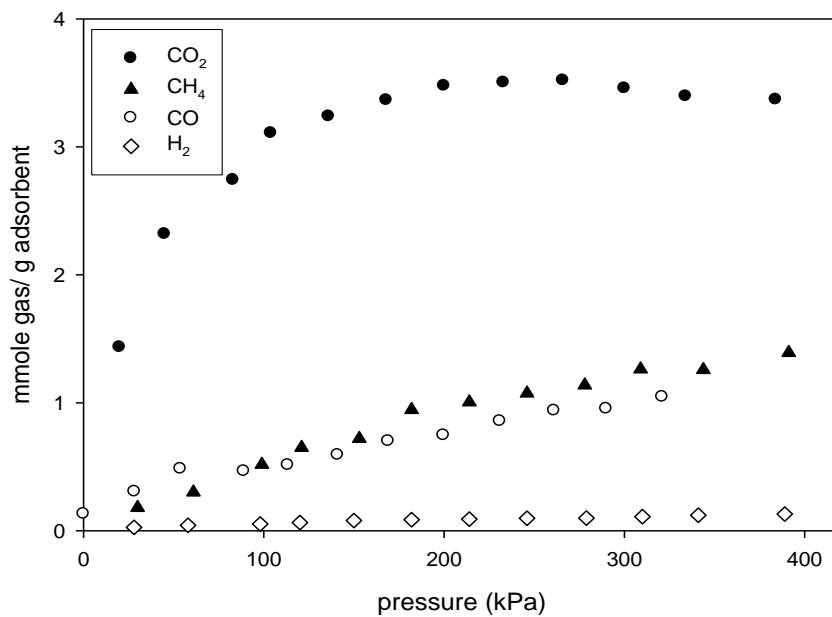
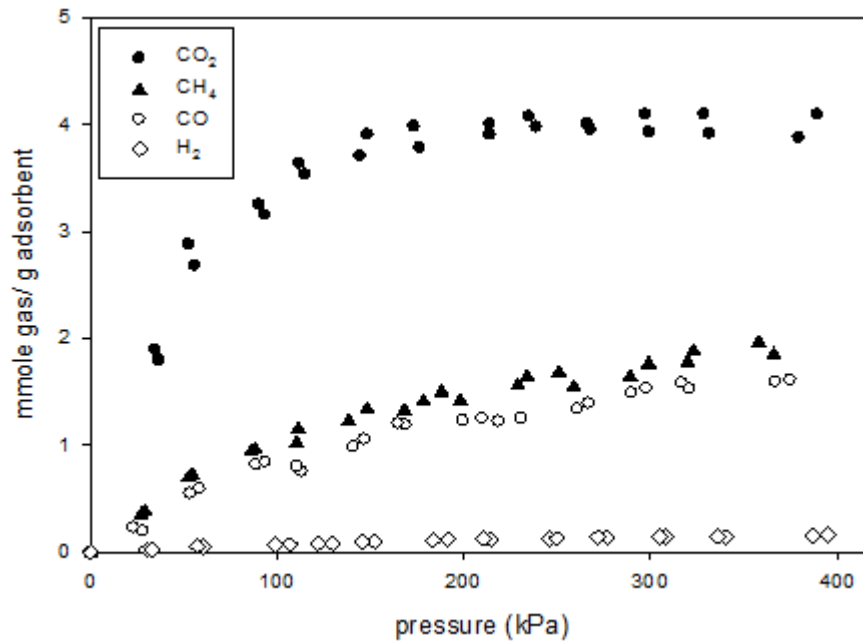


Figure 6.14. CO₂, CH₄, CO, H₂ adsorption equilibrium on zeolite NaX at 298 K (a), 313K(b)

The amount adsorbed at 400 KPa (values in the parenthesis) for zeolite was found to be in the order of CO₂ (3.9, 3.37 mol/kg) > CH₄ (1.8, 1.39 mol/kg) > CO (1.6, 1.04 mol/kg) > H₂ (0.16, 0.13 mol/kg) for 298K and 313K respectively. Amount adsorbed decreases with increasing temperature as expected from physisorption.

Comparison CO₂ adsorption isotherms given in Figure 6.11 and 6.14a (on NaX zeolite at 298K) shows that the amount adsorbed obtained from home made volumetric

system is lower than that from ASAP 2010M depending on the degassing procedure applied; a known mass of adsorbent (10 g in these experiments) was regenerated prior to each isotherm measurement at 573 K under vacuum (10 mbar) for 4h. Prior to adsorption, the samples were degassed for 24 h under vacuum better than 10^{-5} mbar at 350 °C. On the other hand amount adsorbed at 400kPa and 313K 3.5 mmol/g in closed home-made system for NaX zeolite is (Si/Al: 1.12) lower that obtained from open volumetric system for NaX zeolite (Si/Al:1.23) in (5 mmol/g zeolite) another study (Silva et al., 2012).

Our error analysis indicated that the average uncertainties for CO₂, CH₄, CO and H₂ gases adsorption measurements were approximately 3.5% (0.01 mmol/g), 3.2% (0.03 mmol/g), 2.6% (0.01 mmol/g) and 2.3% (0.0095 mmol/g), respectively as depicted by the error bars in Figure 6.15. The error bars generated by error propagation are uncertainties in all measured quantities. The repeated isotherms confirmed the estimated precision of the measurements. Two replicated runs conducted to confirm our measurements shows good agreement between the replicated runs, which yield an expected uncertainty of about 3%.

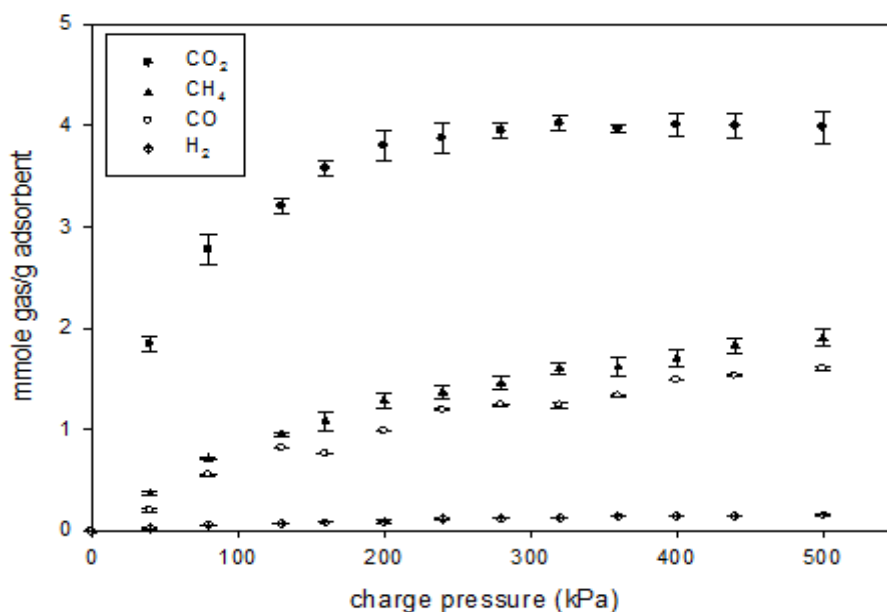


Figure 6.15. Change in amount adsorbed amount with charge pressure

As we have seen in Figure 6.15, the CO₂ adsorption increased rapidly when the pressure was increased up to 50 kPa but the adsorption after 50 kPa appeared to be gradual. At all pressures, adsorption isotherms of CH₄ and CO were lower than those of CO₂, and adsorption isotherm of hydrogen was significantly lower than those of CO₂.

The H₂ amount adsorbed on zeolite NaX was small, and the linearity of the isotherm was clearly seen. On the other hand, the CO₂ isotherm on zeolite NaX showed a high steepness, with an amount adsorbed of 3.9 mol/kg (at 298K and 5atm). This data obtained is slightly lower than the reported one in the literature 4.5 mol/kg (at 298K and 5atm) (Sriwerdane et al., 2001(a); 2001(b), and (Sriwerdane et al., 2001)).

The adsorption isotherm curves for both temperatures obtained reveal that CO₂ has greater affinity to adsorb rather than CH₄. Even though the kinetic diameter of CH₄ (3.8 Å) and CO₂ (3.3 Å) are comparable and small enough to pass through the pore opening of zeolites (Table 4.1). The specific interaction of quadrupole of CO₂ molecule with electric field created by cation is also likely the reason for higher adsorption of CO₂. Non-polar molecules CH₄ have low adsorption affinity towards zeolites as observed in literature (Hernández-Huesca et al., 1999 and Maurin et al., 2005). Henry's constants were obtained by using the Langmuir adsorption equation to calculate the pure component selectivity (Table 6.4).

At 298K and 5atm, the CH₄ amount adsorbed on the zeolite sample was found as 1.8 mol/kg which is comparable with literature. For the same temperature and pressure the CH₄ amount adsorbed was found 1.2 mol/kg (Silva et al., 2012). The data presented compared very well with the low-pressure data in the linear range and up to 100 kPa (Rege et al., 2000, Triebe et al., 1996). At higher pressures, deviation of the data with previous literature was around 15% (Rolniak et al., 1980). This difference at high pressures may be due to different assumptions used for the adsorbed amount calculations and the differences in properties of NaX zeolite.

Hydrogen is the less adsorbed (0.1 mol/kg at 298 K and 4 atm) compound on zeolite. For comparison purposes, higher adsorption equilibrium capacities of hydrogen on NaX zeolite at the same conditions in the literature were reported, i.e., 0.2 mol/kg (Sriwerdane et al., 2001(a), (b)).

The high CO₂ adsorption can be attributed to an electrostatic interaction of the quadrupole moment of this molecule with the Na⁺ cations present in the adsorbent micropores. It was also observed that the isotherms for CO₂ are much more favorable than others due to a stronger CO₂-NaX interaction. As can be seen from the equilibrium isotherms in Figure 6.16, the NaX was found to be very selective to CO₂.

Adsorption isotherms were evaluated by using adsorption equilibrium models. All experimental isotherms were fitted to the models which were described above gas

adsorption models section. The fitted parameter values were listed in Table 6.4 and the model curves were plotted in Figure 6.16.

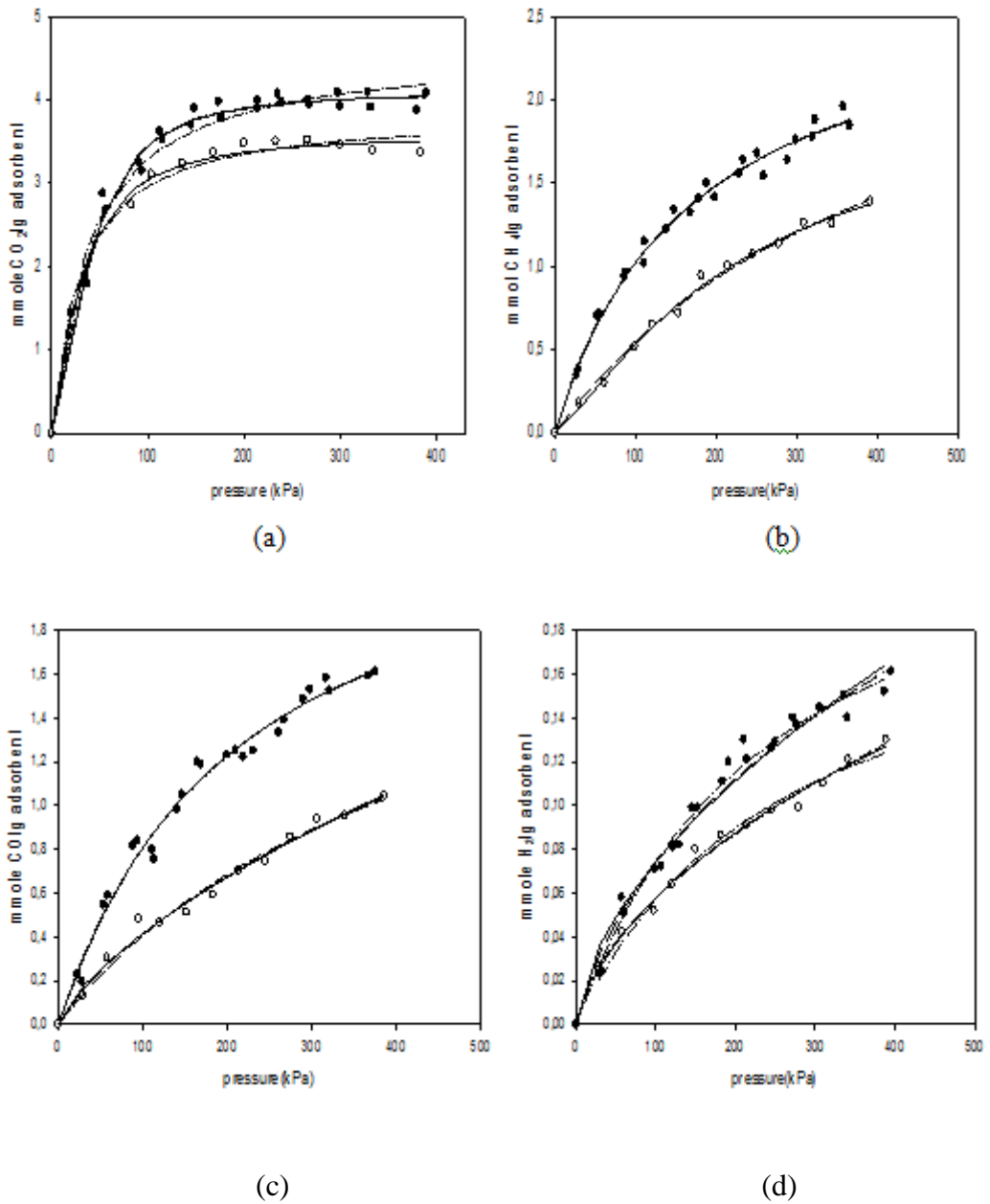


Figure 6.16. Adsorption isotherms of CO_2 , CH_4 , CO , H_2 (●: experimental points at 298K and ○: experimental points at 313K, curve fitting lines Sips: - - - Langmuir - · - · - Toth: ——— model equations)

Table 6.4. Model Fitting and parameters of CO₂, CH₄, CO and H₂ adsorption on NaX zeolite (\pm 95 % confidence interval)

Isotherm model	Parameter	CO ₂		CH ₄		CO		H ₂	
		298K	313K	298K	313K	298K	313K	298K	313K
Langmiur $q = \frac{q_m bP}{1 + bP}$	$q_m(SE)$	4.6 (0.09)	4.3 (0.07)	2.7 (0.08)	2.6 (0.082)	2.5 (0.12)	2.3 (0.11)	0.25 (0.01)	0.22 (0.01)
	$b(SE)$	0.02 (0.002)	0.015 (0.0016)	0.06 (0.0005)	0.05 (0.00043)	0.0046 (0.0005)	0.0042 (0.0003)	0.004 (0.0004)	0.003 (0.0004)
	R^2	0.968	0.976	0.9893	0.9987	0.9848	0.9748	0.98	0.974
	SE	0.17	0.18	0.05	0.04	0.05	0.05	0.0052	0.0032
	SSE	0.7	0.6	0.07	0.06	0.07	0.04	0.006	0.005
	$F\text{-ratio}$	702	700	2117	2200	1488	1502	1760	1800
	$q_m b$	0.09	0.064	0.16	0.13	0.011	0.0096	10 ⁻³	0.00066
Sips $q = \frac{q_m (bP)^{1/n}}{1 + (bP)^{1/n}}$	$q_m(SE)$	4.1 (0.06)	3.48 (0.09)	2.8 (0.03)	2.07 (0.03)	2.4 (0.35)	2.38 (0.3)	1.2(0.1)	1.1(0.09)
	$b(SE)$	0.025 (0.001)	0.021 (0.01)	0.056 (0.001)	0.0043 (0.001)	0.05 (0.001)	0.04 (0.001)	0.004 (0.0001)	0.003 (0.0001)
	$n(SE)$	1.56 (0.053)	0.7 (0.015)	1.1 (0.1)	0.79 (0.009)	1.2 (0.01)	1.16 (0.001)	1.3 (0.01)	1.2 (0.02)
	R^2	0.986	0.987	0.9893	0.991	0.9848	0.986	0.9724	0.98
	SE	0.11	0.09	0.05	0.037	0.05	0.05	0.078	0.082
	SSE	0.31	0.28	0.06	0.05	0.07	0.06	0.08	0.074
	$F\text{-ratio}$	771	790	2300	2390	714	800	1020	1100
Toth $q = \frac{q_m bP}{(1 + (bP)^t)^{1/t}}$	q_m	4 (0.06)	3.5 (0.05)	3 (0.6)	2.37 (0.4)	2.5 (0.6)	2.4	1.2 (0.1)	1.1 (0.1)
	$b(SE)$	0.1 (0.001)	0.094 (0.0001)	0.006 (0.0005)	0.003 (0.0004)	0.0046 (0.0005)	0.0044 (0.0004)	0.0021 (0.0002)	0.0019 (0.0001)
	$t(SE)$	0.21 (0.003)	0.18 (0.003)	0.8 (0.02)	0.7 (0.015)	0.9 (0.01)	0.8 (0.01)	0.8 (0.01)	0.71 (0.01)
	R^2	0.9855	0.989	0.9894	0.99	0.9848	0.985	0.986	0.988
	SE	0.12	0.11	0.05	0.04	0.05	0.05	0.04	0.04
	SSE	0.32	0.26	0.06	0.05	0.07	0.06	0.005	0.004
	$F\text{-ratio}$	746	870	3120	3200	1500	1550	1880	1900
$q_m b$	0.4	0.32	0.018	0.0071	0.011	0.01	2.5*10 ⁻³	2*10 ⁻³	

P: pressure (kPa), q_m : amount adsorbed (mmole / g zeolite)

As seen from Table 6.4 Toth and Sips isotherm models well described the experimental data (with higher R^2 value (>0.98) and F-ratio values (>700) and small error values) than Langmiur isotherm model parameters (When parameter n and t are unity, we recover the Langmuir equation applicable for ideal surfaces). The parameter n for sips model, t for Toth model can be regarded as the parameter characterizing the

system heterogeneity. As seen in Tables 6.4 t and n values were deviates from unity. This could be attributed to the presence heterogeneity of all adsorbent-adsorbate system. As we have seen from Table, highest n and lowest t values were obtained for CO_2 as 1.56, 0.21, respectively. We have noted that the parameter n decreased with temperature, suggesting that the system was "apparently" less heterogeneous as temperature increased (Do 1990).

Parameter b is called as an affinity constant. It is a measure of how strong an adsorbate molecule is attracted onto a surface. When the affinity constant b is larger, the surface is covered more with adsorbate molecule as a result of the stronger affinity of adsorbate molecule towards the surface. As seen in Table 6.4 highest b value was obtained for CO_2 and lowest b value was obtained for H_2 as expected.

Toth model and Langmiur model expression reduces to Henry's law at low adsorbate pressure, in other words (Do, 1998):

$$\lim_{p \rightarrow 0} (b / q) = bq_m = K \quad (6.3)$$

where K is Henry's law constant. Henry constant is related to the interaction energy between the adsorbent and the adsorbate. K values were calculated for Langmuir and Toth models. According to the Henry's constants in Table 6.4, the interaction with CO_2 was the highest for NaX zeolite (as 0.09 for Langmuir model and 0.4 for Toth model) while, the interaction with H_2 was the lowest for both models (as 0.001 for Langmuir model and 0.0025 for Toth model).

The primary requirement for an economic separation process is an adsorbent with sufficiently high capacity, and selectivity based on difference in either adsorption kinetics or adsorption equilibrium. Most of the adsorption processes in current use depend on equilibrium selectivity. The selectivity for one adsorbate at a given pressure is proportional to its adsorbed concentration at that pressure. For NaX zeolite the selectivity order in all the pressure range was the following: $\text{CO}_2 > \text{CH}_4 > \text{CO} > \text{H}_2$. Preferential adsorption of CO_2 on zeolite NaX indicated that this material can be used for the separation of CO_2 from this gas mixture.

6.3. Adsorption Kinetic Studies: Zero Length Column (ZLC)

ZLC is a macroscopic technique for measurement of diffusivity of pure and multicomponent gases in porous solids. It is well mixed cell minimizing the external heat and mass transfer resistance. In this study, CO₂, H₂, CO and CH₄ adsorbed MIL53(Al) in a ZLC is purged at 34 °C, 70 °C or 100 °C. ZLC are subsequently used after regeneration. Regeneration time applied before each adsorption step, and purge flow rate (30- 100 ml/min) and temperature applied in desorption steps are investigated.

Effect of regeneration time on ZLC desorption curves and diffusion coefficients

Period of regeneration time (3h, 6h, 20h) were altered to investigate its effect on transport parameters. CO₂ desorption curve is shown in Fig. 6.17, along with a typical run at 100° C and purge rate 100 ml/min. Only % 0, 02 deviations in the diffusivity was calculated with change in regeneration time. This reveals that the effect of regeneration time on desorption curve may be ignored.

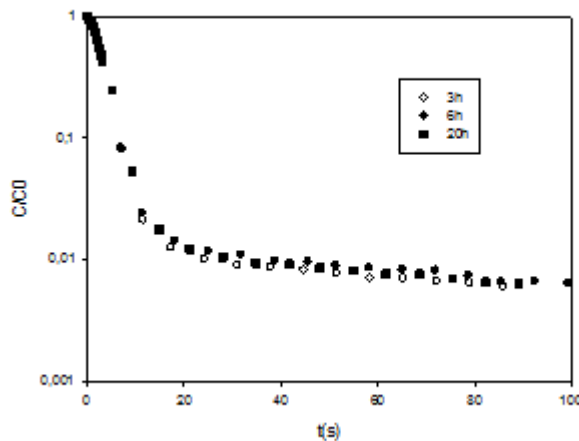


Figure 6.17. CO₂ desorption curves at 100 °C for 3h, 6h, 20h regeneration periods (purge flow rate of 100 ml/min).

Controlling Step in ZLC: equilibrium or kinetic

The response curves measured at different flow rates are simple experimental test to confirm the equilibrium or kinetic control as stated by Loos et al., (2000) and

Iliyas et al., (2008). Figure 6.17 and 6.18 show the response curves obtained in flow rate range of 30-100 ml min⁻¹. Response curves given in the figures did not overlap showing that mass transfer is not controlled by equilibrium.

The L value, at a given temperature, is proportional to the flow rate (F) and used to calculate the equilibrium constant (K) by using Eq. (5.16). The effect of purge flow rate on the key parameter L is also appeared in the same equation;

$$L = \frac{1 \text{ purge flow rate } r^2}{3 \text{ crystals volume } KD_c} = \frac{\left(\frac{r^2}{D_c}\right)}{\left(\frac{3KV_s}{F}\right)} \quad (5.16)$$

The L value is an important parameter for determining whether the transport process is controlled by equilibrium or diffusion (Brandani et al., 1996). If the L value is very low (<0.5), i.e., intraparticle transport is much faster than interparticle one and desorption process will be controlled by equilibrium effects. if L is higher than 10, mass transfer in ZLC is controlled by only diffusion.

The response curves were fitted well (the Sum of square error, SSE \cong 10⁻⁷) with equation 2.22 and to obtain parameters D_c and L (Table 6.5) by using the crystal size (R_c=31.5x10⁻⁵ cm) volume (V_s =5.68x10⁻⁴ cm³) and mass of solid (m_s =2.02 mg):

$$\frac{C}{C_o} = 2L \sum_{n=1}^{\infty} \frac{\exp(-\beta_n^2 D_c t / r^2)}{\beta_n^2 + L(L-1)} \quad (2.22)$$

Considering the L values obtained (L=1.1-5.1) it can be concluded that diffusion is the controlling step. From table, it may be seen that the diffusion time constant, D_c/R², is depend on purge flow rate. The consistency of diffusivity for different purge rate indicates that transport process is controlled by intraparticle diffusion rather than by equilibrium.

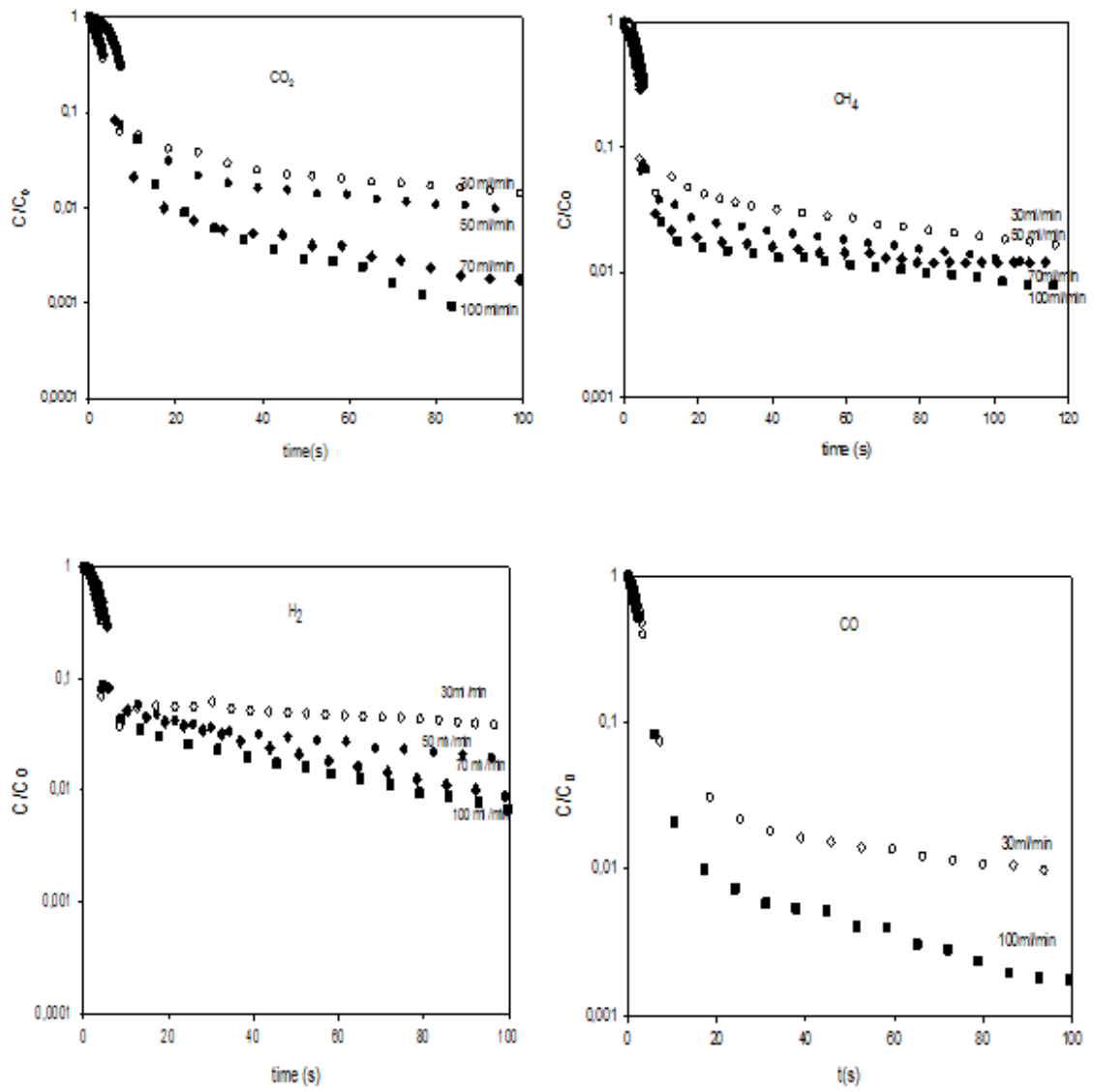


Figure 6.18a. Effect of flow rates on CO_2 response curve at 100 °C. and CO , CH_4 , H_2 response curves at 34 °C.

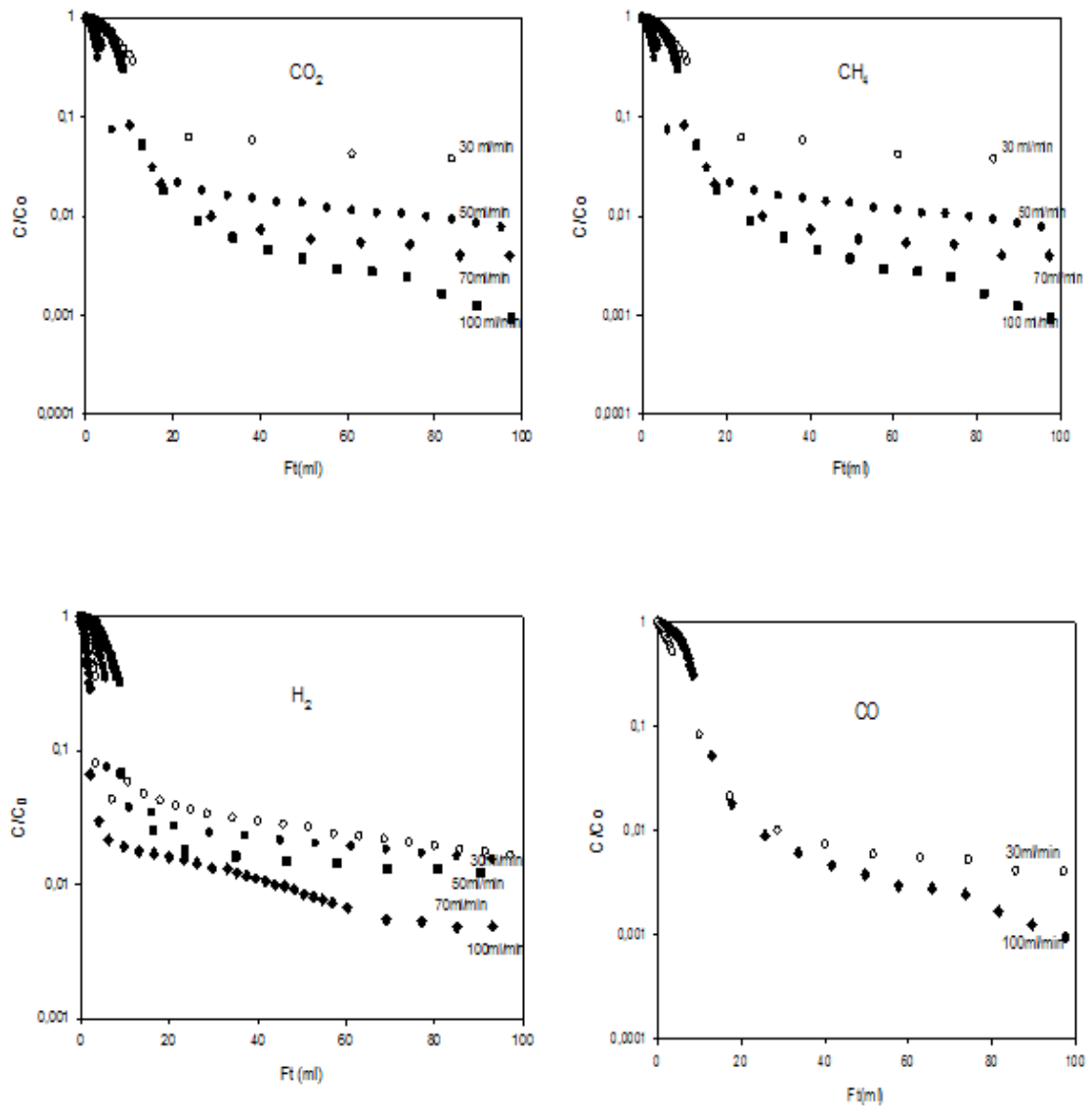


Figure 6.18b. Effect of flow rates on CO_2 response curve at 100 °C. and CO , CH_4 , H_2 response curves at 34 °C.

Table 6.5. Transport parameters of CO₂, CH₄, H₂, CO adsorption on MIL 53 (Al)

T (°C)	F(ml/min)	L	F/L(ml/min)	100*D/R ² (s ⁻¹)	D (m ² /s)	KV _s (ml)	K×10 ⁻³
CO₂							
34.00	100.00	2.88	34.72	1.40	3.44E-12	829.33	146.00
70.00	100.00	2.95	33.90	3.27	8.07E-12	345.13	60.76
100.00	30.00	1.30	23.08	3.29	8.10E-12	193.68	34.09
	50.00	2.39	20.92	3.61	8.90E-12		
	70.00	2.70	25.93	3.69	9.10E-12		
	100.00	3.10	32.26	3.81	9.40E-12		
CH₄							
34.00	30.00	1.11	27.03	1.05	2.60E-12	667.34	117.49
	50.00	1.90	26.32	1.24	3.06E-12		
	70.00	2.69	26.02	1.42	3.50E-12		
	100.00	3.56	28.09	1.54	3.80E-12		
70.00	100.00	3.82	26.18	3.29	8.10E-12	265.54	46.74
100.00	100.00	5.10	19.61	4.05	9.98E-12	161.43	28.42
H₂							
34.00	30.00	1.13	26.55	0.99	2.45E-12	1153.59	203.09
	50.00	1.16	43.10	1.25	3.07E-12		
	70.00	2.2	31.82	1.26	3.10E-12		
	100.00	2.3	43.48	1.38	3.40E-12		
70.00	100.00	2.65	37.74	2.47	6.10E-12	508.27	89.48
100.00	100.00	2.72	36.76	2.60	6.40E-12	471.98	83.09
CO							
34.00	30.00	1.11	27.0	0.97	2.4E-12	925.26	162.89
	100.00	1.22	81.96	1.54	3.8E-12		
70.00	100.00	3.82	26.17	2.79	6.9E-12	311.72	54.88
100.00	100.00	4.2	23.80	3.23	7.9E-12	245.14	43.15

Effect of the temperature on ZLC desorption curves and diffusion coefficients

CO₂, CH₄, H₂, CO desorption curves at different temperatures are given in Fig 6.19. It reveals a temperature dependence of the curves. The parameters obtained (Table 6.6) are affected by temperature in a consistent way; the diffusivity of CO₂, CH₄, H₂, CO in the pores increases with increasing temperature; equilibrium constant on the surface of the pores decreases with increasing temperature.

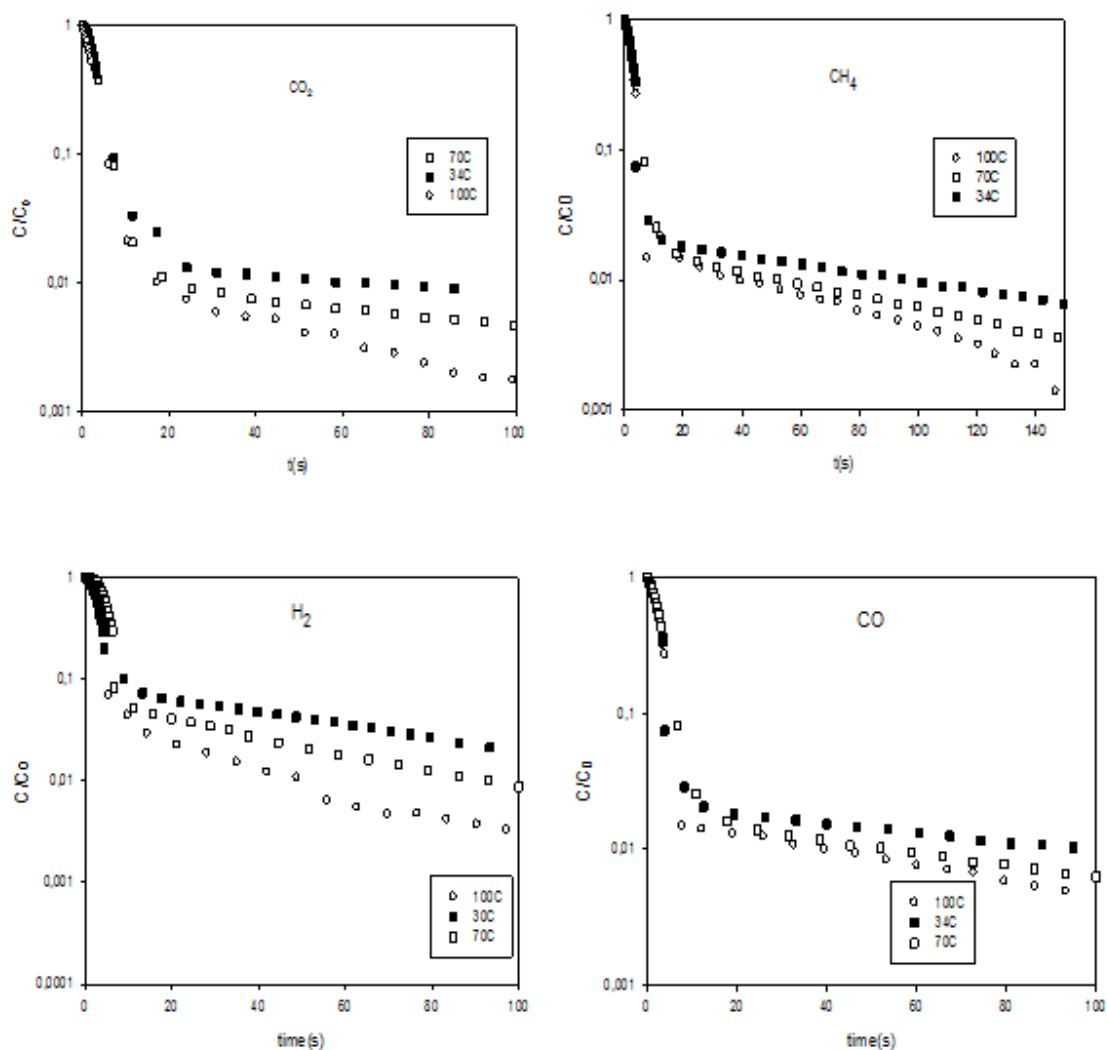


Figure 6.19. Effect of temperature on the response curves of CO₂, CH₄, H₂, CO (Helium flow rate=100 ml/min).

There are evident for Knudsen diffusivity in the pores: the calculated lowest mean free path 10^3 times higher than average pore diameter of MIL 53(Al); temperature dependency is lower for transport diffusivity than molecular diffusivity.

Activation Energy and Isotheric heat of adsorption

Figure 6.21 shows the change in Henry's constant with reciprocal temperature. It can be seen that the Henry's law constant decreases with increasing temperature, as expected for physical adsorption. The Van't Hoff equation (2.29) with neglecting the differences in heat capacities between the adsorptive and adsorbate, can be used to calculate heat of adsorption after integration of Van't Hoff equation:

$$K = K_0 \exp(-\Delta H / RT) \quad (2.30)$$

The heat of adsorption, determined from the slope of the Ln K vs 1/T line, according to Eq. 2.29, is listed in Table 6.27. The temperature dependence of the diffusivity is correlated by the Arrhenius equation (2.27) was used to calculate the diffusive activation energy E;

$$E = -R \left(\frac{\partial \ln D}{\partial (1/T)} \right) \quad (2.28)$$

where T is the temperature and R is the ideal gas constant. The activation energies derived from the diffusivity data as described above are listed in Table 6.7.

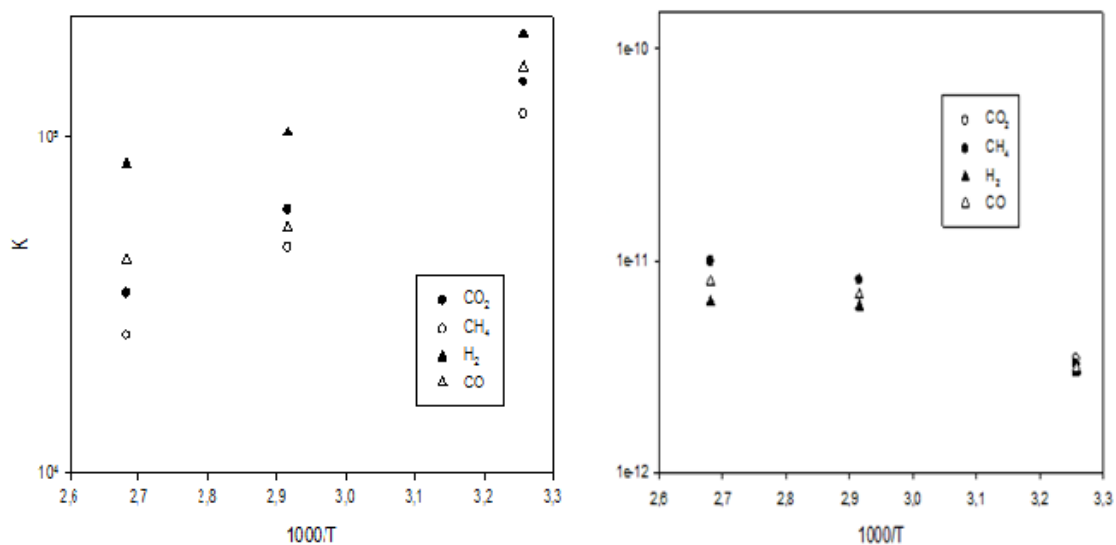


Figure 6.20. Variation of Henry's law constant and diffusivity and with temperature for adsorption of CO₂, CH₄, H₂, CO

Negative heat of adsorption values indicates the adsorption is exothermic; heat is evolved. It can be seen that similar heat of adsorption values are obtained for CO₂ and CH₄ (49,4 and 47,1 kJ/ mol , respectively) and CO and H₂ (38.7 and 34.1 kJ/ mol , respectively). Specific (Dipole moment and quadropole moment) and Nonspecific (polarizability, dispersion and repulsion) contributions are affected to the heat of adsorption values. Even though polarizabilities are nearly same (Table 6.6), it is expected higher specific interactions for CO₂ due to high quadropole moment. As a result, higher heat of adsorption and Henry's law constant values were obtained for CO₂. Low polarizability of CO and H₂ results with lower heat of adsorption than CO₂ and CH₄.

Table 6.6 Sorbate properties and heat of adsorption, activation energy values

Adsorptive	Temperature range(°C)	E (kJ/mol)	ΔH (kJ/mol)	Polarizability $\times 10^{25}/\text{cm}^3$	Kinetic diameter Å	Dipole moment $\times 10^{18}$ esu cm	Quadropole moment $\times 10^{26}$ esu cm ²
CH ₄	34-100	41.4	-47.1	25.93	3.8	0	0
CO		40.9	-38.7	19.5	3.6	0.1098	2.5
CO ₂		43.9	- 49.4	29.11	3.3	0	4.30
H ₂		41.2	-34.1	8.04	2.8	0	0.662

Method Validation

The accuracy of diffusivities obtained above can be validated by using a long time method (tail of the response curve)

$$\frac{C}{C_o} = \frac{2L}{\beta_1^2 + L(L-1)} \exp\left(-\frac{\beta_1^2 D_c t}{r^2}\right) \quad (2.23)$$

which is appropriate for kinetic conditions. It was found that the errors in using equation 2.24 are in the range of 2–8.2%, which provides strong support for the values obtained by full range procedure. Nevertheless, while the consistency of the results between the two methods is reassuring, it is desirable to compare the results with those using FR method since all entire desorption curve is considered. It can be concluded that the desorption process is significantly diffusion affected at which can be further confirmed a long time analysis method (as described above) suggested for the range of $0.5 < L < 5$. Since CO₂, CH₄, H₂, CO are strongly adsorbed.

Selectivity

The kinetic selectivity gives an idea about which adsorbent is the best to separate gas mixture. The kinetic selectivity of gas A over gas B, $S_{A/B}$ depends on both adsorption rate and equilibrium.

$$S_{A/B} = \frac{K_A}{K_B} \sqrt{\frac{D_A}{D_B}} \quad (2.32)$$

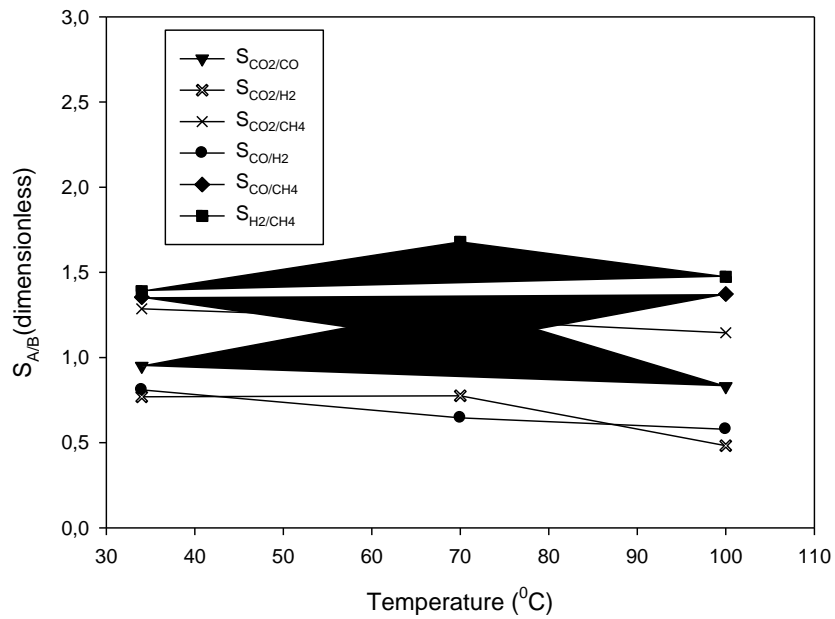


Figure 6.21. The kinetic selectivity, $S_{A/B}$, for MIL 53(A1)

The selectivities $S_{CO_2/CO}$, S_{CO_2/H_2} , S_{CO_2/CH_4} , S_{CO/H_2} , S_{CO/CH_4} , S_{H_2/CH_4} were calculated and presented as a function of temperature (Figure 6.22). The kinetic selectivities are found as around 1 values all temperatures. The lowest selectivities are obtained for CO_2/CH_4 , CO/H_2 pair that found as lower than 1 values.

Selectivities are not a strong function of temperature. As seen from ZLC results MIL 53(A1) is a good adsorbent for H_2 compared to the others.

CHAPTER 7

CONCLUSION

NaX zeolite, a porous crystalline aluminosilicate, has three dimensional open framework consisting of AlO_4 and SiO_4 tetrahedra linked to each other by sharing all of the oxygens. The framework bears negative charges on AlO_4 tetrahedron which are balanced by an extra-framework cation such as alkaline or alkaline earth ions. These cations are mobile and undergo ion exchange. In this study, the introduction of K^+ ions into NaX frameworks was performed. The effect of the temperature ($50\text{ }^\circ\text{C}$ and $70\text{ }^\circ\text{C}$) in the exchange were examined in the presence of ultrasound. The results were compared with those obtained from traditional batch method. The exchange levels were increased with temperature and ultrasound effect. Maximum exchange percent was obtained as 86 for K^+ ions exchange. The ultrasonic method applied in this study was found to effective on the exchange amount at equilibrium as similar to Erten et al., studies (Erten et al., 2012). Due to cavitation effect of ultrasound field, ultrasound acted like a co-driven force of concentration of counter ions in solution. This can be caused an increasing the equilibrated values in ion exchange process.

Additional to KNaX zeolites, MIL 53 (Al) adsorbent evaluated as a potential adsorbent for CO_2 adsorption. The MIL 53 (Al) adsorbent has a langmuir specific surface area of $1473\text{ m}^2/\text{g}$. For MIL 53 adsorbent at temperatures of 278 and 298 K all systems show linear adsorption isotherm (Yang 1987). Highly favorable CO_2 adsorption isotherm was obtained at 278K and 298K for zeolite adsorbents. The orders for zeolite adsorbents are not changed with respect to temperature which are as follows; NaX >S50 (76) >U50 (79)>S70 (81)> U70 (83). From the order, it can be concluded that NaX zeolite has the highest adsorption capacity and among the modified zeolites. CO_2 adsorption data fitting to the theoretical models allows to conclude that carbon dioxide adsorption on the adsorbents is related to the surface heterogeneity of the adsorbent materials, the data better reproduced by Tóth model. Therefore this equation is used to calculate the isosteric heat of adsorption. Isosteric heat of adsorption of carbondioxide on adsorbents decreases with loading, which indicates the heterogeneity of the CO_2 -adsorbent systems.

We have provided adsorption equilibrium of the gases exiting SMR of-gases. Adsorption equilibrium of CO_2 , CH_4 , CO and H_2 was measured at 278K, 298K between 0–5

atm in zeolite NaX. The Langmuir, Sips, Toth models were employed to fit the experimental data of H₂, CO₂, CH₄, CO. It was found that Toth, Sips models could describe the adsorption isotherms. The following orders of adsorption (from the most adsorbed compound to the less adsorbed gas) CO₂>CH₄>CO>H₂ were observed in the sample of NaX zeolite.

The diffusion kinetics for SMR off-gas on MIL 53(Al) were measured in the 34-100 °C temperature range by the ZLC method. Thus it minimizes the external resistance to heat and mass transfer. The experimental data were well correlated with the model ($R^2 > 0.98$ and $SSE > 10^{-7}$). The low value of the micropore time constant ($D_c/r^2 \ll 0.05$) also shows that internal mass transfer resistance is the controlling step. A full time range analysis of desorption curves was taken to derive diffusion coefficients. The diffusivity obtained is in range (2,6–9.98) 10^{-12} cm²/s. The diffusivity values are dependent on temperature, flow rate and independent from the regeneration time. The study shows that the ZLC method is an effective tool for studying the diffusion kinetics of SMR off-gas on MIL 53 (Al).

REFERENCES

- Babarao, R.; Jiang, J. W., Molecular screening of metal-organic frameworks for CO₂ storage. *Langmuir* **2008**, *24* (12), 6270-6278.
- Bae Sang Omar K. Farha, Alexander M. Spokoyny, Chad A. Mirkin, Joseph T. Hupp and Randall Q. Snurr Chem Carborane-based metal-organic frameworks as highly selective sorbents for CO₂ over methane *Youn-Commun.* **2008**, 4135-4137.
- Banerjee, R.; Phan, A.; Wang, B.; Knobler, C.; Furukawa, H.; O'Keeffe, M.; Yaghi, O. M., High-throughput synthesis of zeolitic imidazolate frameworks and application to CO₂ capture. *Science* **2008**, *319* (5865), 939-943.
- Barcia, P. S.; Silva, J. A. C.; Rodrigues, A. E., Adsorption equilibrium and kinetics of branched hexane isomers in pellets of BETA zeolite. *Micropor Mesopor Mat* **2005**, *79* (1-3), 145-163.
- Barman, S.; Pradhan, N.C.; Basu, J.K. Kinetics of Alkylation of Phenol with Methanol over Ce-Exchanged NaX Zeolite. *Catalysis Letters.* **2006**, *111*, 67-73.
- Bekum, H.V.; Flanigen, E.M.; Jacobs, P.A.; Jansen, J.C. *Introduction to Zeolite Science and Practice*; 2nd completely revised and expanded edition, Elsevier Science Publishing Company Inc. Newyork, **2001**
- Bourrelly, S.; Llewellyn, P. L.; Serre, C.; Millange, F.; Loiseau, T.; Ferey, G., Different adsorption behaviors of methane and carbon dioxide in the isotopic nanoporous metal terephthalates MIL-53 and MIL-47. *J Am Chem Soc* **2005**, *127* (39), 13519-13521.
- Brandani, F.; Brandani, S.; Coe, C.G.; Ruthven, D.M. Measurement of Henry Constants and Equilibrium Isotherms by the ZLC Technique. *Fundamentals of Adsorption.* **2002**, *7*, 21 - 28.
- Brandani, F.; Ruthven, D. ZLC response for systems with surface resistance control, *Adsorption*, **2005**, *11*, 31-34.
- Brandani, F.; Ruthven, D.; Coe, C.G. Measurement of Adsorption Equilibrium by the Zero Length Column (ZLC) Technique Part 1: Single-Component Systems, *Ind. Eng. Chem. Res.*, **2003**, *42*, 1451-1461.
- Brandani, S.; Gunadi, A. Diffusion of Linear Paraffins in NaCaA Studied by the ZLC Method. *Microporous and Mesoporous Materials.* **2006**, *90*, 278-283.
- Brandani, S.; Ruthven, D.M. Analysis of ZLC Desorption Curves for Gaseous Systems. *Adsorption*, **1996**, *2*, 133-143.
- Breck, D.W. *Physical Properties of Crystalline Zeolites in Zeolite Molecular Sieves: Structure, Chemistry and Use*; A Wiley-Interscience Publication: New York, **1974**.

- Buhl, J.-Ch.; Gerstmann, M.; Lutz, W.; Ritzmann, A. Hydrothermal Stability of the Novel Zeolite Type LSX in Comparison to the Traditional 13X Modification, Hannover, *Institut für Mineralogie*, **2003**.
- Buhl, J.-Ch.; Gerstmann, M.; Lutz, W.; Ritzmann, A. Hydrothermal Stability of the Novel Zeolite Type LSX in Comparison to the Traditional 13X Modification. *Z. Anorg. Allg. Chem.* **2004**, 630, 604-608.
- Chen, B. L.; Eddaoudi, M.; Hyde, S. T.; O'Keeffe, M.; Yaghi, O. M., Interwoven metal-organic framework on a periodic minimal surface with extra-large pores. *Science* **2001**, 291 (5506), 1021-1023.
- Chui, S. S. Y.; Lo, S. M. F.; Charmant, J. P. H.; Orpen, A. G.; Williams, I. D., A chemically functionalizable nanoporous material [Cu-3(TMA)(2)(H₂O)(3)](n). *Science* **1999**, 283 (5405), 1148-1150.
- Delgado, J. A.; Uguina, M. A.; Gomez, J. M.; Ortega, L., Adsorption equilibrium of carbon dioxide, methane and nitrogen onto Na- and H-mordenite at high pressures. *Sep Purif Technol* **2006**, 48 (3), 223-228.
- Dinca M. and Long J. R., Strong H₂ Binding and Selective Gas Adsorption within the Microporous Coordination Solid Mg₃(O₂C-C₁₀H₆-CO₂)₃. *J. Am. Chem. Soc.*, **2005**, 127, 9376-9377.
- Do, D.D. *Adsorption Analysis: Equilibria and Kinetics*; Imperial College Press: London, **1998**.
- Drage, T. C.; Blackman, J. M.; Pevida, C.; Snape, C. E., Evaluation of Activated Carbon Adsorbents for CO₂ Capture in Gasification. *Energ Fuel* **2009**, 23, 2790-2796.
- Dunne, J. A.; Rao, M.; Sircar, S.; Gorte, R. J.; Myers, A. L., Calorimetric heats of adsorption and adsorption isotherms .2. O-2, N-2, Ar, CO₂, CH₄, C₂H₆, and SF₆ on NaX, H-ZSM-5, and Na-ZSM-5 zeolites. *Langmuir* **1996**, 12 (24), 5896-5904.
- Dybtsev, D. N.; Chun, H.; Yoon, S. H.; Kim, D.; Kim, K., Microporous manganese formate: A simple metal-organic porous material with high framework stability and highly selective gas sorption properties. *J Am Chem Soc* **2004**, 126 (1), 32-33.
- Eic, M.; Micke, A.; Kocirik, M.; Jama, M.; Zikanova, A. Diffusion and Immobilization Mechanisms in Zeolites Studied by ZLC Chromatography. *Adsorption*, **2002**, 8: 15–22.
- Eic, M.; Micke, A.; Kocirik, M.; Jama, M.; Zikanova, A. Diffusion and Immobilization Mechanisms in Zeolites Studied by ZLC Chromatography. *Adsorption*, **2002**, 8: 15–22.
- Entezari, M.H.; Tahmasbi, M. Water Softening by Combination of Ultrasound and Ion Exchange. *Ultrason. Sonochem.* **2009**, 16, 356-360.
- Faghihian, H.; Amini, M.K.; Nezamzadeh, A.R. Cerium Uptake by Zeolite A Synthesized from Natural Clinoptilolite Tuffs. *Journal of Radioanalytical and Nuclear Chemistry.* **2005**, 264, 577-582.

- Forster, P. M.; Thomas, P. M.; Cheetham, A. K., Biphasic solvothermal synthesis: A new approach for hybrid inorganic-organic materials. *Chem Mater* **2002**, *14* (1), 17-20
- Grande, C.A.; Silva, V.M.T.M.; Gigola, C.; Rodrigues, A.E. Adsorption of Propane and Propylene onto Carbon Molecular Sieve. *Carbon*. **2003**, *41*, 2533-2545.
- Guimarães, A.P.; Möller, A.; Staudt R.; Azevedo D.C.; Lucena, S.M.P.; Cavalcante C.L. Diffusion of Linear Paraffins in Silicalite Studied by the ZLC Method in the Presence of CO₂. *Adsorption*, **2010**, *16*, 29–36.
- Harlick, P. J. E.; Tezel, F. H., An experimental adsorbent screening study for CO₂ removal from N₂. *Micropor Mesopor Mat* **2004**, *76* (1-3), 71-79.
- Hayashi, H.; Cote, A. P.; Furukawa, H.; O'Keeffe, M.; Yaghi, O. M., Zeolite a imidazolate frameworks. *Nat Mater* **2007**, *6* (7), 501-506.
- Huften, R.J.; Ruthven, M.D. Diffusion of Light Alkanes in Silicalite Studied by the Zero Length Column Method. *Ind. Eng. Chem. Res.* **1993**, *32*, 2379-2386.
- Jasra, R.V.; Tyagi, B.; Badheka, Y.M.; Choudary, V.N.; Bhat, T.S.G. Effect of Clay Binder on Sorption and Catalytic Properties of Zeolite Pellets. *Ind. Eng. Chem. Res.*, **2003**, *42*, 3263-3272.
- Karge, H.; Weitkamp, J. *Adsorption and Diffusion: Molecular Sieves, Science and Technology*; Springer-Verlag Berlin Heidelberg, **2008**.
- Keller, J.U.; Staudt, R. *Gas Adsorption Equilibria: Experimental Methods And Adsorptive Isotherms*; Springer Science and Business Media: Boston, **2005**.
- Kim, J. B. Li⁺- and H⁺- Exchanged Low Silica X Zeolite as Selective Nitrogen Adsorbent for Air Separation. *Bull. Korean Chem. Soc.* **2003**, *24*, 1814-1817.
- Kim, K-H.; Kim, K-B. Ultrasound Assisted Synthesis of Nano-sized Lithium Cobalt Oxide. *Ultrasonics Sonochemistry*. **2008**, *15*, 1019-1025.
- Kitagawa, S.; Kitaura, R.; Noro, S., Functional porous coordination polymers. *Angew Chem Int Edit* **2004**, *43* (18), 2334-2375.
- Kitaura, R.; Seki, K.; Akiyama, G.; Kitagawa, S., Porous coordination-polymer crystals with gated channels specific for supercritical gases. *Angew Chem Int Edit* **2003**, *42* (4), 428-431
Li Y, Yang R T. (2007), Gas adsorption and storage in metal-organic framework MOF-177. *Langmuir*, *23*: 12 937-12 944.
- Li, C. J.; Lin, Z. J.; Peng, M. X.; Leng, J. D.; Yang, M. M.; Tong, M. L., Novel three-dimensional 3d-4f microporous magnets exhibiting selective gas adsorption behavior. *Chem Commun* **2008**, (47), 6348-6350.
- Liu, X. W.; Li, J. W.; Zhou, L.; Huang, D. S.; Zhou, Y. P., Adsorption of CO₂, CH₄ and N₂ on ordered mesoporous silica molecular sieve. *Chem Phys Lett* **2005**, *415* (4-6), 198-201.

- Llewellyn, P. L.; Bourrelly, S.; Serre, C.; Filinchuk, Y.; Ferey, G., How hydration drastically improves adsorption selectivity for CO₂ over CH₄ in the flexible chromium terephthalate MIL-53. *Angew Chem Int Edit* **2006**, *45* (46), 7751-7754.
- Loiseau, T.; Lecroq, L.; Volkringer, C.; Marrot, J.; Ferey, G.; Haouas, M.; Taulelle, F.; Bourrelly, S.; Llewellyn, P. L.; Latroche, M., MIL-96, a porous aluminum trimesate 3D structure constructed from a hexagonal network of 18-membered rings and $\mu(3)$ -oxo-centered trinuclear units. *J Am Chem Soc* **2006**, *128* (31), 10223-10230.
- Loiseau, T.; Serre, C.; Huguenard, C.; Fink, G.; Taulelle, F.; Henry, M.; Bataille, T.; Ferey, G., A rationale for the large breathing of the porous aluminum terephthalate (MIL-53) upon hydration. *Chem-Eur J* **2004**, *10* (6), 1373-1382.
- Loos, J-B W.P.; Verheijen, P.J.T.; Moulijn, J.A. Improved Estimation of Zeolite Diffusion Coefficients from Zero-Length Column Experiments. *Chemical Engineering Science*. **2000**, *55*, 51-65.
- Loos, J-B W.P.; Verheijen, P.J.T.; Moulijn, J.A. Improved Estimation of Zeolite Diffusion Coefficients from Zero-Length Column Experiments. *Chemical Engineering Science*. **2000**, *55*, 51-65.
- Ma, S. Q.; Wang, X. S.; Manis, E. S.; Collier, C. D.; Zhou, H. C., Metal-organic framework based on a trinickel secondary building unit exhibiting gas-sorption hysteresis. *Inorg Chem* **2007**, *46* (9), 3432-3434..
- Ma, S. Q.; Wang, X. S.; Yuan, D. Q.; Zhou, H. C., A coordinatively linked Yb metal-organic framework demonstrates high thermal stability and uncommon gas-adsorption selectivity. *Angew Chem Int Edit* **2008**, *47* (22), 4130-4133.
- Malekian, A.; Vinh-Thang, H.; Huang, Q.; Eić, M.; Kaliaguine, S. Evaluation of the Main Diffusion Path in Novel Micro-Mesoporous Zeolitic Materials with the Zero Length Column Method. *Ind. Eng. Chem. Res.* **2007**, *46*, 5067-5073.
- Meek, S. T.; Greathouse, J. A.; Allendorf, M. D., Metal-Organic Frameworks: A Rapidly Growing Class of Versatile Nanoporous Materials. *Adv Mater* **2011**, *23* (2), 249-267.
- Millward, A. R.; Yaghi, O. M., Metal-organic frameworks with exceptionally high capacity for storage of carbon dioxide at room temperature. *J Am Chem Soc* **2005**, *127* (51), 17998-17999
- Moon, H. R.; Kobayashi, N.; Suh, M. P., Porous metal-organic framework with coordinatively unsaturated Mn-II sites: Sorption properties for various gases. *Inorg Chem* **2006**, *45* (21), 8672-8676.
- Mueller, U.; Schubert, M.; Teich, F.; Puetter, H.; Schierle-Arndt, K.; Pastre, J., Metal-organic frameworks - prospective industrial applications. *J Mater Chem* **2006**, *16* (7), 626-636.
- Navarro, J. A. R.; Barea, E.; Rodriguez-Dieguez, A.; Salas, J. M.; Ania, C. O.; Parra, J. B.; Masciocchi, N.; Galli, S.; Sironi, A., Guest-induced modification of a magnetically active ultramicroporous, gismondine-like, Copper(II) coordination network. *J Am Chem Soc* **2008**, *130* (12), 3978-3984.

- Pan, L.; Adams, K. M.; Hernandez, H. E.; Wang, X. T.; Zheng, C.; Hattori, Y.; Kaneko, K., Porous lanthanide-organic frameworks: Synthesis, characterization, and unprecedented gas adsorption properties. *J Am Chem Soc* **2003**, *125* (10), 3062-3067.
- Rege, S.U.; Yang, R.T.; Qian, K.; Buzanowski, M.A. Air-Prepurification by Pressure Swing Adsorption Using Single/layered Beds. *Chemical Engineering Science*. **2001**, *56*, 2745-2759.
- Rouquerol, F.; Rouquerol, J.; Sing, K. S. W. *Adsorption by Powders and Porous Solids: Principles, Methodology and Applications*; Academic Press, San Diego, **1999**.
- Ruthven, D.M.; Brandani, S. Analysis of ZLC Desorption Curves for Liquid Systems. *Chemical Engineering Science*. **1995**, *50*, 2055-2059.
- Ruthven, D.M.; Brandani, S. Analysis of ZLC Desorption Curves for Liquid Systems. *Chemical Engineering Science*. **1995**, *50*, 2055-2059.
- Ruthven, M.D. Molecular Sieve Separations. *Chemie Ingenieur Technik*. 2011, *83*, 44–52.
- Ruthven, M.D. *Principles of Adsorption and Adsorption Processes*; A Wiley- Interscience Publication, Newyork, **1984**.
- Ruthven, M.D.; Reyes, S.C. Adsorptive Separation of Light Olefins from Paraffins. *Microporous and Mesoporous Materials*. **2007**, *104*, 59–66.
- Saha, D.; Wei, Z. J.; Deng, S. G., Equilibrium, kinetics and enthalpy of hydrogen adsorption in MOF-177. *Int J Hydrogen Energ* **2008**, *33* (24), 7479-7488
- Hernandez, H. E.; Wang, X. T.; Zheng, C.; Hattori, Y.; Kaneko, K., Porous lanthanide-organic frameworks: Synthesis, characterization, and unprecedented gas adsorption properties. *J Am Chem Soc* **2003**, *125* (10), 3062-3067.
- Salles, F.; Jobic, H.; Ghoufi, A.; Llewellyn, P. L.; Serre, C.; Bourrelly, S.; Ferey, G.; Maurin, G., Transport Diffusivity of CO₂ in the Highly Flexible Metal-Organic Framework MIL-53(Cr). *Angew Chem Int Edit* **2009**, *48* (44), 8335-8339.
- Savitz, S.; Siperstein, F.R.; Huber, R.; Tieri, S. M.; Gorte, R.; Myers, A.; Grey, C.P.; Corbin, D.R. Adsorption of Hydrofluorocarbons HCF-314 and HCF-314A on X and Y Zeolites: Effect of Ion-Exchange on Selectivity and Heat of Adsorption. *J.Phys.Chem.B*. **1999**, *103*.
- Sheldrick, W. S.; Wachhold, M., Solventothermal synthesis of solid-state chalcogenidometalates. *Angewandte Chemie-International Edition in English* **1997**, *36* (3), 207-224.
- Shen, D.; Bülow, M.; Jale, S.R.; Fitch, F.R.; Ojo, A.F. Thermodynamics of Nitrogen and Oxygen Sorption on Zeolites LiLSX and CaA. *Microporous and Mesoporous Material*. **2001**, *48*, 211-217.
- Shinde, P.D.; Mahajan, V.A.; Borate, H.B.; Tillu, V.H.; Bal, R.; Chandwadkar, A.; Wakharkar, R.D. Li-X Type Zeolite Mediated Michael Addition of Thiols to Cyclic

- Enones and its Application in the Synthesis of 13-Thiaprostaglandins. *Journal of Molecular Catalysis A: Chemical*. **2004**, 216, 115-119.
- Silva, F.A.; Rodrigues, E.A. Adsorption Equilibria and Kinetics for Propylene and Propane over 13X and 4A Zeolite Pellets. *Ind. Eng. Chem. Res.* **1999**, 38, 2051-2057.
- Silva, J. A.C.; Da Silva, F. A.; Rodrigues, A.E. An Analytical Solution for the Analysis of Zero-Length-Column Experiments with Heat Effects. *Ind. Eng. Chem. Res.* **2001**, 40, 3697-3702.
- Silva, J. A.C.; Da Silva, F. A.; Rodrigues, A.E. An Analytical Solution for the Analysis of Zero-Length-Column Experiments with Heat Effects. *Ind. Eng. Chem. Res.* **2001**, 40, 3697-3702.
- Surble, S.; Millange, F.; Serre, C.; Duren, T.; Latroche, M.; Bourrelly, S.; Llewellyn, P. L.; Ferey, G., Synthesis of MIL-102, a chromium carboxylate metal-organic framework, with gas sorption analysis. *J Am Chem Soc* **2006**, 128 (46), 14889-14896.
- Uemura, K.; Matsuda, R.; Kitagawa, S., Flexible microporous coordination polymers. *J Solid State Chem* **2005**, 178 (8), 2420-2429.
- Walton, K.S.; Abney, M.B.; LeVan, M.D. CO₂ Adsorption in Y and X Zeolites Modified by Alkali Metal Cation Exchange. *Microporous and Mesoporous Material*. **2006**, 91, 78-84.
- Walton, K.S.; Abney, M.B.; LeVan, M.D. CO₂ Adsorption in Y and X Zeolites Modified by Alkali Metal Cation Exchange. *Microporous and Mesoporous Material*. **2006**, 91, 78-84.
- Wang, B.; Cote, A. P.; Furukawa, H.; O'Keeffe, M.; Yaghi, O. M., Colossal cages in zeolitic imidazolate frameworks as selective carbon dioxide reservoirs. *Nature* **2008**, 453 (7192), 207-U
- Xue, M.; Ma, S. Q.; Jin, Z.; Schaffino, R. M.; Zhu, G. S.; Lobkovsky, E. B.; Qiu, S. L.; Chen, B. L., Robust metal-organic framework enforced by triple-framework interpenetration exhibiting high H-2 storage density. *Inorg Chem* **2008**, 47 (15), 6825-6828.
- Yaghi, O. M.; Li, H. L.; Davis, C.; Richardson, D.; Groy, T. L., Synthetic strategies, structure patterns, and emerging properties in the chemistry of modular porous solids. *Accounts Chem Res* **1998**, 31 (8), 474-484.
- Yang, J.; Hand, D. W.; Crittenden, J. C.; Hokanson, D. R.; Oman, E. J.; Audeves, D. Dynamic Mathematical Modeling of an Isothermal Three-Phase Reactor: Model Development and Validation. *Journal of Environmental Engineering*. **2003**, 129:7, 586-594.
- Yang, S. Y.; Long, L. S.; Jiang, Y. B.; Huang, R. B.; Zheng, L. S., An exceptionally stable metal-organic framework constructed from the Zn-8(SiO₄) core. *Chem Mater* **2002**, 14 (8), 3229-3231.
- Yazaydin, A. O.; Benin, A. I.; Faheem, S. A.; Jakubczak, P.; Low, J. J.; Willis, R. R.; Snurr, R. Q., Enhanced CO₂ Adsorption in Metal-Organic Frameworks via Occupation of

- Open-Metal Sites by Coordinated Water Molecules. *Chem Mater* **2009**, *21* (8), 1425-1430.
- Zhan, B.Z.; White, M.A.; Lumsden, M.; Mueller-Neuhaus, J.; Robertson, K.N.; Cameron, T.S.; Gharghour, M. Control of Particle Size and Surface Properties of Crystals of NaX Zeolite. *Chem. Mater.* **2002**, *14*, 3636-3642.
- Zhao, Z. X.; Li, Z.; Lin, Y. S., Adsorption and Diffusion of Carbon Dioxide on Metal-Organic Framework (MOF-5). *Ind Eng Chem Res* **2009**, *48* (22), 10015-10020.
- Zou, Y.; Hong, S.; Park, M.; Chun, H.; Lah, M. S., Selective gas sorption property of an interdigitated 3-D metal-organic framework with 1-D channels. *Chem Commun* **2007**, (48), 5182-5184.

VITA

ALEV GÜNEŞ YERKESİKLİ

Date of Birth: 22.04.1980
Place of Birth: Ankara
Citizenship: Turkish

EDUCATION

[1998-2003] B.Sc. (Chemical Engineering)

Ege University
Department of Chemical Engineering, Izmir, Turkey
Dissertation: Hydrogen Production

[2002-2005] M.Sc. (Chemical Engineering)

İzmir Institute of Technology
Department of Food Engineering, İzmir, Turkey
Dissertation: The Production of Thymoquinone From Thymol and Carvacrol by Using Zeolite Catalysts

[2005-2013] Ph. D. (Chemical Engineering)

İzmir Institute of Technology
Department of Chemical Engineering, İzmir, Turkey
Dissertation: Adsorption of Reformer Off-Gas on NaX Zeolite and Metal Organic Framework (MIL53(Al)): Equilibria and Kinetics

PUBLICATIONS

A. Güneş, O. Bayraktar, S. Yılmaz, Liquid Phase Oxidation of Carvacrol by Using Zeolite Encapsulated Metal Complexes, Ind. Eng. Chem. Res., 2006, 45, (54-61)

B.B.Pekşen, C. Üzelakçıl, A. Güneş, Ö.Malay, O. Bayraktar, A Novel Silk Fibroin-Supported Iron Catalyst for Hydroxylation of Phenol, Journal of Chemical Technology and Biotechnology, 2006, 81, (1218-1224)

Y. Erten, A. Güneş-Yerkesikli, A. E.Çetin and F. Çakıcıoğlu-Özkan, CO₂ Adsorption and Dehydration Behavior of LiNaX, KNax, CaNaX and CeNaX Zeolites, Journal of Thermal Analysis and Calorimetry, Vol. 94 (2008) 3, 715–718.

Alev Güneş Yerkesikli, Fehime Çakıcıoğlu Özkan, CO₂ adsorption on K⁺ exchanged NaX zeolite via ultrasound and MOFs (in preparation)